Synergistic Anti-Tumor Immune Response to Combination Immunotherapy Consisting of Anti-Tumor Antibodies, Extended Half-Life Interleukin-2, and Other Immunomodulatory Agents

by

Eric F. Zhu

B.S., Chemical Engineering
University of California – Berkeley, 2011

Submitted to the Department of Chemical Engineering
in partial fulfillment of the requirements for the degree of

Doctor of Philosophy in Chemical Engineering

at the

MASSACHUSETTS INSTITUTE OF TECHNOLOGY

June 2016 [September 2016]

Signature of Author: Signature redacted
Department of Chemical Engineering
June 2016

Certified by: Signature redacted
K. Dane Wittrup
C.P. Dubbs Professor of Chemical Engineering and Biological Engineering
Thesis Supervisor

Accepted by: Signature redacted
Daniel Blankschtein
Herman P. Meissner (1929) Professor of Chemical Engineering, Graduate Officer
Committee for Graduate Students

Synergistic Anti-Tumor Immune Response to Combination Immunotherapy Consisting of Anti-Tumor Antibodies, Serum-Persistent Interleukin-2, and Other Immunomodulatory Agents

by

Eric F. Zhu

Submitted to the Department of Chemical Engineering on June 24, 2016
in partial fulfillment of the requirements for the degree of
Doctor of Philosophy in Chemical Engineering

Abstract

Cancer immunotherapies under development have generally focused on either stimulating T-cell immunity or driving antibody-directed effector functions of the innate immune system such as antibody-dependent cell-mediated cytotoxicity (ADCC). However, as our understanding of anti-tumor immune responses grows, it has become increasingly apparent that single agent therapies may be insufficient to effectively stimulate all aspects of a complex robust anti-tumor response in a large proportion of patients. Thus, rational combination of single agent immunotherapies has become an area of increasing interest.

In this work, we find that a combination of an anti-tumor antigen antibody and an untargeted IL-2 fusion protein with delayed systemic clearance induces significant tumor control in aggressive isogenic tumor models via a concerted innate and adaptive response. We find that this therapy induces the infiltration of various immune effectors such as neutrophils, eosinophils NK cells, and $CD8^+$ T-cells that appear to direct cytolytic activity against tumor cells. This combination therapy also induces an intratumoral "cytokine storm," potentially re-polarizing the tumor microenvironment into one that is immunologically anti-tumor. We also identify cross-talk between NK cells and macrophages to induce intratumoral recruitment of neutrophils but with the requisite presence of anti-tumor antibodies and IL-2 simultaneously.

We further enhanced the efficacy of this two-component therapy with the addition of a potent amphiphile-based anti-tumor peptide vaccine in combination with checkpoint blockade of anti-PD-1 and anti-CTLA-4. This multi-component therapy was tested in a setting of a low-

mutational burden GEM lung cancer model with a single known and targetable antigen: human carcinoembryonic antigen (CEA). We find that in the subcutaneous setting and autochthonous setting, both components of checkpoint blockade are necessary for full efficacy. While a 5-component therapy is admittedly unwieldy for clinical translation, understanding the complementary yet non-overlapping contributions of each agent may inform improved development of additional immunotherapy agents and their combinations in the clinic.

Thesis Supervisor: K. Dane Wittrup
Title: C.P. Dubbs Professor of Chemical Engineering and Biological Engineering

Acknowledgements

Although a Ph.D. thesis has but a single author, the body of this work could not have been accomplished without the invaluable contribution and support from a number of individuals.

My deepest gratitude goes out to my advisor K. Dane Wittrup for the success of this work. His incredible mind, constant support, and patient mentoring have shaped me for the past 5 years. My thesis committee members—Darrell Irvine, Chris Love, and Arlene Sharpe—have also been invaluable with their striking insights and ideas, strongly directing the progression of my project.

I am also indebted to the assistance and camaraderie of all the members of the Wittrup Lab. Annie Gai was my first mentor, having first laid the groundwork for the Fc/IL-2 + TA99 project. John Rhoden transitioned me into the role of Mouse Czar and KP mouse expert. Katie Maass and I worked closely in the first year chemical engineering office and joined the Wittrup Lab together. Tiffany Chen proved to be an invaluable resource for any technical questions that I had as a graduate student and even past her graduation, we remain close friends over brunch. Byron Kwan made working in lab an adventure, both mental and physical, but his presence always engendered joy. I have learned much from his wealth of knowledge and strong sense of self-confidence. Tina Zhou and her constant cheerfulness have been a panacea for many dour moments. I have been deeply influenced by Cary Opel, his rigor in both statistics and the scientific method, and his ineffable ability to be critical and questioning. Seymour de Picciotto, Nicole Yang, Xiaosai Yao, and Alice Tzeng possessed deep-wells of knowledge and experience from which I could draw succor when needed. Ryan Kelly brought levity; he was a good sport when I kicked him out of the lab. Monique Kauke was an incredible colleague and a wonderful friend, whose steadfastness I hope I can learn from. I always looked forward to sharing a meal and coffee with Alessandro Angelini. His scientific curiosity is an inspiration and his unending support is something I have come to depend on.

I am truly grateful to have been able to work closely with Kavya Rakhra and Wuhbet Abraham from the Irvine Lab. Embarking on a challenging new project is always a daunting task, but collaboration with these two has never felt more natural and amiable. Within the Koch Institute, I would like to thank all the staff of the animal facility that have cared for countless of mice. The experienced staff of the Swanson Biotechnology Center also accelerated this project in

all aspects: cloning and sequencing flow cytometry, histology, microscopy, and live animal imaging.

I could not have made it through this process without the deep connections forged with my classmates and friends. Mark Weidman has been a constant source of laughter and wit in my life at MIT. I could not ask for a better travel companion on our many adventures together. I admire Steven Edgar and his unshakeable nature; he remains gregarious and upbeat in any situation. His ability to make people feel at ease and converse without pretense is a gift. Xiao Su has also enriched my travels and I am glad to have shared many a meal with him. Sean Hunt, Lionel Lam, Karthik Narsimhan, David Nicholson, Julia Haftel, William Ho, Helen Luo, and Jennifer Lewis have all made graduate school that much more enjoyable. I am always uplifted when spending time with Aanchal Jain; my guard is never up in her presence. She possesses such a genuine personality and an insurmountable spirit from on which I can always rely. Su Luo has always been incredibly supportive and a source of mirth; I am only sad that we could not have been friends sooner.

My journey was first conceived at UC Berkeley, and I give particular thanks to the three individuals who were with me at the outset. Dat Tien Hoang who gave me strength during the trying times of first semester MIT classes and our continual care for each other during the graduate school process despite the tribulations and evolution of our lives. Rosanna Lim has remained my dear roommate from start to finish during graduate school, and in times of crisis I draw on all her good qualities: intelligence, perseverance, kindness, and her never-ending smile. She will always remain a dear friend. My time at MIT would be unfathomable without Thomas Willems, my closest friend. Our conversations have always been unreserved, our moments together always cherished, and our understanding of each other always unquestionable. He is a source of encouragement and guidance, and someone who inspires me to reach untiringly for a higher level of achievement. I look to him as family and I hope our bond of friendship continually strengthens as we embark on the new chapters of our lives.

Finally, my sister and parents have been an eternal wellspring of support. I thank my sister Ying for her assured confidence in my success and her wise outlook on life. Her own experiences as a graduate student and beyond have greatly informed my own path. I am immeasurably grateful for my parents, Xinmin and Geibao. They have made unimaginable sacrifices in their own lives to ensure the future successes in mine. That knowledge has always

pushed me to work harder in moments of self-doubt or when my drive has been nearly exhausted, because I know that they overcame worse odds than I ever shall. Knowing that I can always fall back on their love and care has allowed me to take risks and strive for things that were seemingly out of reach. Mom and Dad, you have taken your son to where he is now and I hope to go farther still for your sakes. I could never return to you what you have given me but I will always try.

To all the people that have shaped my life here at MIT, thank you.

Eric Zhu
June 2016

Table of Contents

1. Background

The first cancer immunotherapy was administered over 100 years ago by Dr. William Coley, a surgical oncologist (Coley, 1894). Although crude in form, Coley's toxin nevertheless was evidence that our immune system, so capable of protecting us against various pathogens, also had the capacity to recognize cancer as a malignant form of the self and eliminate it (Dunn et al., 2002, 2004a, 2004b; Schreiber et al., 2011). It is therefore surprising that advances in cancer immunotherapy as a field have only taken off in the last few decades, proving it to be an exciting area of fundamental biology research and active drug development.

Tumors, being highly mutable, are able to develop resistance to traditional anti-cancer regimens such as chemotherapy (Tsuruo et al., 2003) or targeted therapy (Chong and Jänne, 2013; Katayama et al., 2011; Rini and Atkins, 2009). Thus, the promise of immunotherapy is a highly compelling one, as heterogeneously mutating tumors can actually be countered by a similarly evolving adaptive immune response (Blattman and Greenberg, 2004; Smyth et al., 2001). Perhaps the first cancer immunotherapy was recombinant interleukin-2 (IL-2), one of the first type I cytokines discovered and was first named T-cell growth factor, due to the proliferative effects it had on T lymphocytes (Malek, 2008).

IL-2 is an important signaling molecule involved in various responses of the immune system. $CD4^+$ T-cells are the main source of endogenous IL-2, produced after appropriate TCR engagement and co-stimulatory signals, but other cells such as $CD8^+$ T-cells may also contribute to its secretion to a lesser degree (Malek, 2008). The IL-2 receptor (IL-2R) is composed of three subunits—**1.** IL-2Rα or CD25; **2.** IL-2Rβ or CD122; and **3.** the common γ chain or γ_c or CD132—which can complex together in various ways to produce three distinct receptors, with different affinities for IL-2 and signaling capabilities (Nelson and Willerford, 1998).

The low affinity receptor of IL-2 is simply CD25 itself. This chain has only a K_d of approximately 10 nM. The medium affinity receptor is a heterodimer of CD122 and CD132, with signaling possible through IL-2Rβ and CD132 (γ_c). This receptor has a K_d for IL-2 of approximately 1 nM. This receptor is found constitutively on resting lymphoid cells such as NK cells and $CD8^+$ T-cells. Finally, the high affinity receptor is a heterotrimer of CD25, CD122, and CD132. Again, signaling is transduced in this complex through IL-2Rβ and γ_c, and has an

extremely high affinity for IL-2, with a K_d of approximately 10 pM. This form of IL-2R is only expressed on activated $CD8^+$ T-cells, but is constitutively expressed on the surface of regulatory T-cells. (Nelson and Willerford, 1998; Sakaguchi et al., 1995).

IL-2 forms a signaling complex in a sequential manner, with initial CD25 binding leading to subsequent recruitment of CD122 and CD132 (Nelson and Willerford, 1998). When IL-2 binds to its cognate receptor, it induces signaling through the JAK-STAT pathway, in particular through JAK1, JAK3, and the STAT5 transcription factor although STAT1 and STAT3 are also implicated. Most of this signaling is associated with IL-2Rβ chain. STAT5 is an important but weak transcription factor for the CD25 gene, requiring co-activators for significant transcription of CD25. On the opposing spectrum, another target for STAT5 is FasL, responsible for activation-induced cell death. Another prominent pathway induced by IL-2 is the PI3K pathway, involved in survival and anti-apoptosis responses. Additionally, the γ_c also has signaling capabilities, mostly through JAK3 association, for T-cell development. Interestingly, the γ_c in contrast to IL-2Rβ also has a role in receptor internalization, reducing the half-life of CD25 on the cell surface. Moreover, the γ_c is downregulated upon T-cell expansion. Thus, to maintain homeostasis, IL-2 signaling can have opposing outcomes: activation signals to naïve T-cells but also apoptotic signals in activated T-cells. (Gaffen, 2001).

Clinically, IL-2 was able to show durable responses in a small subset of patients of metastatic melanoma and metastatic renal carcinoma, in some cases generating long-term cures. However, its use was often associated with severe adverse events, and therefore was not given extensively as a first-line therapy. Nevertheless, IL-2 provided an early indication that immunotherapies were able to deliver on their promise of durable regression. (Atkins et al., 1999; Fyfe et al., 1995).

Since then, perhaps the most successful class of cancer immunotherapy has been monoclonal antibodies, although ironically they were not necessarily developed with immunotherapy in mind. Despite being an integral part of the adaptive immune system, antibodies were originally utilized for their exquisite selectivity to certain antigens. In this sense, successful clinical antibodies such as Herceptin or Cetuximab were developed as binders to overexpressed tumor-associated growth receptors such as those of the EGFR family, to inhibit growth signaling. (Weiner et al., 2010).

Unsurprisingly, it has come to be appreciated that there is likely an immune-component to their efficacy as well. These antibodies still possessed activating isotypes, human IgG1, and it is not unreasonable that part of their mechanism of action was engaging effectors through FcγR binding (Schneider-Merck et al., 2010; Weiner et al., 2009; Weng and Levy, 2003). Indeed, even with current checkpoint blockade antibodies such as CTLA-4, this important aspect of the innate immune system has been highlighted (Selby et al., 2013).

Perhaps the true excitement around cancer immunotherapy came only in the last few years, with the advent of checkpoint inhibitors. Checkpoint receptors such as CTLA-4 and PD-1 had been recognized for decades as mechanisms through which the immune response could be controlled (Freeman et al., 2000; Leach et al., 1996; Nishimura et al., 1999).

CD28 and CTLA-4 are important modulators of T-cell activation; where the former is involved in activation of T-cells, the latter is involved in the inhibition of such responses. While T-cell activation is a critical component of the overall immune response, aberrant activation of self-reactive T-cells is also undesired. While normally absent on resting T-cells, CTLA-4 expression becomes apparently hours after activation and reaches a peak after 48-72 hours. Both CD28 and CTLA-4 bind to the same cognate ligands CD80 (B7-1) and CD86 (B7-1), although differences in the receptors mediate the ultimate outcome of binding. CD28 is expressed in much higher density on the cell-surface than CTLA-4 even during T-cell activation, although CTLA-4 could be considered a higher-affinity receptor than CD28. Thus, one route through which CTLA-4 can inhibit activation is through limiting the available pool of CD80/86 that can bind to CD28. While CTLA-4 does not outnumber CD28 with regards to density, CTLA-4 does traffic specifically to immune synapses from intracellular vesicles, generating a high local density of CTLA-4. The other route of CTLA-4 inhibition of T-cell activation is through inhibitory signaling. CTLA-4 does possess a cytoplasmic tail and thus could have intracellular signaling capabilities, although it lacks enzymatic activity and other traditional inhibitory motifs such as ITIM. Although the exact mechanism remains unclear, evidence suggests that the signaling may involve PP2A downstream of early TCR signaling, either competing with PI3K or PKB/Akt inhibition. Despite our incomplete understanding of CTLA-4, its importance as inhibiting unwanted T-cell activation is clear. CTLA-4 knock-out mice quickly succumb to lethal autoimmunity, suggesting that without this negative regulator, even weakly self-reactive T-cells can be activated. (Sansom, 2000; Teft et al., 2006).

Although both CTLA-4 and PD-1 are important for peripheral tolerance, CTLA-4 functions primarily on at the T-cell priming level in the lymph nodes whereas PD-1 functions at the periphery. Similarly to CTLA-4, PD-1 is also absent on resting T-cells but becomes expressed upon activation. Furthermore, the effects of PD-1 ligation are quite rapid, apparent within a few hours of activation. PD-1 expression is not limited to T-cells, but is also found on other immune cell populations such as B-cells, NK cells, and dendritic cells (DCs). PD-1 possesses two ligands—PD-L1 and PD-L2—although the former has a much wider tissue expression than the latter. PD-L1 is expressed constitutively on cells of hematopoetic lineage such as T and B cells but can also found on non-hematopoietic cells after induction through type I and type II interferons, including those of the heart, lung, and spleen, among others. This could be an important mechanism of peripheral tolerance against weakly self-reactive T-cells, and is exhibited by the expression of PD-L1 across a wide spectrum of host tissues. In terms of signaling, PD-1 signaling predominantly regulates cytokine production with weaker effects on proliferation. Interestingly, PD-1 inhibition is stronger during lower levels of TCR engagement. Upon ligation of PD-1, downstream PI3K and Akt are inhibited. Erk activation is also reduced with PD-1 ligation but can be overcome with activation of STAT5 primarily through cytokine-mediated signaling such as through IL-2. (Keir et al., 2008; Nishimura and Honjo, 2001).

Yet the PD-1/PD-L1 axis has also been subverted by neoplasia as a mechanism of immune suppression, preventing immune responses by effector T-cells that in fact recognize tumor-associated antigens. It was found that PD-L1 was overexpressed in many types of cancer, and that this was correlated with poorer prognosis. PD-L1 was also found to be up-regulated on tumor cells with exposure to IFNγ, strongly suggesting that tumors were able to respond to and blunt an incipient anti-tumor immune response. Incredibly, the PD-1/PD-L1 axis was also found to have bi-directional signaling capacity. PD-1 engagement of PD-L1 on cancer cells can actually transmit signals in those cancer cells, increasing their resistance to apoptosis by immune effectors. (Azuma et al., 2008; Dong et al., 2002; Flies et al., 2011).

Antibodies developed against anti-CTLA-4 and anti-PD-1 have given clinical recourse to those patients whose disease had essentially progressed too far for treatment, such as metastatic melanoma or metastatic non-small cell lung cancer (NSCLC). It is an amazing feat that these agents have been able to induce complete regression in patients of these advanced diseases, often for several years without sign of relapse. Yet, despite the "raising of the tail" effect, only a small

subset of patients benefit from these drugs, reminiscent of the days of IL-2. (Borghaei et al., 2015; Brahmer et al., 2015; Hodi et al., 2010a; Wolchok et al., 2013).

As the field continues to develop such drugs, it has been recognized and accepted that single agent therapies may be insufficient to induce durable responses for a large swathe of patients (Overwijk, 2005; Stagg et al., 2007). Therefore, researchers are now focusing on combination immunotherapy, in hopes of meeting all the postulated criteria required for robust efficacy (Stagg et al., 2007). Even early clinical development of immunotherapies demonstrated this thinking, as clinical trials of anti-CTLA-4 were first done with not just anti-CTLA-4 alone, but also in combination with a vaccine against gp100 (Hodi et al., 2010b). Recent clinical trials in the combination of anti-CTLA-4 and anti-PD-1 suggest that the combination of the two may be greatly superior to either one alone, as although these agents work to reverse the same general phenomena—immune suppression—they work in complementary but distinctly different ways (Hammers et al., 2014; Wolchok et al., 2013). For example, subsequent research on the mechanism of action of anti-CTLA-4 revealed that enhanced T-cell priming may not have been the only effect. As it turns out, tumor-associated Tregs express extremely high levels of CTLA-4, higher than other tumor-infiltrating lymphocytes (Beyer and Schultze, 2006; Selby et al., 2013). Therefore, it was found that anti-CTLA-4 had maximal efficacy only when it was of an activating isotype, suggesting that beyond its enhancement of T-cell priming, it also acted as a potent depleting antibody of Tregs (Selby et al., 2013).

In fact, it seems now that combination with anti-PD-1 is a matter of course for any new immunotherapy development. In particular, clinical trials with cancer vaccines have been particularly enthusiastic about combination with anti-PD-1 (Sznol and Chen, 2013). This may be because effective priming of T-cells may remain insufficient for an anti-tumor response at the tumor locale. For example, it has been shown that an amphiphile-based vaccine as monotherapy was not particularly efficacious, despite generation of a large number of tumor-specific T-cells, over 20-30% in peripheral blood (Liu et al., 2014). This may very well be because of immunosuppressive effects at the tumor microenvironment level.

It has been recognized that the anti-tumor immune response is a multi-faceted process, with various steps that remain spatially and temporally distinct (Chen and Mellman, 2013). A single agent simply cannot address all the complexity of such a process. As the field moves forward, the development of single agents addressing multiple steps in the development of anti-

tumor immunity will be critical. But it is also inevitable that only rational combinations of such monotherapies will engender more successful clinical outcomes.

2. Characterization and Generalization of Serum-Extended Half-Life IL-2 and Anti-Tumor Antibodies

2.1. Introduction

Monoclonal antibodies against target tumor antigens, such as trastuzumab, rituximab, and cetuximab, have achieved tremendous clinical successes (Weiner et al., 2009). Although such antibodies generally possess direct growth-inhibitory bioactivity, their capability to enlist innate effector functions is a critical component of their therapeutic efficacy (Ferris et al., 2010). In mechanistic studies of anti-tumor monoclonal antibodies in xenograft mouse models, innate effector cells expressing activating FcγR, particularly NK cells, were shown to be required for therapeutic efficacy (Clynes et al., 2000; Sliwkowski et al., 1999; Tokuda et al., 1996). In fact, it was found that lymphoma patients expressing higher affinity alleles of FcγRIII responded better to rituximab therapy (Weng and Levy, 2003), consistent with a major contribution of ADCC to the efficacy of anti-tumor antigen antibody therapy.

Encouragingly, studies demonstrated that IL-2 enhanced NK cell activity against antibody-coated tumor cells in cell culture bioassays (Carson et al., 2001; Eisenbeis et al., 2004). Thus, efforts to strengthen clinical NK cell-mediated ADCC combined monoclonal antibodies with IL-2, marketed as monotherapy for metastatic renal cell carcinoma and metastatic melanoma (Atkins et al., 1999; Fyfe et al., 1995). However, these results did not prove translatable to the clinic. IL-2 combined with antibodies such as trastuzumab and rituximab consistently failed to provide significant clinical benefit over antibody alone (Khan et al., 2006; Mani et al., 2009; Poiré et al., 2010).

Part of this failure may stem from the nature of IL-2 itself. As a small protein, approximately 18 kDa in molecular mass, IL-2 is rapidly cleared from the body when given as an intravenous bolus (Konrad et al., 2009). That is why much of the clinical benefit seen with IL-2 as a monotherapy is derived only when IL-2 is dosed at a level where patients experience severe toxicities. It is possible that the concentration of systemic IL-2 required to enhance anti-tumor antibody function is not achievable simply with bolus injections of IL-2. Either the delivery method must be altered, for example the use of continuous infusion of IL-2 at a finely calibrated concentration (Dillman et al., 1993; Legha et al., 1996), or the protein nature of IL-2 must be changed.

One way to alter the pharmacokinetics of a protein is to attach an additional moiety on it. In this case, we wish to increase the serum half-life of IL-2, such that a sufficient level of IL-2 can be maintained in the blood that can synergize with anti-tumor antibody function. Increasing the molecular weight of IL-2 can be done through chemical modifications such as conjugation to PEG (Zimmerman et al., 1989). IL-2 can also be directly fused to other protein moieties such as with the Fc fragment of an antibody (Baden et al., 2011) or mouse serum albumin (MSA) (Melder et al., 2005). Both moieties have the auspicious properties of being proteins found abundantly in the blood already, and both have an additional method of half-life extension through FcRn recycling.

We also hypothesized that the signaling resulting from parenteral IL-2 administration may be temporally inappropriate, as repeated bolus doses can lead to highly oscillatory cytokine exposure. The cellular response to such IL-2 spikes can be dramatically different than the response to more stable concentration trajectories (Rao et al., 2005). Both the duration and strength of IL-2 signaling determines the balance between effector and memory cytolytic T-cell development (Feau et al., 2011; Kalia et al., 2010; Pipkin et al., 2010), a balance critical to the success of immunotherapies such as adoptive cell therapy (June, 2007). It is noteworthy that in the previous clinical trials combining IL-2 and antibodies, IL-2 was administered as a subcutaneous pulse either once per day (Mani et al., 2009; Poiré et al., 2010) or three times per week(Khan et al., 2006). Consequently, these patients' T-cells were exposed to short, strong bursts of IL-2 signaling, unlike the sustained exposure in cell culture plates that had initially motivated the clinical studies (Carson et al., 2001; Eisenbeis et al., 2004; Rao et al., 2004).

Finally, by maintaining a more constant serum concentration of IL-2 with fewer injections, the toxicity normally associated with bolus IL-2 administration may be mitigated. In this study, we explore how fusing IL-2 to either Fc of MSA can enhance the therapeutic efficacy of IL-2 as a monotherapy, in addition to how it may synergize with anti-tumor antibodies. Moreover, we also investigate the potential mitigation of toxicity when administering IL-2 fusions compared to soluble IL-2.

2.2. Materials and Methods

Cloning

Vectors encoding the heavy and light chains of mouse TA99 antibody were gifts of Jeffrey V. Ravetch (The Rockefeller University). The DNA sequences encoding the heavy and light chains were cloned into gWIZ (Genlantis), yielding gWIZ-TA99-HC and gWIZ-TA99-LC. A vector encoding the scFv sequence of 237 mAb (Ward et al., 1989) was a kind gift from David M. Kranz (University of Illinois at Urbana-Champaign). The DNA sequences encoding the variable heavy and light chains were isolated and used to replace the variable regions of the previous gWIZ-TA99-HC and gWIZ-TA99-LC, yielding gWIZ-237-HC and gWIZ-237-LC, respectively. A vector encoding the heavy chain of mouse IgG2a from C57BL/6 mice was a gift of Jeffrey V. Ravetch (The Rockefeller University). A D265A mutation was introduced and the DNA encoding the non-lytic D265A Fc, henceforth referred to simply as Fc, was cloned into gWIZ. For cloning of Fc/IL-2, murine IL-2 (InvivoGen) with C-terminal 6xHis tags was subsequently cloned C-terminal to the Fc, separated by a short G_3S linker, yielding gWIZ-Fc/IL-2. To enable expression of monovalent heterodimeric Fc/IL-2, a vector encoding the Fc with a C-terminal FLAG tag, gWIZ-Fc/FLAG, was also constructed using similar methods. Plasmid DNA was transformed into XL-1 Blue (Agilent) for amplification and purified using EndoFree Plasmid Maxi Kit (Qiagen). For cloning of the recombinant fusion protein of mouse serum albumin fused to murine IL-2 (MSA/IL-2), the coding sequence for mouse serum albumin (Origene) was used to replace the sequence encoding the Fc in the existing gWIZ-Fc/IL-2 vector, generating the vector gWIZ-MSA/IL-2.

Protein Production

TA99, 237 mAb, Fc/IL-2, and MSA/IL-2 fusion proteins were produced using HEK293 cells (Life Technologies) according to manufacturer's instructions. HEK293 cells were transfected with gWIZ-TA99-HC and gWIZ-TA99-LC; gWIZ-237-HC and gWIZ-237-LC; gWIZ-Fc/IL-2 and gWIZ-Fc/FLAG; or gWIZ-MSA/IL-2 for TA99, Sm3e, Fc/IL-2 or MSA/IL-2, respectively, using polyethylenimine in FreeStyle 293 media supplemented with OptiPro (Life Technologies). TA99 and 237 mAb were purified by Protein A Agarose (Genscript), Fc/IL-2 was purified by TALON Metal Affinity Resin (Clontech) and followed by anti-FLAG M2 Affinity Gel (Sigma-Aldrich), and MSA/IL-2 was purified by TALON Metal Affinity Resin and further purified using a HiLoad™ 16/600 Superdex™ 200 pg column (GE Healthcare Life Sciences) on an ÄKTAFPLC protein purification system (GE Healthcare Life Sciences). All in-house produced

protein were ensured to contain minimal levels of endotoxin (< 0.1 total EU/injection within 1 hour) using the QCL-1000 assay (Lonza).

Mice

C57BL/6NTac mice (Taconic) and C3H/HeNTac mice (Taconic) were aged between 6-10 weeks of age before tumor induction. All animal work was conducted under the approval of the MIT Division of Comparative Medicine, in accordance with federal, state, and local guidelines.

CTLL-2 Viability Assay

CTLL-2 cells (ATCC) were cultured in RPMI 1640 (ATCC), supplemented with fetal bovine serum, L-alanyl-L-glutamine, sodium pyruvate, and penicillin-streptomycin, all purchased from Life Technologies, as well as T-STIM with ConA (BD Biosciences). For maintenance, cells were passaged to a density of 10,000 cells/mL. For viability assays, cells were seeded at 150,000 cells/mL to which various forms of IL-2—murine IL-2 produced in *E. coli* (mIL-2), human, IL-2 produced in *E. coli* (Proleukin), Fc/IL-2 produced in HEK cells, or MSA/IL-2 produced in HEK cells, were added at indicated concentrations on an IL-2 basis, in a final volume of 100 □L. Cells were grown for 48 hours before assaying viability using CellTiter-Glo Luminescent Cell Viability Assay (Promega), according to manufacturer's instructions. Luminescence was measured using an Infinite M1000 microplate reader (Tecan) using an integration time of 1 second. A dose response curve was fit via nonlinear regression using GraphPad Prism 5 software (GraphPad).

Fc/IL-2 *in vitro* Serum Stability

Blood was drawn from mice retro-orbitally, allowed to clot, and serum isolated via centrifugation in Microvette 100 tubes (Sarstedt), according to manufacturer's instructions. Equivalent amounts of Fc/IL-2 were incubated in serum at 37 °C for up to 3 days. Incubations were staggered such that all incubations (0 days-3 days) finished on the same day. Protein was run on a 4-12% Bis-Tris protein gels (Life Technologies) and transferred to a nitrocellulose membrane using iBlot transfer stacks and the iBlot gel transfer device (Life Technologies), according to manufacturer's instructions. Membranes were blocked with non-fat dry milk in TBST, probed with biotinylated anti-IL-2 antibody (clone JES6-5H4; eBioscience), and subsequently probed with Avidin-HRP (eBioscience). Detection of HRP chemiluminescence was performed using Thermo Scientific Super Signal West Dura Chemiluminescent Substrate (Fisher Scientific) and imaged using an ImageQuant LAS 4000 (GE Healthcare Life Sciences).

Pharmacokinetic Studies

Wild-type murine IL-2 (Peprotech), Fc/IL-2, and MSA/IL-2 were labeled with IRDye® 800CW NHS Ester (Li-Cor) and degree of labeling determined, according to manufacturer's instructions. 25 μg of IL-2 or 50 μg of Fc/IL-2 or MSA/IL-2 was injected retro-orbitally into C57BL/6 mice and blood was drawn from the tail at indicated time points and collected in heparin coated tubes (VWR). Tubes were protected from light and kept at 4 °C until blood collection was complete. IR luminescence was measured using the Odyssey Infrared Imaging System (Li-Cor) and analyzed using ImageJ (NIH).

Tumor Cells

B16F10 cells (ATCC), RM9 cells (Baley et al., 1995), and Ag104A cells (Ward et al., 1989) were maintained in DMEM, supplemented with fetal bovine serum, L-alanyl-L-glutamine, and penicillin-streptomycin, all purchased from Life Technologies. D5-HER2 cells (Wang et al., 2012) were maintained in RMPI 1640, supplemented with fetal bovine serum, L-alanyl-L-glutamine, and pencillin-streptomycin, all purchased from Life Technologies. The RM9 prostate cancer cell line was a kind gift from Dr. Timothy C. Thompson (MD Anderson Cancer Center). The Ag104A fibrosarcoma cancer cell line was a kind gift from Dr. Hans Schreiber (University of Chicago).

Tumor Inoculation and Treatment

For induction of B16F10 tumors, 10^6 cells in 100 μL of PBS were injected subcutaneously into the flanks of C57BL/6 mice and allowed to establish for 6 days before treatment. These tumors are on average 25-30 mm^2 in area and equivalently sized tumors could be achieved through other methods, such as inducing with 10^5 cells with a 10-14 day establishment period, based on the natural doubling time of B16F10 in C57BL/6 mice. Retro-orbital injection of PBS, IL-2 (6 μg; PeproTech), Fc/IL-2 (25 μg), MSA/IL-2 (30 μg), and/or TA99 (100 μg) was done on day 6, 12, 18, 24, and 30 after tumor inoculation for a total of five treatments. Daily intraperitoneal injections of Proleukin (36 μg), provided under a research grant from Prometheus Laboratories, started on day 6 and ended on day 30 after tumor inoculation. For induction of D5-HER2 tumors, hmHER2 Tg mice were inoculated subcutaneously in the flank with $3x10^3$ D5-HER2 cells. Beginning on day 1 after tumor induction, animals received intraperitoneal injections of either PBS, trastuzumab (Herceptin) biweekly (200 μg; Genentech), Fc/IL-2 weekly (25 μg), or the combination of the two. For induction of RM9 tumors, 250,000 cells in 50 μL of PBS were

injected subcutaneously into the flanks of C57BL/6 mice. Retro-orbital injection of PBS, Fc/IL-2 (25 μg), and/or 3F8 (150 μg) was done on day 6, 12, 18, 24, and 30 after tumor inoculation for a total of five treatments. 3F8 (Zhang et al., 1998), a murine IgG3 antibody against the tumor antigen GD2, was a kind gift from Dr. Nai-Kong V. Cheung (Memorial Sloan Kettering Cancer Center). For induction of Ag104A tumors, 10^6 cells in 50 μL of PBS were injected subcutaneously into the flanks of C3H/HeN mice. Retro-orbital injections of PBS, Fc/IL-2 (10 μg), and/or 237 mAb (100 μg) was done on day 6, 12, 18, 24, and 30 after tumor inoculation for a total of five treatments.

Pulmonary Wet Weight

C57BL/6 mice were injected *i.v.* with a single bolus of PBS, 12 μg IL-2, or 50 μg Fc/IL-2. 4 days after injection, lungs were extracted, placed into scintillation vials (VWR), frozen in liquid nitrogen, and lyophilized for 48 hours at room temperature under vacuum. Pulmonary wet weight was calculated by subtracting the sample weight after lyophilization from the initial sample weight.

Liver Enzymes AST and ALT Activity Assay

C57BL/6 mice were induced with B16F10 as previously described. Mice were bled on the day of first treatment with PBS or Fc/IL-2+TA99 and bled every other day thereafter until the sixth day after treatment for a total of four blood draws. In all cases the blood was allowed to clot, serum isolated via centrifugation in Microvette 100 tubes (Sarstedt), according to manufacturer's instructions, and then immediately flash frozen in liquid nitrogen to allow for subsequent batch processing. Determination of AST and ALT activity was done using AST activity assay kit (Sigma-Aldrich) and ALT activity assay kit (Sigma-Aldrich), respectively, according to manufacturer's instructions.

Serum Cytokine Analysis

For analysis of cytokine levels in the serum, mice were bled on the day of first treatment with PBS or Fc/IL-2+TA99 and bled every other day thereafter until the sixth day after treatment, for a total of four blood draws. In all cases the blood was allowed to clot, serum isolated via centrifugation in Microvette 100 tubes (Sarstedt), according to manufacturer's instructions, and then immediately flash frozen in liquid nitrogen to allow for subsequent batch processing. Samples were evaluated in triplicate using the Mouse 32-Plex Cytokine/Chemokine Panel Luminex Assay as performed by Eve Technologies.

Statistics

AST and ALT liver enzyme and serum cytokine data were analyzed using a 2-way ANOVA with Bonferroni post-test, survival data were determined using a log-rank Mantel-Cox test.

2.3. Results

2.3.1. Characterization of IL-2 and TA99 Treatment Conditions

To explore the effects of differing IL-2 exposure combined with a monoclonal antibody targeting a tumor antigen, established B16F10 melanoma were treated either with soluble recombinant murine IL-2 and/or the anti-TYRP-1 antibody, TA99 (Figure 2.1). TYRP-1 is a melanocyte marker but becomes surface expressed on B16F10. With infrequent IL-2 exposure, neither agents dosed separately nor together provided survival benefit (Figure 2.1). However, when extended daily dosing was performed, a notable synergistic effect was observed when TA99 was added, significantly extending survival (Figure 2.2). Despite this promising response, daily IL-2 dosing resulted in poor body condition for many of the mice treated (data not shown) and such a regimen could be arduous and expensive for clinical translation. Therefore, we sought to achieve similar synergistic effects through a form of IL-2 that provides similar long-term IL-2 exposure but requiring fewer and smaller doses.

2.3.2. Characterization of Fc/IL-2 and TA99 Treatment Conditions

To increase the persistence of IL-2 exposure *in vivo*, wild-type murine IL-2 was fused to the Fc fragment of murine IgG2a, termed Fc/IL-2 (Figure 2.3). We introduced the D265A mutation to the Fc—previously shown to abrogate FcgR binding and complement activation (Baudino et al., 2008)—to eliminate cytotoxic effects on the IL-2R$^+$ cells we wished to stimulate. We chose a monovalent heterodimeric form of the fusion protein in order to avoid avidity effects from two IL-2 molecules on the same protein. Fc/IL-2 possessed similar specific bioactivity to murine IL-2 produced either from *E. coli* or the clinical drug Proleukin (Figure 2.4). Fc/IL-2 demonstrated an increase in serum duration, with a beta half-life nearly three times that of wild type murine IL-2 (Figure 2.5 and Table 2.1). Fc/IL-2 exhibited significant degradation after *in vitro* incubation in serum at 37 °C for 48 hours (Figure 2.6).

We proceeded to evaluate the efficacy of Fc/IL-2 against established B16F10 tumors and its potential synergism with TA99. Cohorts were administered equimolar Fc/IL-2 to that of the IL-2 given in the infrequent exposure case with identical dosing schedules. Impressively, administration of Fc/IL-2 with TA99 (Fc/IL-2+TA99) resulted in a strong synergy between the two agents that fully controlled B16F10 growth during treatment, extending survival further than

either single agent (Figure 2.7). The dosing of Fc/IL-2+TA99 appeared well-tolerated by the mice which continued to gain weight during treatment (Figure 2.8) and showed no changes in pulmonary wet weight (Figure 2.9), although splenomegaly (Figure 2.10) and an acute increase in the serum level of liver enzymes (Figure 2.11) and various inflammatory cytokines (Figure 2.12) was observed.

2.3.3. Generalization of Serum-Extended Half-Life IL-2 using Mouse Serum Albumin

To confirm that the synergistic efficacy was solely due to the serum half-life extension of Fc/IL-2 as opposed to immunological effects conferred by the Fc region, we fused IL-2 to mouse serum albumin (MSA/IL-2) to generate an alternative form of IL-2 with extended serum half-life (Figure 2.5 and Table 2.1) and bioactivity (Figure 2.4), as albumin is similarly recycled by FcRn (Anderson et al., 2006). MSA/IL-2+TA99 and Fc/IL-2+TA99 were essentially identical in efficacy (Figure 2.13), suggesting that any form of IL-2 with increased serum half-life, or perhaps a continuous infusion of IL-2, will exhibit this synergistic therapeutic effect.

2.3.4. Generalization of Serum-Extended Half-Life IL-2 and Anti-Tumor Antibodies in Different Tumor Models

We further tested three additional tumor models with three different monoclonal antibodies to demonstrate the generalizability of this strategy:

D5-HER2 melanoma in hmHER2 transgenic mice (Wang et al., 2012) using Fc/IL-2 and trastuzumab (Herceptin) (Figure 2.14);

RM9 prostate cancer (Baley et al., 1995) in C57BL/6 mice using Fc/IL-2 and 3F8 (Zhang et al., 1998), a murine IgG3 antibody targeting the GD2 antigen expressed on RM9 (Figure 2.14);

Ag104 fibrosarcoma in C3H/HeN mice using Fc/IL-2 and 237 mAb, a murine IgG2a targeting the OTS8 antigen found on Ag104A (Ward et al., 1989) (Figure 2.14).

In every case, the combination of Fc/IL-2 with an anti-tumor IgG showed superior efficacy to either agent alone, even where the antibody itself provided no benefit (Figure 2.14).

Thus, the strong tumor-suppressive effect is generalized to four different tumor models with a unique anti-tumor antigen and antibody pairing plus a serum-persistent form of IL-2.

2.4 Discussion

There have been determined clinical attempts to combine anti-tumor antigen antibodies with pulsed IL-2 treatment in Phase I (Bajorin et al., 1990; Bleumera et al., 2006; Eisenbeis et al., 2004; Fleming et al., 2002; Repka et al., 2003) and Phase II (Khan et al., 2006; Mani et al., 2009; Poiré et al., 2010) clinical trials, all without evidence of efficacy. PEGylated IL-2 with increased serum half-life has also been tested clinically as monotherapy, and found not to be clinically superior (Yang et al., 1995). This suggests that a critical aspect missing may be more persistent IL-2 signaling, and in fact the clinical administration of anti-GD2 antibody, continuous infusion of IL-2, subcutaneous GM-CSF, and isotretinoin led to increased survival in children with high-risk neuroblastoma (Yu et al., 2010). Indeed, our own combination of an anti-tumor antibody and a fusion protein bestowing prolonged IL-2 signaling, despite its greater simplicity, demonstrated significant efficacy in various syngeneic murine tumor models.

With our initial construct Fc/IL-2, we demonstrated that the enhanced efficacy observed over soluble wild-type IL-2 is likely solely due to the extension in half-life provided by the fusion to the Fc fragment. This is further bolstered by the fact that Fc/IL-2 is monovalent with respect to IL-2, so there is no avidity when considering binding to IL-2R. Moreover, given the D265A mutation present within the Fc, the Fc fragment becomes non-lytic as it can no longer engage FcγR or activate the complement cascade, rendering it completely as a vehicle to increase half-life of whatever is attached to it.

We further demonstrate that half-life extension is likely the most important factor and not an unconsidered immunological function attributed to the Fc, as IL-2 fusion to mouse serum albumin (MSA/IL-2) in combination with an anti-tumor antibody provides identical responses. In this case, while both MSA and Fc can recycle through FcRn binding, MSA itself has no immunological function.

We also show that this synergistic effect derived from this combination immunotherapy strategy is not limited to B16F10. Indeed, it is applicable to other related melanoma models that express alternative antigens, such as D5-HER2, as well as completely unrelated models such as prostate, in the case of RM9, or fibrosarcoma, in the case of Ag104A. It is notable that in the latter two cases, the antibody targeting the tumor-associated antigen was ineffective in providing any survival benefit whatsoever. Yet upon the addition of Fc/IL-2, tumor growth was strongly controlled, and in the case of Ag104A tumor-bearing mice, all the mice were completely cured.

We therefore believe that this combination therapy is likely to be efficacious in a variety of models, so long as a cognate tumor antigen-antibody is known.

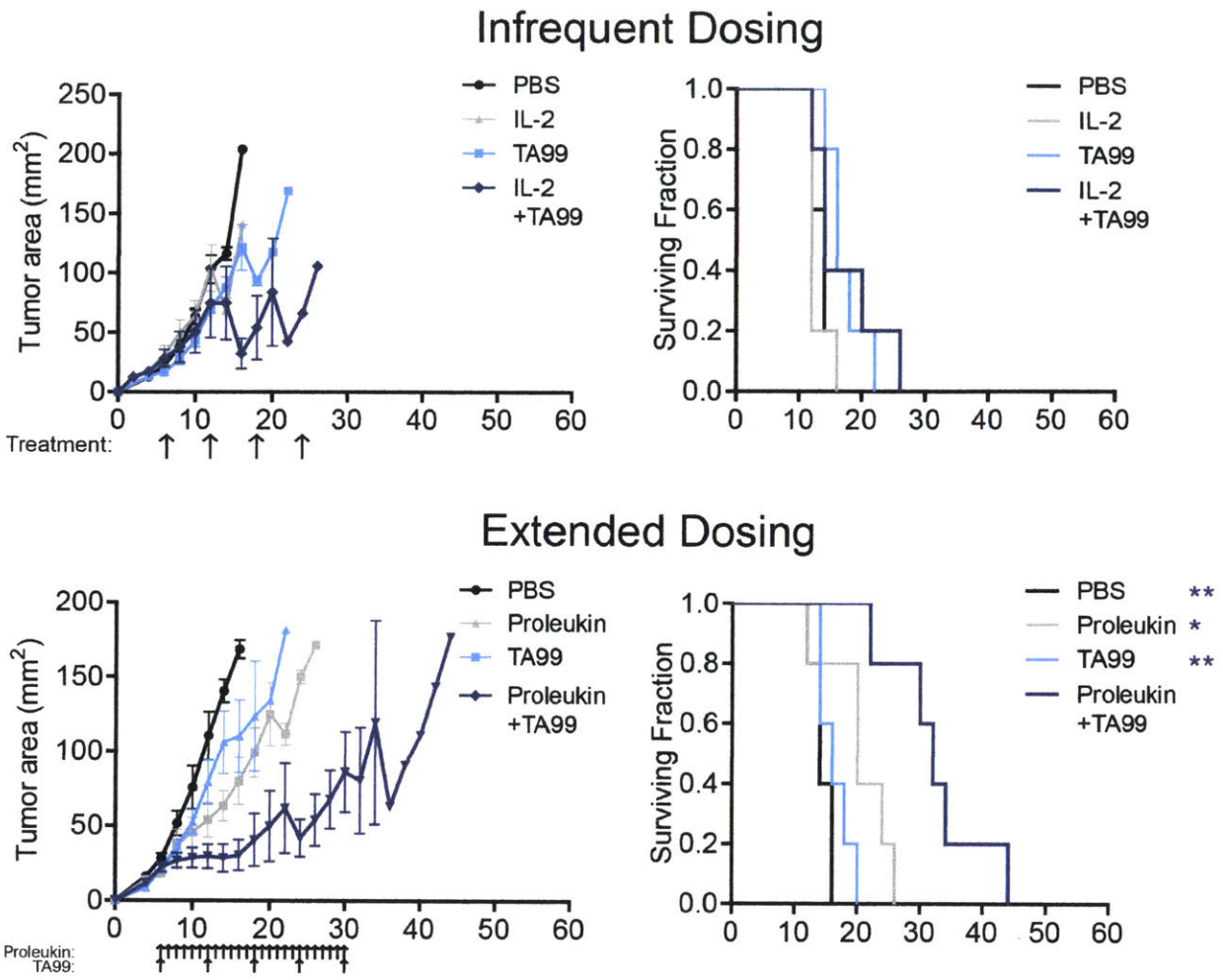

Figure 2.1 Tumor growth and survival curves of C57BL/6 mice bearing subcutaneous B16F10 tumors treated with Infrequent Dosing: PBS, murine IL-2 and/or TA99; or Extended Dosing: PBS, Proleukin and/or TA99. Arrows indicate points of treatment. n = 5 per group. *$p < 0.05$, **$p < 0.01$ v. corresponding color group in legend. Data are mean ± SEM.

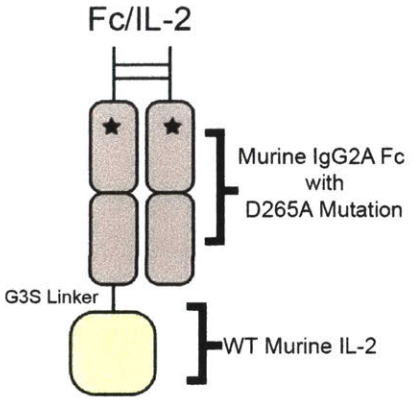

Figure 2.2 Schematic of Fc/IL-2. Wild-type murine IL-2 is fused to the C-terminus of a murine IgG2a Fc fragment containing a D265A mutation (indicated by asterisks), where the protein fusion is monomeric with respect to IL-2.

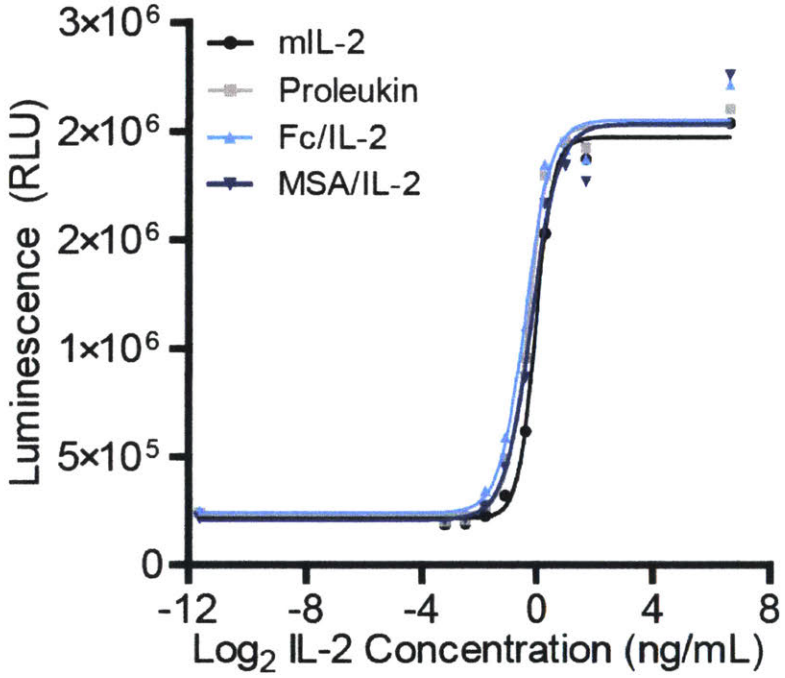

Figure 2.3 CTLL-2 cells were cultured in media with murine IL-2 produced in *E. coli* (mIL-2), human IL-2 produced in *E.* coli (Proleukin), Fc/IL-2 or MSA/IL-2, both produced in HEK cells, at the indicated concentrations on an IL-2 basis. Proliferation analyzed by CellTiter-Glo Luminescent Cell Viability Assay. n = 3 per group.

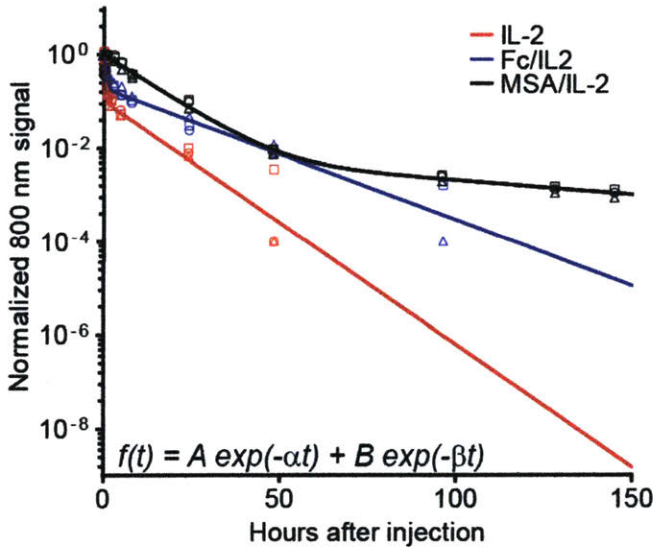

Figure 2.4 Normalized 800 nm signal of blood samples taken at various time points from mice injected retro-orbitally with 25 μg of IL-2 or 50 μg of Fc/IL-2 or MSA/IL-2 labeled with IRDye 800CW. Mean fluorescence intensity data were fit to a bi-phasic exponential decay. See Table 2.1 for fitted parameter values. n = 3 per group.

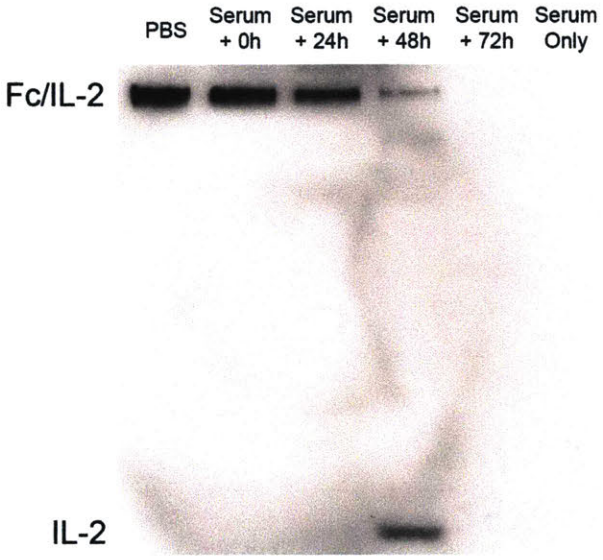

Figure 2.5 Equal amounts of Fc/IL-2 were incubated in serum isolated from C57BL/6 mice at 37 °C for the indicated time. A western blot against IL-2 was performed to detect Fc/IL-2 and any degradation products in these samples, compared to an equal amount of Fc/IL-2 from the stock solution in PBS, as well as serum alone. Representative blot is shown.

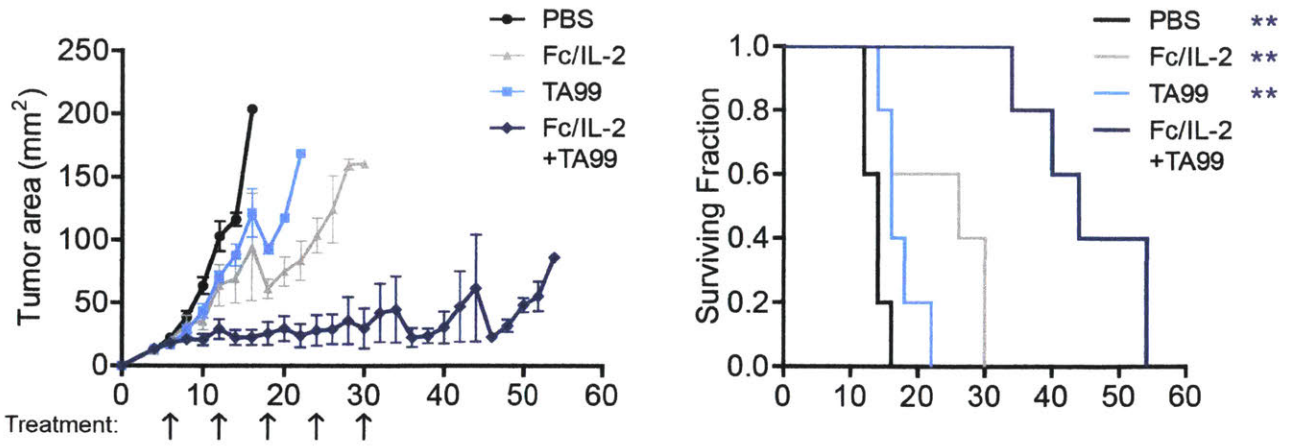

Figure 2.6 Tumor growth and survival curves of C57BL/6 mice bearing subcutaneous B16F10 tumors treated with PBS, Fc/IL-2 and/or TA99. Arrows indicate points of treatment. n = 5 per group. **p < 0.01 v. corresponding color group in legend. Data are mean ± SEM.

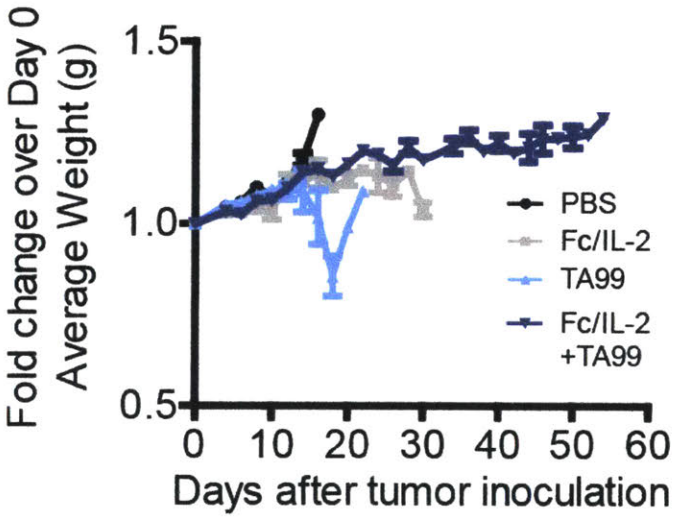

Figure 2.7 Weight progression of C57BL/6 mice bearing B16F10 tumors during the course of treatment with PBS, Fc/IL-2 and/or TA99. n = 5 per group. Data are mean ± SEM.

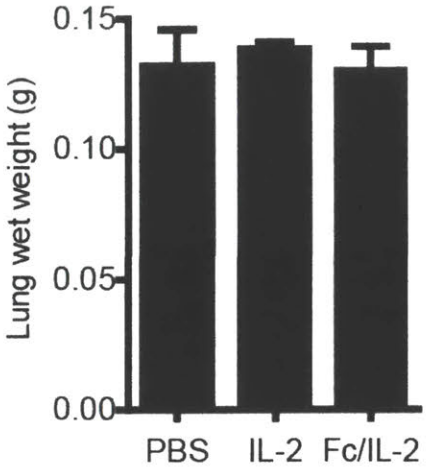

Figure 2.8 C57BL/6 mice were injected i.v. with a single bolus of PBS, 12 μg IL-2, or 50 μg Fc/IL-2. 4 days after injection, lung weight was determined by lyophilization. n = 3 per group. Data are mean ± SEM.

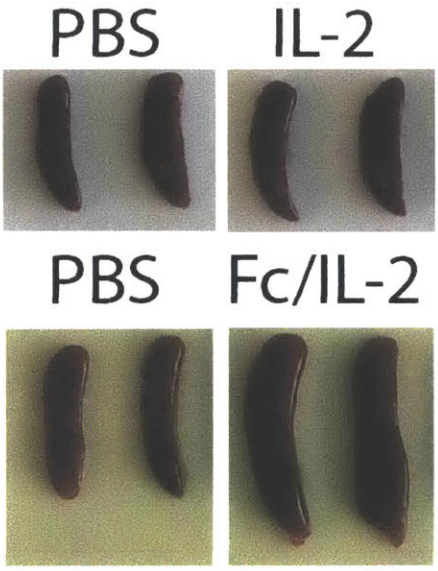

Figure 2.9 C57BL/6 mice were injected i.v. with a single bolus of PBS, 12 μg IL-2, or 50 μg Fc/IL-2. 4 days after injection, spleens were extracted and photographed. 2 representative spleens are shown.

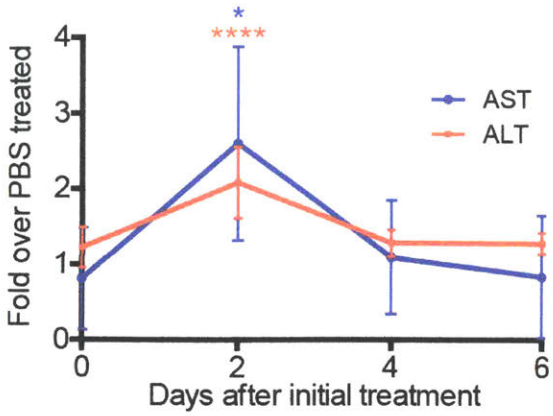

Figure 2.10 C57BL/6 mice bearing B16F10 tumors were injected i.v. with a single bolus of PBS or Fc/IL-2+TA99. At the indicated time points, blood was drawn, serum isolated, and activity of liver enzymes AST and ALT was assayed. n = 3 per group. Data are mean ± SEM.

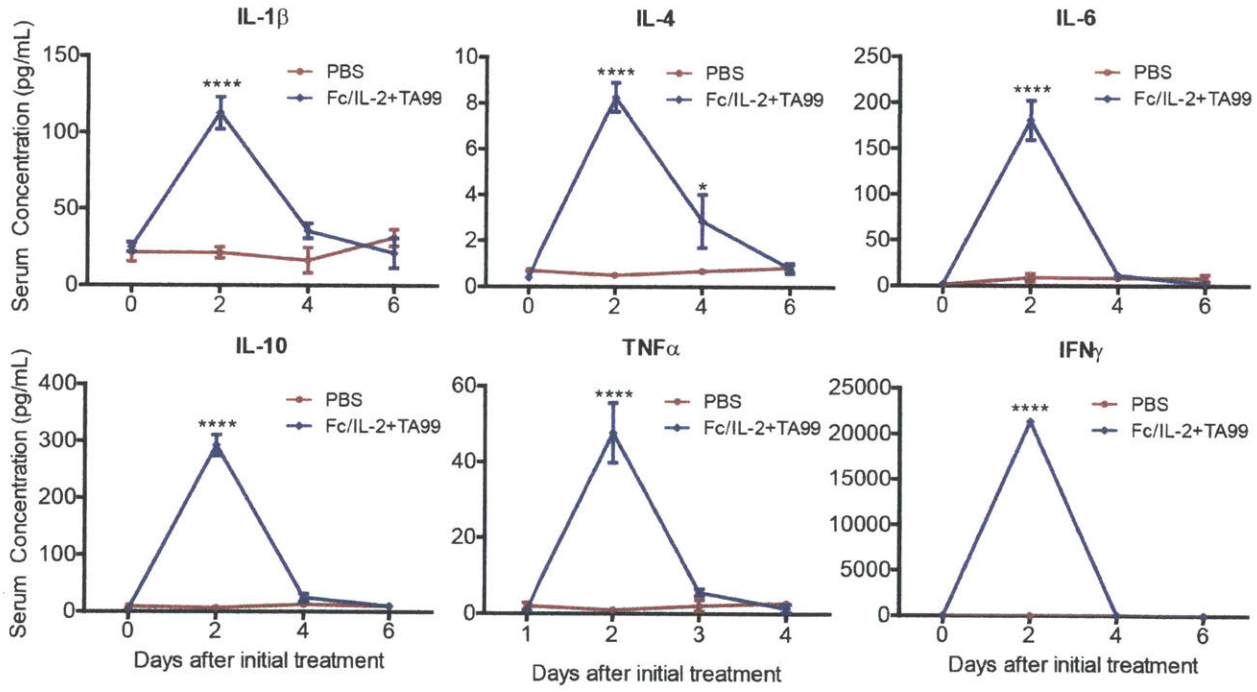

Figure 2.11 C57BL/6 mice bearing B16F10 tumors were injected i.v. with a single bolus of PBS or Fc/IL-2+TA99. At the indicated time points, blood was drawn, serum isolated, and the serum concentration of various inflammatory cytokines was assayed. n = 3 per group. Data are mean ± SEM.

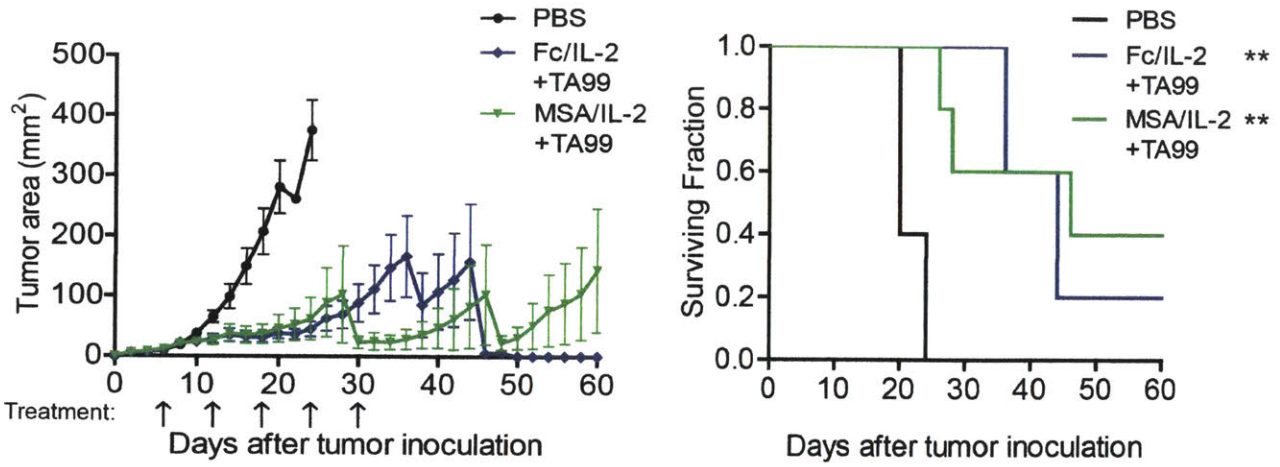

Figure 2.12 Tumor growth and survival curves of C57BL/6 mice bearing subcutaneous B16F10 tumors treated with PBS, Fc/IL-2+TA99, or MSA/IL-2+TA99. Arrows indicate points of treatment. n = 5 per group. **$p < 0.01$ v. corresponding color group in legend. Data are mean $\pm$ SEM.

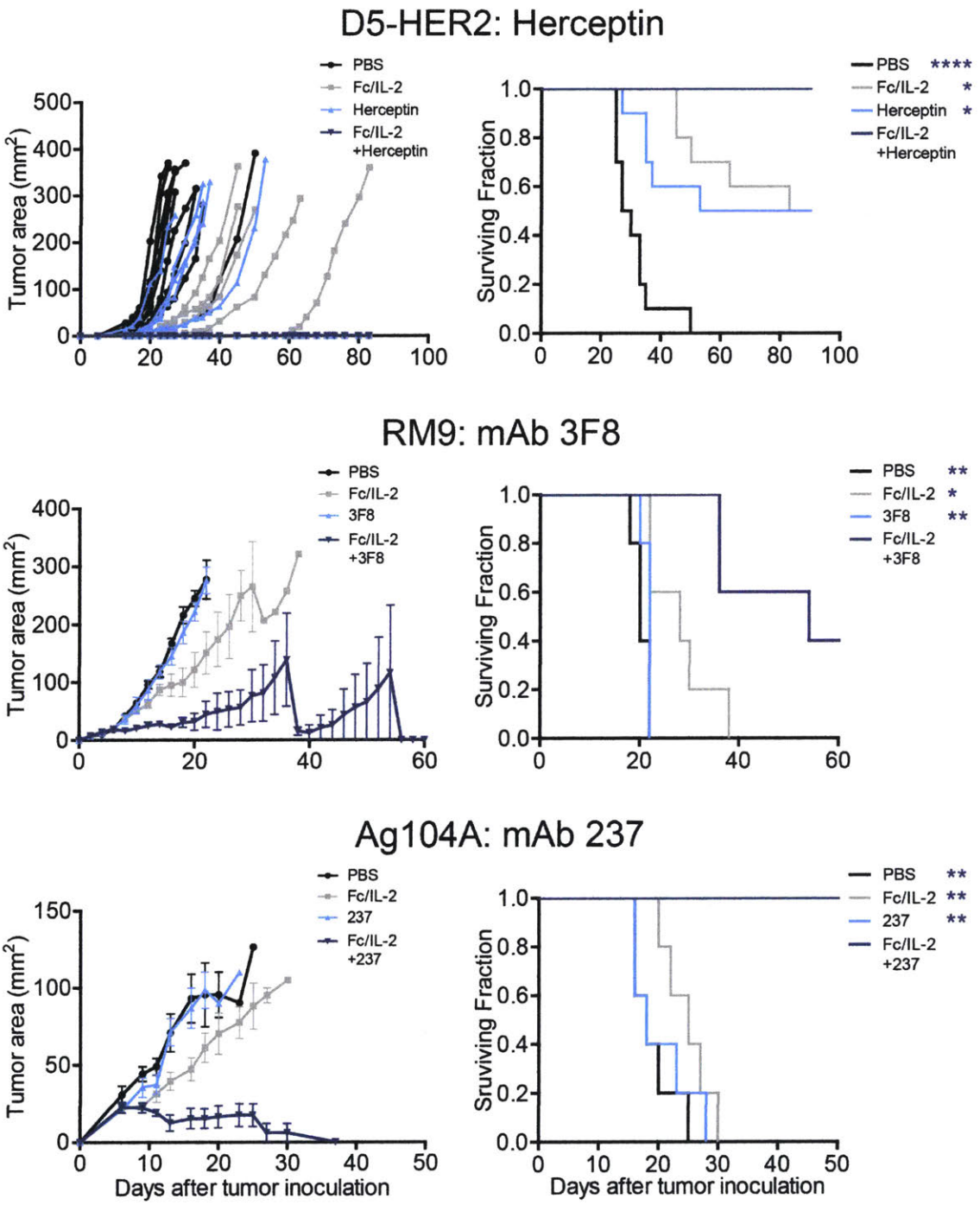

Figure 2.13 Tumor growth and survival curves of 1) hmHER2 Tg mice bearing subcutaneous D5-HER2 tumors treated with PBS, Fc/IL-2 and/or Herceptin. n = 10 per group. 2) C57BL/6 mice bearing subcutaneous RM9 tumors treated with PBS, Fc/IL-2 and/or 3F8 mAb. n = 5 per group. 3) C3H mice bearing subcutaneous Ag104A tumors treated with PBS, Fc/IL-2 and/or 237 mAb. n = 5 per group. *$p < 0.05$, **$p < 0.01$, ****$p < 0.0001$ v. corresponding color group in legend. Data are mean $\pm$ SEM.

Table 2.1: Pharmacokinetics parameters of IL-2, Fc/IL-2, and MSA/IL-2 administered as single *i.v.* bolus.

	A	α (hr^{-1})	B	β (hr^{-1})	$\tau_{1/2,\alpha}$ (hr)	$\tau_{1/2,\beta}$ (hr)
IL-2	0.88 ± 0.02	2.61 ± 0.25	0.12 ± 0.02	0.44 ± 0.03	$0.3 \pm 2.8\times10^{-2}$	4.8 ± 1.8
Fc/IL-2	0.86 ± 0.054	1.99 ± 0.086	0.14 ± 0.054	$0.056 \pm 8.7\times10^{-3}$	0.4 ± 0.01	12.5 ± 1.3
MSA/IL-2	$0.99 \pm 7.6\times10^{-4}$	$0.11 \pm 4.8\times10^{-3}$	$8.2\times10^{-3} \pm 7.6\times10^{-4}$	0.014 ± 0.0014	6.3 ± 0.3	49.9 ± 4.9

C57BL/6 mice were injected *i.v.* with a single bolus of 25 μg IL-2, 50 μg Fc/IL-2, or 50 μg MSA/IL-2 labeled with IRDye800 ($n = 3$). Serum levels were fit to a bi-phasic exponential decay of form: $MFI(t) = Ae^{-\alpha t} + Be^{-\beta t}$. Fast- and slow half-lives, $\tau_{1/2,\alpha}$ and $\tau_{1/2,\beta}$, were calculated as $\ln 2/\alpha$ and $\ln 2/\beta$, respectively.

3. Synergistic Innate and Adaptive Immune Response Induced by Fc/IL-2 and TA99

3.1. Introduction

The efficacy of immunotherapies is largely derived from an anti-tumor response from the immune system, although different immunotherapies can possess different mechanisms of action. For example, antibodies that target tumor antigens are thought largely to work through ADCC by the innate immune system via effectors such as macrophages, neutrophils, and NK cells (Weiner et al., 2010). IL-2 can act upon cells of both innate and adaptive immunity, but are restricted to those that possess IL-2R: NK cells and T-cells (Malek, 2008). Checkpoint blockade using anti-CTLA-4 is largely restricted to modulating the adaptive response, through a combination of depletion of tumor-associated Tregs (Selby et al., 2013) and potentiating the priming of T-cells weakly reactive against tumor antigens potentially associated with self (Leach et al., 1996). Finally, strategies such CAR T-cells focus only a monoclonal genetically engineered population of cytotoxic T-cells to confer the majority of anti-tumor effects (Leen et al., 2007).

Combination immunotherapy thus derives its benefit from the ability to draw anti-tumor responses from a wider pool of immune effectors. In our work, we have found that combining such extended serum half-life IL-2 constructs with anti-tumor antigen monoclonal antibodies creates a strong synergistic therapeutic effect that requires elements of both innate and adaptive immunity, in particular neutrophils and $CD8^+$ T-cells (Zhu et al., 2015).

Moreover, combination immunotherapy can enhance various immune responses through the enhancement of signaling through certain cytokines and chemokines. For example, neutrophils are one of the most robust effectors for an inflammatory response but are typically disregarded in tumor immunotherapy (Carlo et al., 2001). But neutrophils can still be drawn to a local site if the appropriate cytokines and chemokines are present (Homey et al., 2002). In a typical inflammatory response, release of G-CSF by an initial population of infiltrating neutrophils is observed, to both increase the PMN progenitor pool and enhance PMN effector function. This enhanced neutrophil population is then drawn to the site through a gradient of MIP-2, a neutrophil chemoattractant that is largely released by macrophages (Carlo et al., 2001; Mantovani et al., 2011; Wolpe et al., 1989). When neutrophils reach the site of insult or injury, they undergo degranulation, further releasing factors that can enhance neutrophil effector

function but also the effector function of cells from both innate and adaptive immunity (Cassatella, 1995; Kowanko and Ferrante, 1987; Mantovani et al., 2011; Müller et al., 2009).

It may be possible to induce such a cascade systemically without exogenous delivery of G-CSF and MIP-2, but the correct combination of immunotherapies must be identified. Indeed, if one could identify an immunotherapeutic agent that could induce anti-tumor neutrophil responses, this could indirectly enhance a second immunotherapeutic agent that induces an anti-tumor T-cell response. By combining these two together, a synergistic response could be achieved that would be far more efficacious than either agent alone. In this study, we explore the immunological mechanism of action involved in the synergistic anti-tumor response of combining Fc/IL-2 + TA99 in treating B16F10. This includes both identifying effector cells that are infiltrating into the tumor and the cytokines and chemokines that are involved in their function. We also hope to identify the source of synergy in any of the effectors or factors interrogated, showing further evidence that two complementary immunotherapeutic agents can be combined to induce an enhanced response over either monotherapy.

3.2. Materials and Methods

Cloning

Vectors encoding the heavy and light chains of mouse TA99 antibody were gifts of Jeffrey V. Ravetch (The Rockefeller University). The DNA sequences encoding the heavy and light chains were cloned into gWIZ (Genlantis), yielding gWIZ-TA99-HC and gWIZ-TA99-LC. A vector encoding the heavy chain of mouse IgG2a from C57BL/6 mice was a gift of Jeffrey V. Ravetch (The Rockefeller University). A D265A mutation was introduced and the DNA encoding the non-lytic D265A Fc, henceforth referred to simply as Fc, was cloned into gWIZ. For cloning of Fc/IL-2, murine IL-2 (InvivoGen) with C-terminal 6xHis tags was subsequently cloned C-terminal to the Fc, separated by a short G_3S linker, yielding gWIZ-Fc/IL-2. To enable expression of monovalent heterodimeric Fc/IL-2, a vector encoding the Fc with a C-terminal FLAG tag, gWIZ-Fc/FLAG, was also constructed using similar methods. Plasmid DNA was transformed into XL-1 Blue (Agilent) for amplification and purified using EndoFree Plasmid Maxi Kit (Qiagen).

Protein Production

TA99 and Fc/IL-2 fusion proteins were produced using HEK293 cells (Life Technologies) according to manufacturer's instructions. HEK293 cells were transfected with gWIZ-TA99-HC and gWIZ-TA99-LC; or gWIZ-Fc/IL-2 and gWIZ-Fc/FLAG; for TA99 or Fc/IL-2, respectively, using polyethylenimine in FreeStyle 293 media supplemented with OptiPro (Life Technologies). TA99 was purified by Protein A Agarose (Genscript), Fc/IL-2 was purified by TALON Metal Affinity Resin (Clontech) and followed by anti-FLAG M2 Affinity Gel (Sigma-Aldrich). All in-house produced protein were ensured to contain minimal levels of endotoxin (< 0.1 total EU/injection within 1 hour) using the QCL-1000 assay (Lonza).

Mice

C57BL/6NTac mice (Taconic) were aged between 6-10 weeks of age before tumor induction. All animal work was conducted under the approval of the MIT Division of Comparative Medicine, in accordance with federal, state, and local guidelines.

Tumor Cells

B16F10 cells (ATCC) were maintained in DMEM, supplemented with fetal bovine serum, L-alanyl-L-glutamine, and penicillin-streptomycin, all purchased from Life Technologies.

Tumor Inoculation

For induction of B16F10 tumors, 10^6 cells in 100 μL of PBS were injected subcutaneously into the flanks of C57BL/6 mice and allowed to establish for 6 days before treatment.

Histology, Immunohistochemistry, and Immunofluorescence

Tumor inoculation and treatment were done as previously described. For H&E staining, animals were sacrificed four days after a single dose of PBS, Fc/IL-2, TA99, or Fc/IL-2+TA99, and B16F10 tumors were fixed in 10% formalin, embedded in paraffin, and stained with hematoxylin and eosin.

Depletions

Tumor inoculation and treatment were done as previously described. All depleting or neutralizing antibodies were injected i.p., as indicated until the end of Fc/IL-2+TA99 treatment. Anti-CD8α (clone 2.43), anti-NK1.1 (clone PK136), and anti-Ly-6G (clone 1A8) were injected at a dose of 400 μg per antibody, 4 days after tumor inoculation and every 4 days thereafter. Anti-CSF-1R (clone AFS98) was injected at a dose of 300 μg, 4 days after tumor inoculation and every other day thereafter. All antibodies were purchased from BioXCell unless otherwise indicated.

Flow Cytometry

Tumor inoculation and treatment were done as previously described. Single cell suspensions were prepared by mechanically dissociating tumors or spleens between two frosted glass slides. Cell suspensions were passed through 70 μm filters, pelleted, resuspended in 96 well plates, and stained. Red blood cells in spleen and peripheral blood samples were lysed using RBC Lysis Buffer (Biolegend). Cells were first treated with Zombie Aqua Fixable Viability Kit (Biolegend). Cells were subsequently treated with TruStain fcX (clone 95; Biolegend) and then stained with antibodies against CD3ε (clone 145-2C11), CD8α (clone 53-6.7), CD4 (clone GK1.5), CD25 (clone 3C7), NK1.1 (clone PK136), Ly-6G (clone 1A8), CD11b (clone M1/70), F4/80 (clone BM8), Ly-6C (clone HK1.4), I-A/I-E (clone M5/114.15.12), CD206 (clone C068C2), all purchased from Biolegend unless otherwise indicated. For intracellular FoxP3 staining, samples were fixed, permeabilized, and stained with antibodies against FoxP3 (clone FJK-16s; eBioscience) or isotype control (clone eBR2a; eBioscience Samples were analyzed on a BD LSR-II flow cytometer (BD Biosciences) and data analysis was performed using FlowJo software (Tree Star).

Intratumoral Cytokine Analysis

Tumor inoculation and treatment were done as previously described. All relevant depletions were also performed as previously described. All mice were sacrificed and tumors harvested for analysis 24 hours after a single dosing of PBS, Fc/IL-2, or Fc/IL-2+TA99. Tumors were homogenized using 1.00 mm zirconium beads in 2 mL tubes (KSE Scientific) using a Mini-Beadbeater-16 (Biospec Products) in 5 volumes of PBS with Complete Protease Inhibitor Cocktail (Roche). Protein concentrations of all samples were normalized using a BCA Assay (Pierce) and snap-frozen in liquid nitrogen to allow for batch processing. Samples were evaluated in triplicate using the Mouse 32-Plex Cytokine/Chemokine Panel Luminex Assay as performed by Eve Technologies (Eve Technologies, Calgary, AB, Canada).

qPCR Analysis

Tumor inoculation and treatment were done as previously described. All relevant depletions were also performed as previously described. All mice were sacrificed and tumors harvested for analysis 24 hours after a single dosing of Fc/IL-2+TA99. Tumors were made into single cell suspensions and stained as previously described. Samples were then run on a BD FACSAria III sorter (BD Biosciences), isolating $CD11b^{+}F4/80^{+}$ macrophages, $CD11b^{+}Ly\text{-}6G^{+}$ neutrophils, or $CD3^{-}NK1.1^{+}$ NK cells. Cell lysis and RT-PCR were then performed using an Ambion Cells-to-C_t kit (Life Technologies) according to manufacturer's instructions. qPCR was performed using TaqMan probes purchased from Life Technologies for the murine genes *Cxcl2* and *B2m* as internal control, and the TaqMan Universal PCR Master Mix (Life Technologies) according to manufacturer's instructions, on a Roche Lightcycler 480 (Roche).

Statistics

Survival data were determined using a log-rank Mantel-Cox test, flow cytometry data were analyzed using a 1-way ANOVA with Tukey post-test for analyzing all possible comparisons or with Dunnett post-test for analyzing comparisons only to a specific group, and multiplex cytokine/chemokine assay data were analyzed through false discovery rate control using the Benjamini-Hochberg procedure, with $\alpha = 0.05$

3.3. Results

3.3.1. Fc/IL-2 and TA99 Promotes Effector Cell Infiltration

We hypothesized that the strong control of tumor growth observed was due to a combination of adaptive and innate immune activation localized to the tumor microenvironment. H&E staining of tumor sections from mice treated with either Fc/IL-2 or TA99 alone showed some lymphocyte infiltration restricted to the edges (Figure 3.1-II and III); however, Fc/IL-2+TA99 treatment resulted brisk lymphocyte infiltration both at the periphery (Figure 3.1-IV) and within the tumor mass (Figure 3.2), as well as widespread necrosis (Figure 3.3). Additionally, we observed instances of direct lymphocyte engagement with a tumor cell (Figure 3.2).

It has been previously reported that the presence of brisk infiltrating lymphocytes is a favorable prognostic indicator in melanoma (Clemente et al., 1996). This apt observation prompted us to further identify and quantify infiltrating effector cells using flow cytometry. The $CD3^+CD8^+$ T-cell population was significantly increased by over 10-fold with Fc/IL-2 or Fc/IL-2+TA99 (Figure 3.4). The $CD3^+CD4^+$ T-cell and $CD3^+CD4^+CD25^+FoxP3^+$ T_{reg} population were elevated with all three treatment groups (Figure 3.4). The $CD3^-NK1.1^+$ NK cell population was also increased significantly by over 5-fold with Fc/IL-2 or Fc/IL-2+TA99 (Figure 3.4). Interestingly, an increase in the $CD11b^+Ly\text{-}6C^+Ly\text{-}6G^+$ neutrophil population was unique to the combination of Fc/IL-2+TA99 (Figure 3.4), and only Fc/IL-2+TA99 showed a statistically significant difference in the $CD11b^+F4/80^+$ macrophage population relative to PBS-treated control (Figure 3.4).

3.3.2. CD8+ T-Cells, Natural Killer (NK) Cells, and Neutrophils Contribute to Efficacy

We next sought to determine the contribution of distinct effectors to therapeutic efficacy through antibody-mediated depletions. $CD8^+$ T-cell depletion, neutrophil depletion, or NK cell all attenuated therapeutic efficacy, suggesting an important role for each of these cell types in controlling tumor growth (Figure 3.5). Depletion of the tumor-resident $CD11b^+F4/80^+$ macrophage population by an anti-CSF-1R antibody had no apparent effect on the efficacy of the treatment (Figure 3.6). Nevertheless, this population might simultaneously contribute to and hinder the therapeutic effect via a mix of "M1 anti-tumor" or "M2 pro-tumor" macrophages, respectively. To briefly investigate this, we looked at the macrophage polarization through the

ratio of CD206 and MHC-II expression (Gabrilovich et al., 2012), indicative of macrophages tending towards M2 or M1 polarization, respectively. This ratio was slightly lower in Fc/IL-2+TA99 treated tumors but not statistically significant (Figure 3.7).

3.3.3. Fc/IL-2+TA99 Promotes Intratumoral Cytokine Storm

Given the extensive intratumoral immune cell infiltration with Fc/IL-2+TA99, we explored changes in intratumoral cytokine and chemokine levels induced by these infiltrating effector cells through multiplex Luminex assays. Nearly all cytokines and chemokines measured exhibited significant increases in intratumoral concentration when tumor-bearing mice were treated with Fc/IL-2+TA99 relative to PBS (Figure 3.8). The set of elevated cytokines observed in our system broadly overlaps with those seen in clinical presentation of "cytokine storm" (Suntharalingam et al., 2006; Winkler et al., 1999), indicative of a broad and strong immune activation within the tumor. The CXCR2 ligand MIP-2 (CXCL2) showed a striking increase of nearly 40-fold (Figure 4A), an observation consistent with the observed increase in neutrophil infiltration (Figure 3.8), as MIP-2 is a powerful neutrophil attractant (Wolpe et al., 1989).

We next wished to understand how the antibody TA99 was able to drastically improve the mild efficacy of Fc/IL-2 alone. Fc/IL-2 or Fc/IL-2+TA99 induced nearly equivalent intratumoral levels of many different cytokines and chemokines, but there were 8 different cytokines and chemokines that appeared to be elevated in the tumor only with Fc/IL-2+TA99 treatment (Figure 3.9; shown in blue). These included inflammatory cytokines such as IL-6, IL-1α, and IL-1β, but also neutrophil-related factors such as G-CSF and MIP-2 (Figure 3.9). These results further suggest the importance of neutrophils in the therapeutic efficacy of Fc/IL-2+TA99, and highlight that only with the two agents together is this synergistic effect achieved.

3.3.4. Intratumoral Cytokine Storm is Promoted by Various Effectors

To further understand which cells might be mediating these different cytokines, we monitored changes in intratumoral cytokine and chemokine levels when specific effector cells were depleted. $CD8^+$ T-cells, NK cells, neutrophils, and macrophages all appeared to either directly or indirectly affect the levels of various factors (Figure 3.10). Our data suggested that no single cell type was entirely responsible for the increase in any given cytokine or chemokine, but likely a complex interdependent network of cells was involved. We focused on the neutrophil-related

factors MIP-2 and G-CSF, as well as the inflammatory factor IL-6, which was the most elevated inflammatory cytokine. In the case of MIP-2, depletion of NK cells, macrophages, or neutrophils led to a sharp decrease in the intratumoral concentration of this chemokine (Figure 3.11), whereas G-CSF production seemed to be dependent on the presence of NK cells and macrophages (Figure 3.12). Finally, IL-6 appeared to be dependent on the presence of all the interrogated effector cells to various degrees (Figure 3.13).

3.3.5. NK Cells Induce Macrophage-Derived MIP-2

While MIP-2 can be produced by macrophages (Wolpe et al., 1989), and neutrophils can also release MIP-2 (as well as IL-6) from pre-formed granules (Lacy and Stow, 2011), it was interesting to note that depletion of NK cells also reduced intratumoral MIP-2 levels (Figure 3.11). NK cells are not known to generate MIP-2, and indeed, sorted intratumoral $CD3^{-}NK1.1^{+}$ NK cells showed little expression of *Cxcl2* as measured by qPCR (Figure 3.14). We hypothesized that NK cells may be modulating the production of MIP-2 by macrophages. When *Cxcl2* expression in intratumoral $CD11b^{+}F4/80^{+}$ macrophages was quantified, we observed a significant upregulation of the gene when treating with Fc/IL-2+TA99 (Figure 3.15). Furthermore, with NK cell depletion, we observed a significant downregulation of *Cxcl2* expression in these macrophages (Figure 3.15), suggesting that NK cells influence macrophage production of MIP-2, but solely upon Fc/IL-2+TA99 treatment.

3.4 Discussion

We demonstrate that the efficacy derived from the combination of Fc/IL-2 and TA99 is indeed a synergistic anti-tumor immune response, characterized by the infiltration and likely anti-tumor function of a variety of effectors, as well as the induction of an intratumoral cytokine storm. In particular, the chemokine MIP-2 showed an interesting dependence on a network of cells involving macrophages, NK cells, and neutrophils.

In this model, we find that any type of IL-2 administration results in the infiltration of effectors that respond to IL-2, such as $CD8^+$ T-cells and NK cells. Although a concern with IL-2 administration could be the expansion of the intratumoral T_{reg} population, we find that this does not dramatically affect the efficacy of our therapy. Indeed, despite the unchanged $CD8/T_{reg}$ ratio, the enhanced response by the innate immune system via the anti-tumor antibody may aid in overcoming immunosuppression by T_{regs}. However, increased T_{reg} numbers may limit robust overall cures from this two-agent system.

Strikingly, although many other cell types showed infiltration with just one single agent such as Fc/IL-2, intense neutrophil infiltration was observed, but only in the combination immunotherapy case. This provides further evidence of the unique synergistic response of the two agents dosed together. Neutrophils can be polarized as both anti-tumor or pro-tumor (Fridlender et al., 2009), but further depletion studies suggested that the cumulative effect of neutrophil infiltration was anti-tumor, as depletion of neutrophils abrogated therapeutic efficacy. Other depletion studies showed that $CD8^+$ T-cells and NK cells were important effectors in anti-tumor efficacy, the former being the most important of the effectors interrogated.

By further investigating the signaling involved between these various effectors, we were surprised by the particularly high levels of intratumoral MIP-2 induced by the combination immunotherapy. The production of the neutrophil chemoattractant MIP-2 (Wolpe et al., 1989) by macrophages was also shown to be important for efficacy, despite reports that associate the human homologue IL-8 with increased cancer progression (Waugh and Wilson, 2008), potentially through the recruitment of N2 polarized neutrophils by T_{regs} or the tumors themselves (Fridlender and Albelda, 2012). However, in our system, it would appear that the combination of Fc/IL-2+TA99 induces MIP-2 release by macrophages for the purpose of recruiting neutrophils which were clearly anti-tumor in this context. In addition, many other cytokines in the

intratumoral cytokine storm induced by Fc/IL-2+TA99 are known to enhance neutrophil activity, such as TNFα and GM-CSF (Pelletier et al., 2010), or IL-1β and G-CSF (Colotta et al., 1992).

Interestingly, IL-6 was highly elevated as well, where in many cases, tumor-derived IL-6 has been associated with increased disease progression (Allavena et al., 2000; Balkwill et al., 2005; Pollard, 2004). Nevertheless, IL-6 is a pleiotropic cytokine, critical for transitioning from the innate to the adaptive response as it promotes $CD3^+$ T-cell trafficking and survival (Jones, 2005). In our immunotherapy, we observed IL-6 derivation from various effector cells including neutrophils, which would suggest that in addition to tumor killing, neutrophils may also be functioning to modulate the intratumoral T-cell response as well. Overall, there are many indications that through the administration of these two agents simultaneously, the tumor microenvironment may undergo a repolarization, such that with the presence of many inflammatory and pleiotropic cytokines and chemokines, the observed response elicited from the immune system becomes one that is anti-tumor.

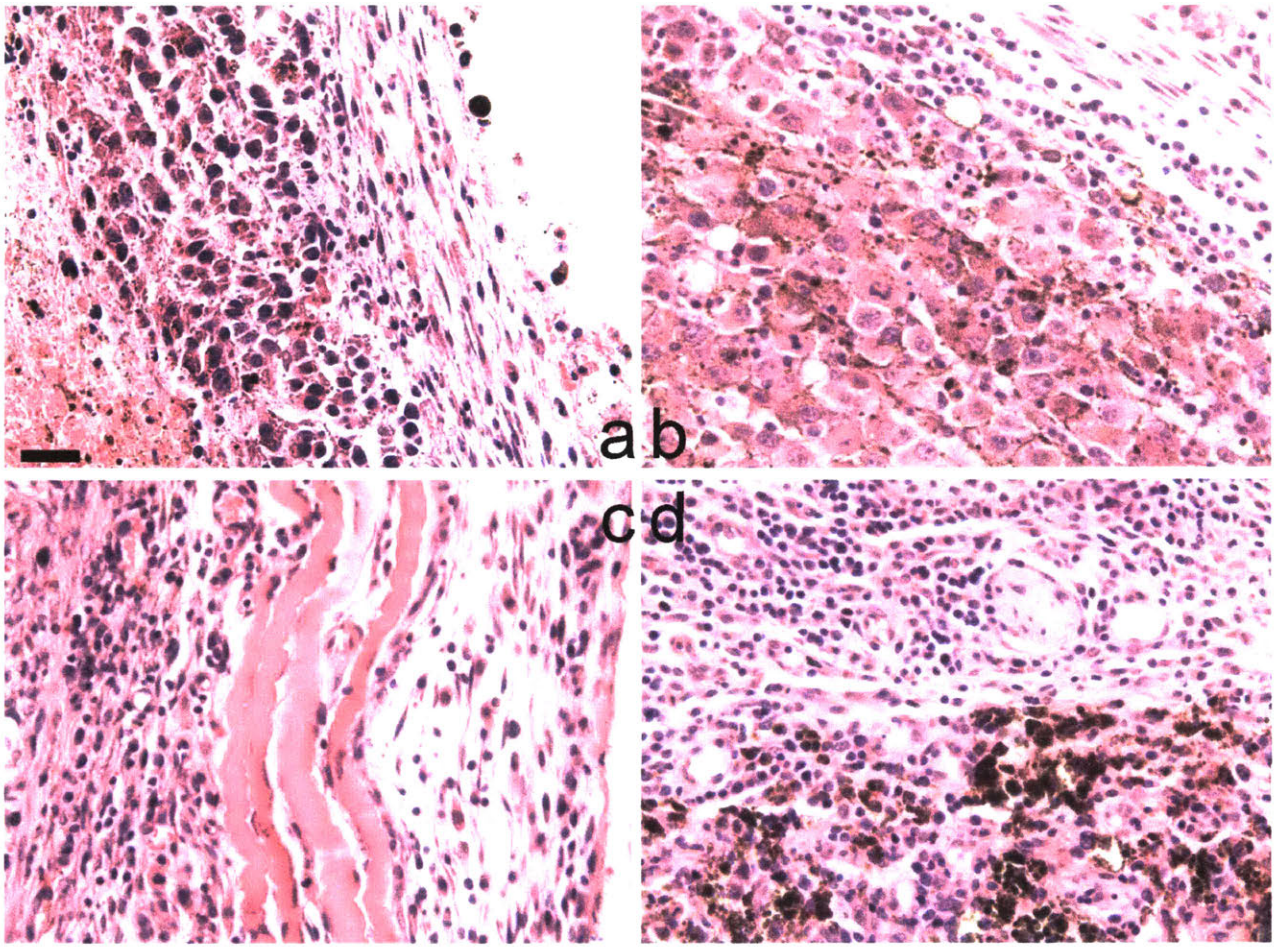

Figure 3.1 Representative images of H&E stained tumor sections. Tumor periphery of different treatment conditions: a) PBS, b) Fc/IL-2, c) TA99, d) Fc/IL-2+TA99. Magnification 40x. Scale bar 25 microns.

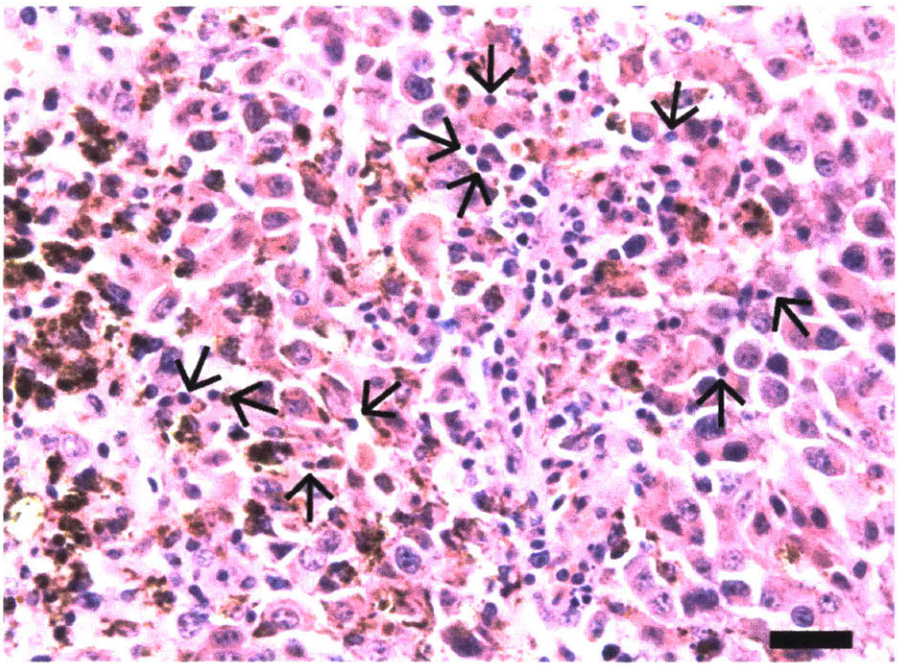

Figure 3.2 Representative images of H&E stained tumor sections. Interior of tumor treated with Fc/IL-2+TA99. Arrows indicate points of lymphocyte:tumor cell engagement. Magnification 40x. Scale bar 25 microns.

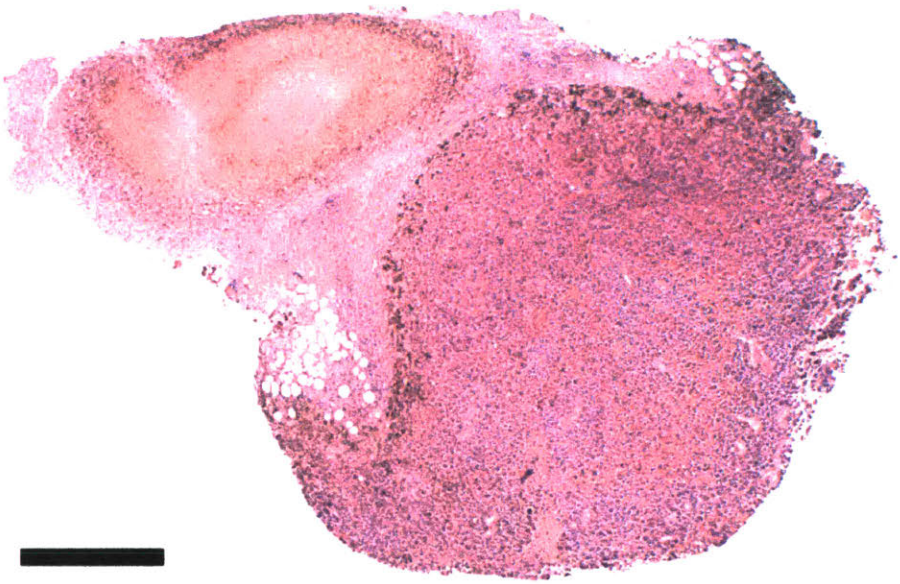

Figure 3.3 Representative image of H&E stained tumor section treated with Fc/IL-2+TA99. Entire tumor section shown. Magnification 4x. Scale bar 600 microns.

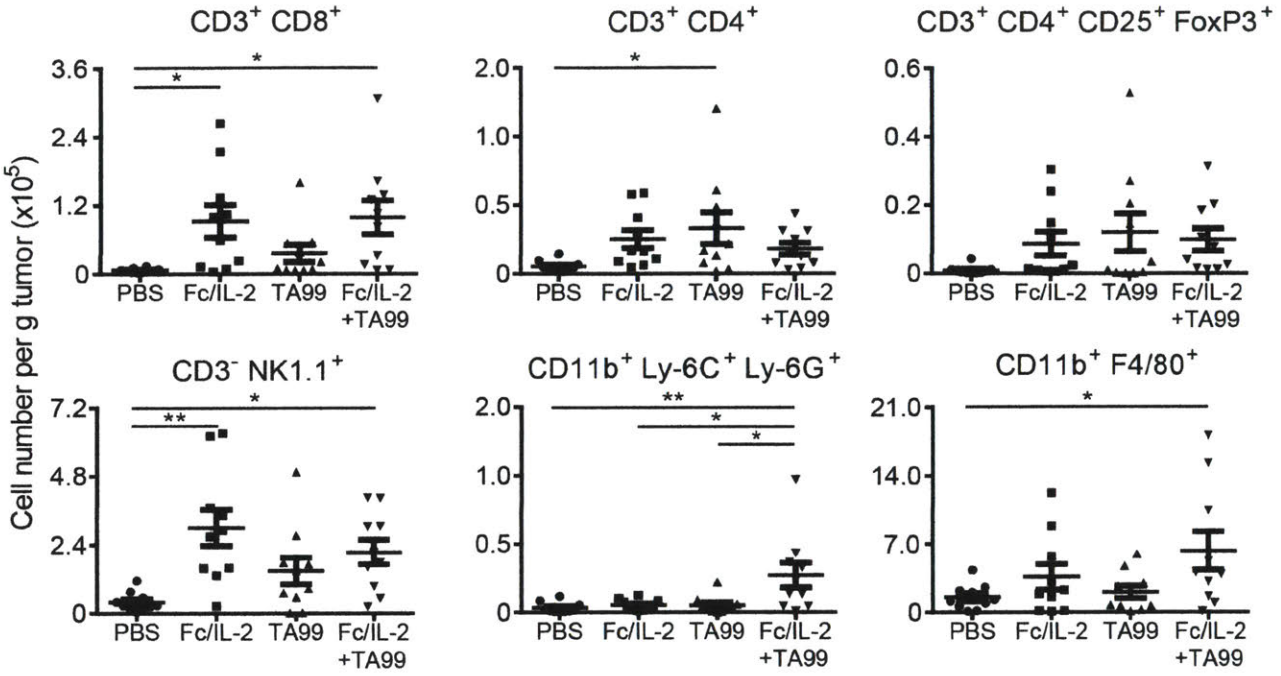

Figure 3.4 Analysis of immune cell infiltrates into treated B16F10 tumors, normalized to total tumor mass, with lineage markers as indicated. n = 10 per group. *p < 0.05, **p < 0.01 between indicated groups. Data are mean ± SEM.

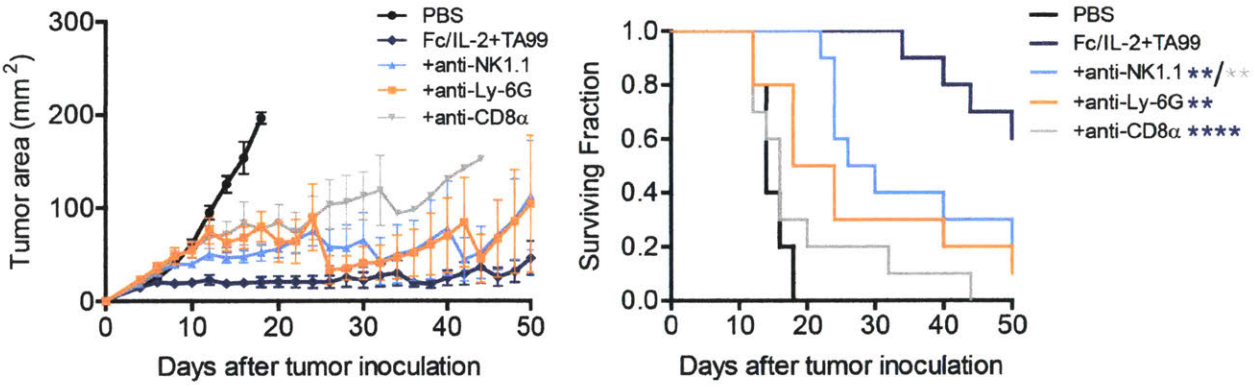

Figure 3.5 Tumor growth and survival curves of C57BL/6 mice bearing subcutaneous B16F10 tumors treated with PBS, Fc/IL-2+TA99, and with depletions as indicated. n = 10 per group. *p < 0.05, **p < 0.01 v. corresponding color group in legend. Data are mean ± SEM.

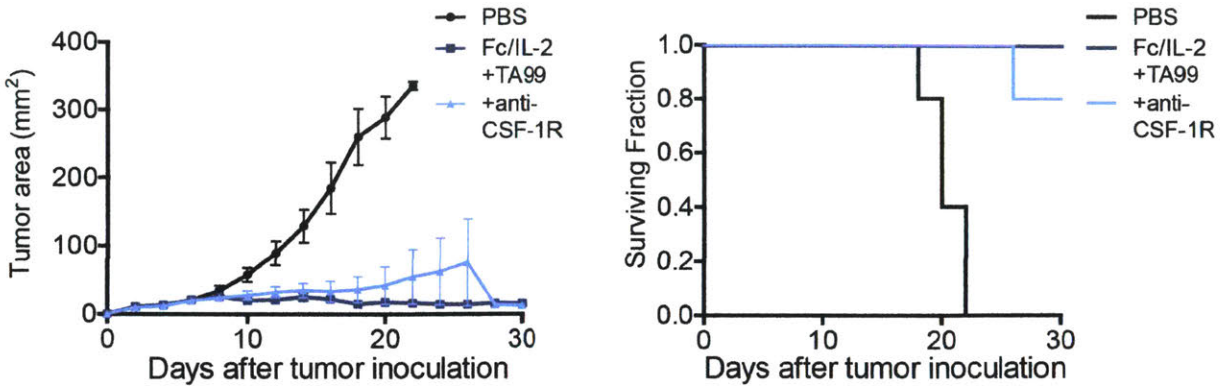

Figure 3.6 Tumor growth and survival curves of C57BL/6 mice bearing subcutaneous B16F10 tumors treated with PBS, Fc/IL-2+TA99, or Fc/IL-2+TA99 with anti-CSF-1R antibody. n = 5 per group. Data are mean ± SEM.

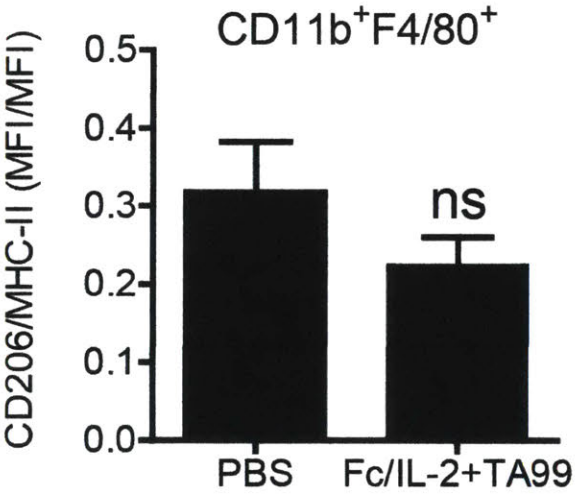

Figure 3.7 B16F10 tumors were treated once with PBS or Fc/IL-2+TA99 and harvested 3 days later to analyze the polarization of intratumoral $CD11b^{+}F4/80^{+}$ macrophages as a ratio of the MFIs of CD206 and MHC-II. ns indicates not significant. n = 3 per group. Data are mean ± SEM.

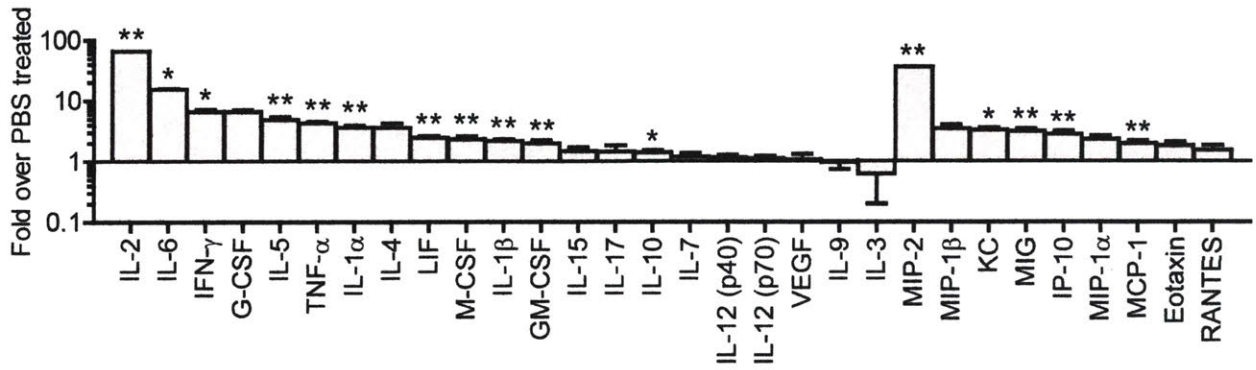

Figure 3.8 Luminex analysis of intratumoral concentrations of a panel of cytokines and chemokines in tumors treated with PBS or Fc/IL-2+TA99. *p < 0.05, **p < 0.01 v. Fc/IL-2+TA99. Data are mean ± SEM.

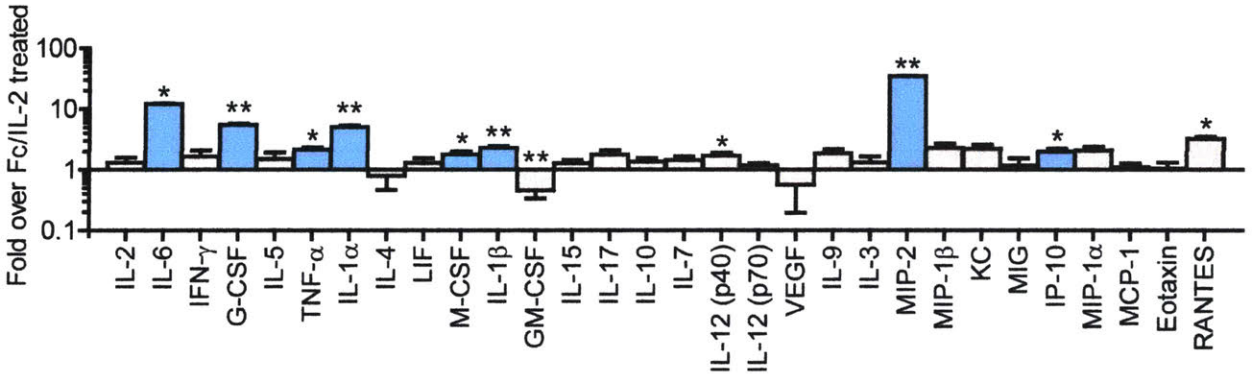

Figure 3.9 Luminex analysis of intratumoral concentrations of a panel of cytokines and chemokines in tumors treated Fc/IL-2 or Fc/IL-2+TA99. Blue bars indicate factors elevated only in Fc/IL-2+TA99 treated tumors. *p < 0.05, **p < 0.01 v. Fc/IL-2+TA99. Data are mean ± SEM.

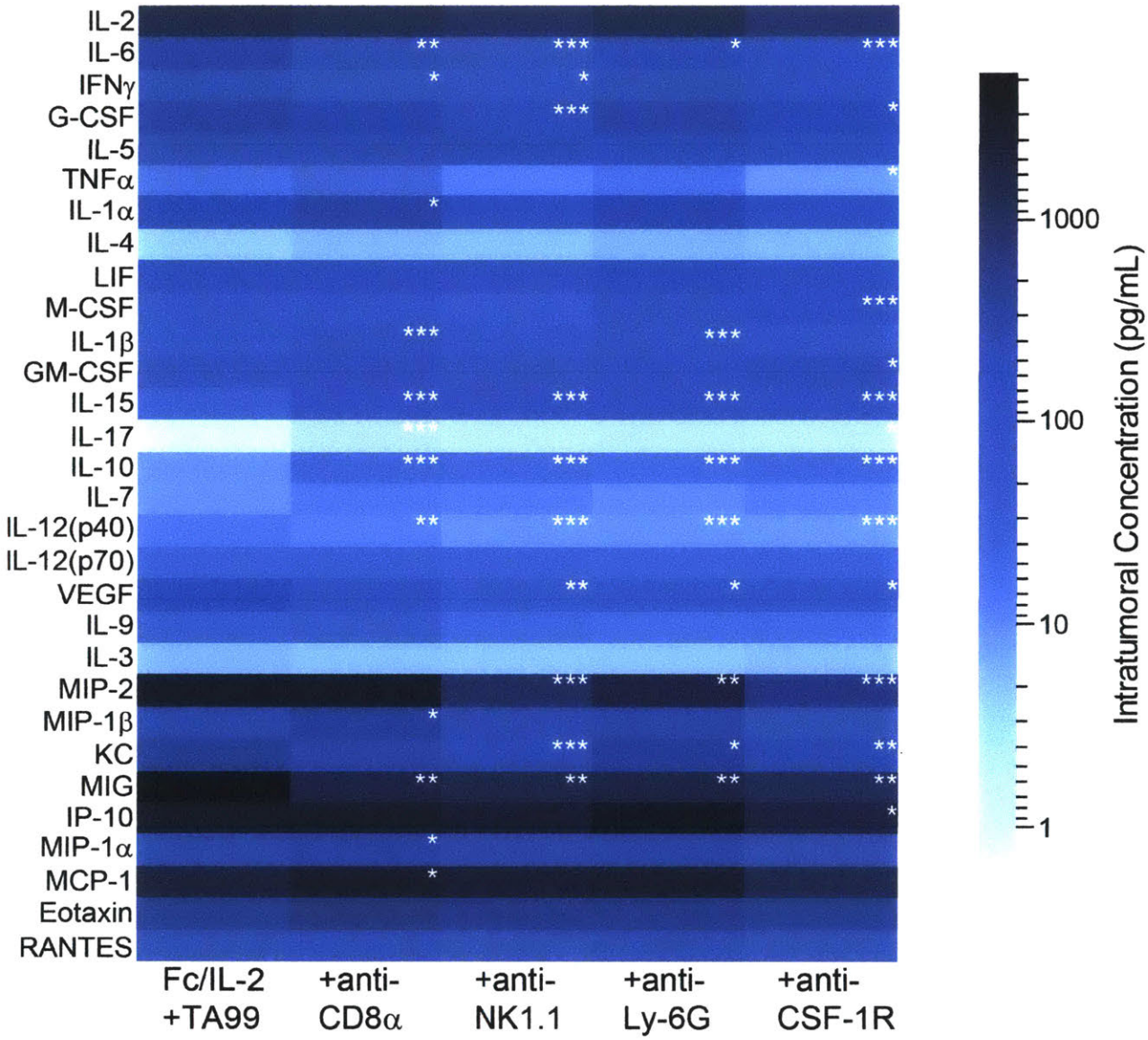

Figure 3.10 Analysis of intratumoral concentrations of a panel of cytokines and chemokines in tumors treated with Fc/IL-2+TA99 and the indicated depletions. Color bar representing intratumoral concentration is on a log scale. *$p < 0.05$, **$p < 0.01$, ***$p < 0.001$ v. Fc/IL-2+TA99. n = 10 per group.

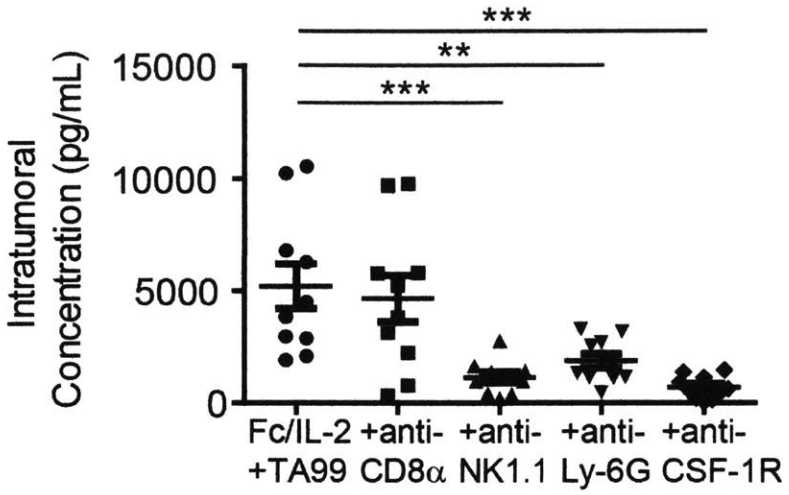

Figure 3.11 Intratumoral concentrations of MIP-2 in tumors treated with Fc/IL-2+TA99 and with depletions as indicated. n = 10 per group. *p < 0.05, **p < 0.01, ***p < 0.001 between indicated groups. Data are mean ± SEM.

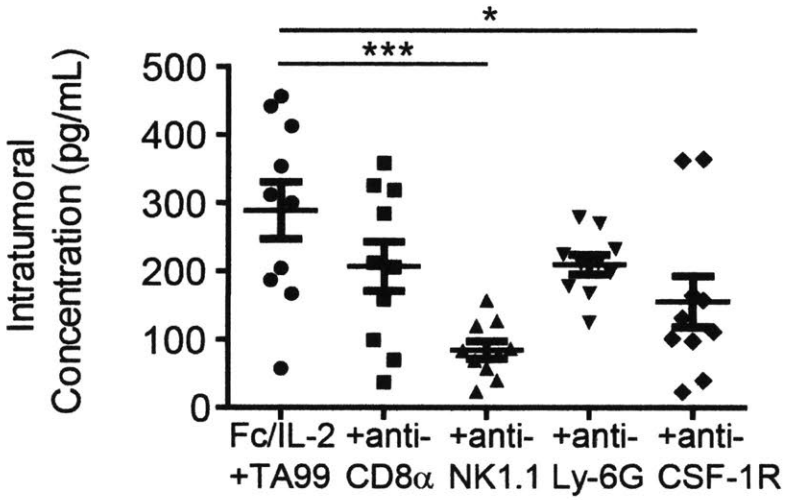

Figure 3.12 Intratumoral concentrations of G-CSF in tumors treated with Fc/IL-2+TA99 and with depletions as indicated. n = 10 per group. *p < 0.05, **p < 0.01, ***p < 0.001 between indicated groups. Data are mean ± SEM.

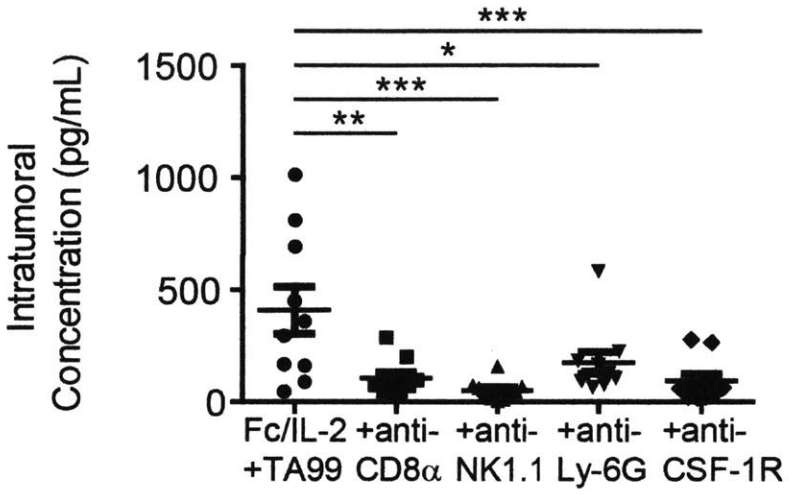

Figure 3.13 Intratumoral concentrations of IL-6 in tumors treated with Fc/IL-2+TA99 and with depletions as indicated. n = 10 per group. *p < 0.05, **p < 0.01, ***p < 0.001 between indicated groups. Data are mean ± SEM.

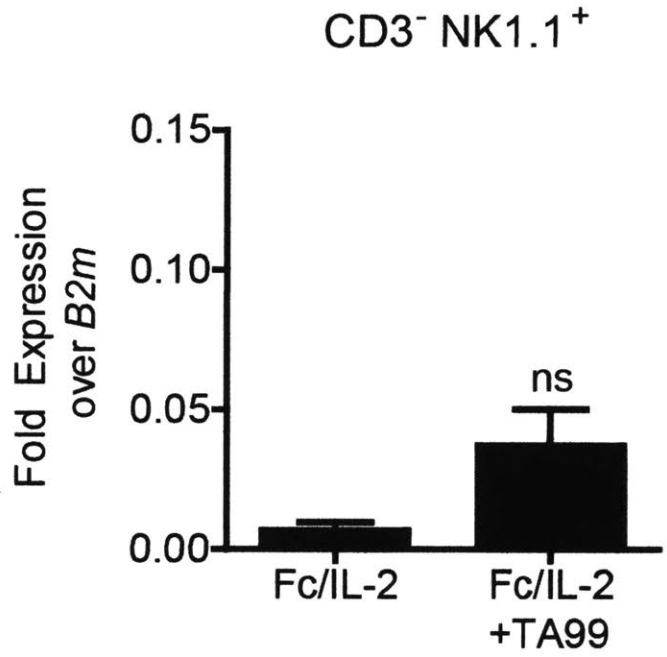

Figure 3.14 *Cxcl2* expression in $CD3^{-}NK1.1^{+}$ NK cells sorted from tumors treated with the indicated conditions, normalized to beta-2 microglobulin (*B2m*) expression. ns indicates not significant. n = 5 per group. Data are mean ± SEM.

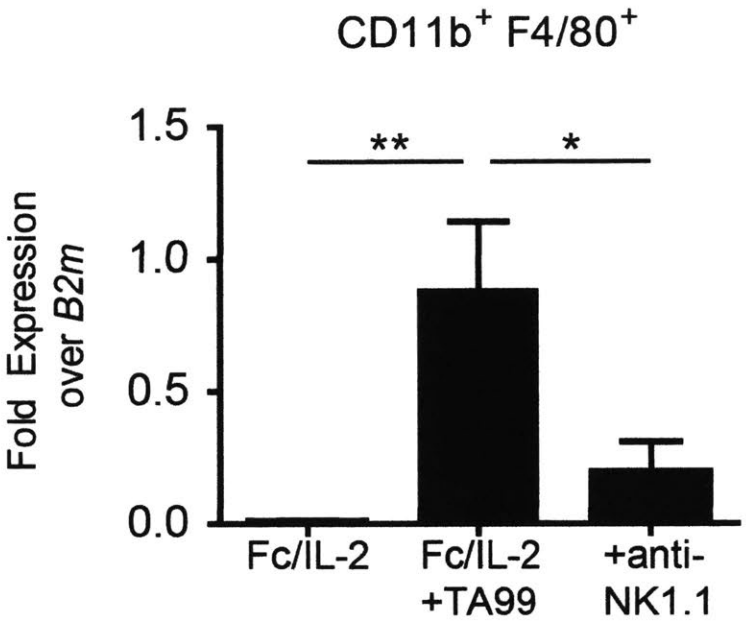

Figure 3.15 *Cxcl2* expression in $CD11b^{+}F4/80^{+}$ macrophages sorted from tumors treated with the indicated conditions, normalized to beta-2 microglobulin (*B2m*) expression. n = 5 per group. *p < 0.05, **p < 0.01, ***p < 0.001 between indicated groups. Data are mean ± SEM.

4. Overall Model of Effector Functions of Synergistic Immune Response Induced by Fc/IL-2 and TA99

4.1. Introduction

There exist many immune cells that are tumor-associated (Gajewski et al., 2013; Grivennikov et al., 2010). Although normally known for their cytotoxic function, effectors such as macrophages (Mantovani et al., 2002; Pollard, 2009; Yang et al., 2010) and neutrophils (Fridlender and Albelda, 2012; Fridlender et al., 2009; Yang et al., 2010) have been shown to infiltrate into the tumor and actually promote a pro-tumor microenvironment. The tumor can also promote the infiltration of immunosuppressive MDSCs (Gabrilovich and Nagaraj, 2009; Gabrilovich et al., 2012; Kusmartsev and Gabrilovich, 2002) and Tregs (Facciabene et al., 2012; Gajewski et al., 2006; Joshi et al., 2015; Liu et al., 2007; Whiteside, 2008). While an anti-tumor response could still in theory be mounted by a polyclonal population of cytotoxic $CD8^+$ T-cells for example, the presence of these immunosuppressive cells could render these CTLs exhausted or anergic (Gajewski et al., 2006; Lindau et al., 2013; Motz and Coukos, 2013; Rabinovich et al., 2007). Therefore, the mere presence of tumor-associated immune cells does not an anti-tumor response make.

In our previous study, we have demonstrated the elevated presence of various effectors within tumors of B16F10-bearing mice treated with a combination of Fc/IL-2 + TA99. Although we have shown indirectly that they may be performing effector functions, as depletion of various cell types causes a decrease in therapeutic efficacy, we have not directly confirmed that they are indeed performing these functions or identified which functions they are performing. Many effectors can have a wide variety of functions, and it is possible that some may be more dominant than others in a tumor setting.

Neutrophils, one of the most prominent effectors elevated in the tumor, were shown to be important for anti-tumor efficacy. However, neutrophils have a variety of functions. They are known to release various factors that can generate toxic reactive oxygen species such as myeloperoxidase (MPO) (Fang, 2004) or promote the development of the immune response by drawing in or enhancing the function of other effectors (Lacy and Stow, 2011; Mantovani et al., 2011). Of a similar vein, other PMNs such as eosinophils can also have generate reactive oxygen species through degranulation of eosinophil peroxidase, but these peroxidases act

through different mechanisms (Carretero et al., 2015; Rosenberg et al., 2013). In general though, oxidative burst is a powerful cytotoxic function that PMNs employ to perform cell-killing.

NK cells also undergo degranulation, but instead of factors that are involved in oxidative burst, factors that are directly cytotoxic such as perforin are released (Smyth et al., 2002; Vivier et al., 2008). NK cells may also release IFNγ, a factor that although is not directly cytotoxic, can enhance the function of effectors such as $CD8^+$ T-cells directly, and also indirectly through the upregulation of MHC-I on tumor cells (Ju et al., 2005; Smyth et al., 2002). $CD8^+$ T-cells also perform their cytotoxic function in a similar manner, and can also release IFNγ in some cases (Ahmadzadeh et al., 2009; Overwijk et al., 2003; Whiteside, 2014). Release of perforin from granules from either NK cells or $CD8^+$ T-cells is characterized by increased surface expression of CD107a (Betts et al., 2003). Moreover, upregulation of certain markers can be indicative of these cells' state as either activated or anergic. These include CD69 as an early activation marker on $CD8^+$ T-cells, CD25 as a mid-to-late marker of activation on $CD8^+$ T-cells, and KLRG-1 as a marker of activation on NK cells (Huntington et al., 2007; Neckers and Cossman, 1983; Schwartz, 2003). Checkpoint receptors, normally associated with a suppressed immune response, are also in fact activation markers, as they are upregulated in response to an activated state on $CD8^+$ T-cells (Keir et al., 2008; Walunas et al., 1994).

In this study, we work to confirm directly that these various infiltrating immune cells are performing anti-tumor effector function and to identify specifically which functions are in play in an anti-tumor immune response.

4.2. Materials and Methods

Cloning

Vectors encoding the heavy and light chains of mouse TA99 antibody were gifts of Jeffrey V. Ravetch (The Rockefeller University). The DNA sequences encoding the heavy and light chains were cloned into gWIZ (Genlantis), yielding gWIZ-TA99-HC and gWIZ-TA99-LC. A vector encoding the heavy chain of mouse IgG2a from C57BL/6 mice was a gift of Jeffrey V. Ravetch (The Rockefeller University). A D265A mutation was introduced and the DNA encoding the non-lytic D265A Fc, henceforth referred to simply as Fc, was cloned into gWIZ. For cloning of Fc/IL-2, murine IL-2 (InvivoGen) with C-terminal 6xHis tags was subsequently cloned C-terminal to the Fc, separated by a short G_3S linker, yielding gWIZ-Fc/IL-2. To enable expression of monovalent heterodimeric Fc/IL-2, a vector encoding the Fc with a C-terminal FLAG tag, gWIZ-Fc/FLAG, was also constructed using similar methods. Plasmid DNA was transformed into XL-1 Blue (Agilent) for amplification and purified using EndoFree Plasmid Maxi Kit (Qiagen).

Protein Production

TA99 and Fc/IL-2 fusion proteins were produced using HEK293 cells (Life Technologies) according to manufacturer's instructions. HEK293 cells were transfected with gWIZ-TA99-HC and gWIZ-TA99-LC; or gWIZ-Fc/IL-2 and gWIZ-Fc/FLAG; for TA99 or Fc/IL-2, respectively, using polyethylenimine in FreeStyle 293 media supplemented with OptiPro (Life Technologies). TA99 was purified by Protein A Agarose (Genscript), Fc/IL-2 was purified by TALON Metal Affinity Resin (Clontech) and followed by anti-FLAG M2 Affinity Gel (Sigma-Aldrich). All in-house produced protein were ensured to contain minimal levels of endotoxin (< 0.1 total EU/injection within 1 hour) using the QCL-1000 assay (Lonza).

Mice

C57BL/6NTac mice (Taconic) were aged between 6-10 weeks of age before tumor induction. p47phox KO mice were aged between 6-10 weeks of age. Generation of p47phox KO mice was previously described (Jackson et al., 1995) and kindly provided by Dr. Michael Yaffe (MIT). All animal work was conducted under the approval of the MIT Division of Comparative Medicine, in accordance with federal, state, and local guidelines.

Tumor Cells

B16F10 cells (ATCC) were maintained in DMEM, supplemented with fetal bovine serum, L-alanyl-L-glutamine, and penicillin-streptomycin, all purchased from Life Technologies.

Tumor Inoculation and Treatment

For induction of B16F10 tumors, 10^6 cells in 100 μL of PBS were injected subcutaneously into the flanks of C57BL/6 mice and allowed to establish for 6 days before treatment. Retro-orbital injection of PBS, Fc/IL-2 (25 μg), and/or TA99 (100 μg) was done on day 6, 12, 18, 24, and 30 after tumor inoculation for a total of five treatments.

Depletions, Neutralizations, and Knock-out Mice

With the exception of IFNγ depletion, tumor inoculation and treatment were done as previously described. All depleting or neutralizing antibodies were injected i.p., as indicated until the end of Fc/IL-2+TA99 treatment. Anti-CD8α (clone 2.43), and anti-NK1.1 (clone PK136) were injected at a dose of 400 μg per antibody, 4 days after tumor inoculation and every 4 days thereafter. Anti-TNFα (clone XT3.11) was injected at a dose of 200 μg, 5 days after tumor inoculation and every other day thereafter. Anti-IL-5 (clone TRFK5) was injected at a dose of 1 mg, 1 day before each treatment of Fc/IL-2+TA99. Anti-MIP-2 (clone MAB452; R&D Systems) was injected at a dose of 150 μg, 5 days after tumor inoculation and every other day thereafter. To evaluate the role of IFNγ in the therapy, mice were inoculated with 10^6 B16F10 in 100 μL PBS and allowed to grow 8 days before administration of Fc/IL-2+TA99, which occurred every 6 days thereafter for a total of 5 treatments. We injected anti-IFNγ (clone XMG1.2) at a dose of 200 μg, 7 days after tumor inoculation and every other day thereafter. All antibodies were purchased from BioXCell unless otherwise indicated. Depletion of complement was achieved through the i.p. administration of cobra venom factor (CVF) from *Naja naja kouthia* (Millipore) at a dose of 30 μg, 1 day before each treatment of Fc/IL-2+TA99. In evaluating therapeutic efficacy in p47phox KO mice, B16F10 tumors were inoculated as previously described and treatment of Fc/IL-2+TA99 was initiated after tumors reached an average area of 25-30 mm^2, with subsequent treatments of Fc/IL-2+TA99 every 6 days for a total of 5 treatments.

Immunohistochemistry

For immunohistochemistry of MHC-I expression, in addition to PBS and Fc/IL-2+TA99 treatment, a cohort of mice was also injected with anti-IFN□ antibody, previously described in

conjunction with Fc/IL-2+TA99 but 5 days after tumor inoculation and every other day thereafter until euthanasia. Animals were sacrificed four days after a single dose of Fc/IL-2+TA99, and B16F10 tumors were embedded in Tissue-Tek OCT compound (Sakura Finetek USA, Inc.) and frozen in isopentane (Alfa Aesar) in liquid nitrogen. Sectioned specimens were air-dried and fixed in acetone for 20 minutes. Endogenous peroxidase activity was quenched with H_2O_2 (3% in PBS) for 15 minutes. Endogenous biotin and avidin was quenched with Avidin/Biotin Blocking Kit (Vector Labs), according to manufacturer's instruction. Samples were washed with TBST and incubated with a biotinylated anti-mouse H-2K^b/H-2D^b (clone 28-8-6; BD Pharmingen), 1:100 dilution, at 4 °C overnight. Slides were then incubated with ABC reagent from VECTASTAIN Elite ABC Kit (Vector Labs), according to manufacturer's instruction, and color development was done using VECTOR NovaRed Peroxidase Substrate Kit (Vector Labs), according to manufacturer's instruction. Slides were counterstained with hematoxylin. Images were captured with a Zeiss Axioplan II upright microscope (Zeiss).

Flow Cytometry

Tumor inoculation and treatment were done as previously described. All relevant depletions were also performed as previously described. For analysis of infiltrating cells numbers and activation markers on NK cells and CD8$^+$ T-cells, mice were sacrificed and tumors harvested for analysis after 3 days of a single dosing of indicated treatment. For analysis of degranulation and IFNγ production of NK cells and CD8$^+$ T-cells, mice were sacrificed and tumors harvested for analysis after 2 days of a single dosing of indicated treatment. For analysis of neutrophil degranulation and activation markers, mice were sacrificed and tumors harvested for analysis after 24 hours of a single dosing of indicated treatment. For confirmation of systemic depletion of an immune cell population via administration of a depleting antibody, mice were sacrificed and either the spleen, blood, or peritoneal lavage were harvested for analysis after 2 days of a single dosing of the depleting antibody, except in the case of anti-IL-5, when the spleen was harvested 2 days after two doses of the depleting antibody. Single cell suspensions were prepared by mechanically dissociating tumors or spleens between two frosted glass slides. Cell suspensions were passed through 70 μm filters, pelleted, resuspended in 96 well plates, and stained. Red blood cells in spleen and peripheral blood samples were lysed using RBC Lysis Buffer (Biolegend). Cells were first treated with Zombie Aqua Fixable Viability Kit (Biolegend). Cells were subsequently treated with TruStain fcX (clone 95; Biolegend) and then stained with

antibodies against CD3ε (clone 145-2C11), CD8α (clone 53-6.7), NK1.1 (clone PK136), Ly-6G (clone 1A8), CD11b (clone M1/70), Ly-6C (clone HK1.4), CD63 (clone H5C6), Siglec-F (clone E50-2440; BD Biosciences), CD69 (clone H1.2F3), CD71 (clone RI7217), KLRG1 (clone 2F1/KLRG1), PD-1 (29F.1A12), CTLA-4 (clone UC10-4B9), all purchased from Biolegend unless otherwise indicated. For intracellular cytokine staining and CD107a staining, samples were first incubated with 0.5 μg/mL Brefeldin A (Sigma-Aldrich) and 0.5 μg/mL Monensin (Sigma-Aldrich) for 5 hours. During this incubation, cells were simultaneously stained with antibodies against CD107a (clone 1D4B; Biolegend). Following surface staining as described above, samples were fixed, permeabilized, and stained with antibodies against IFNγ (clone XMG1.2; Biolegend) or isotype control (clone RTK2071; Biolegend). Samples were analyzed on a BD LSR-II flow cytometer (BD Biosciences) and data analysis was performed using FlowJo software (Tree Star).

Western Blot of iNOS

Tumor inoculation and treatment were done as previously described. All relevant depletions were also performed as previously described. All mice were sacrificed and tumors harvested for analysis 48 hours after a single dosing of Fc/IL-2+TA99. Tumors were homogenized using 1.00 mm zirconium beads in 2 mL tubes (KSE Scientific) using a Mini-Beadbeater-16 (Biospec Products) in 5 volumes of PBS with Complete Protease Inhibitor Cocktail (Roche). Protein concentrations of all samples were normalized using a BCA Assay (Pierce) and snap-frozen in liquid nitrogen to allow for batch processing. Protein was run on a 4-12% Bis-Tris protein gels (Life Technologies) and transferred to a nitrocellulose membrane using iBlot transfer stacks and the iBlot gel transfer device (Life Technologies), according to manufacturer's instructions. Membranes were blocked with non-fat dry milk in TBST and probed with HRP-conjugated anti-iNOS antibody (Santa Cruz Technologies) and HRP-conjugated anti-β-Actin antibody (Abcam). Detection of HRP chemiluminescence was performed using Thermo Scientific Super Signal West Dura Chemiluminescent Substrate (Fisher Scientific) and imaged using an ImageQuant LAS 4000 (GE Healthcare Life Sciences). Images were analyzed using densitometry via Image J (NIH), normalizing to β-Actin as a loading control.

Bioluminescent Imaging of Respiratory Burst *in vivo* using Luminol

Tumor inoculation, treatments, relevant depletions and neutralizations all performed as previously described. Mice were injected with luminol (Santa Cruz Biotechnologies)

resuspended in PBS at a concentration of 50 mg/mL and injected at a dosage of 200 mg/kg, i.p. and imaged with the Xenogen IVIS Imaging System 100 (Xenogen) under the following conditions: f/stop: 1; no optical filter; exposure time: 300 sec; binning: 4.

ELISPOT Assay

Tumor inoculation and treatment were done as previously described. All mice were sacrificed and tumors harvested for analysis 4 days after a single dosing of Fc/IL-2+TA99. Tumors were processed into single cell suspensions and stained as previously described. Samples were then run on a BD FACSAria III sorter (BD Biosciences), isolating $CD3^+CD8^+$ T-cells. Using a Mouse IFN-gamma ELISpot Kit (R&D Systems), following manufacturer's instructions, isolated $CD8^+$ T-cells were co-incubated with B16F10 cells that had been previously treated with 500 U/mL of IFNγ overnight and irradiated at 120 Gy on the day of the assay. Additionally, isolated $CD8^+$ T-cells, B16F10 cells, and media were analyzed individually. Spots were visualized and quantified using CTL-Immunospot S6 Macro Analyzer (C.T.L.).

Statistics

Luminol chemiluminescence data were analyzed using a 2-way ANOVA with Bonferroni post-test, survival data were determined using a log-rank Mantel-Cox test, flow cytometry data, western blot data, and ELISPOT were analyzed using a 1-way ANOVA with Tukey post-test for analyzing all possible comparisons or with Dunnett post-test for analyzing comparisons only to a specific group.

4.3. Results

4.3.1. Infiltration and Function of Neutrophils

A striking aspect of the synergy of Fc/IL-2+TA99 was the increase in the neutrophil population above all other treatment conditions (Figure 3.4). We further explored the causes of this pronounced infiltration by depleting different cell types or neutralizing different factors that may be involved in boosting neutrophil infiltration or function. Both $CD8^+$ T-cell and NK cell depletion resulted in a statistically significant drop of intratumoral neutrophils (Figure 4.1). As NK cells modulated intratumoral MIP-2 levels via macrophages (Figure 3.11 and 3.15), it follows that the absence of NK cells may impair neutrophil infiltration. Moreover, both $CD8^+$ T-cells and NK cells contributed to intratumoral IFNγ (Figure 3.10), which has been shown to play a role in neutrophil longevity (Pelletier et al., 2010). Indeed, intratumoral neutrophils also decreased when IFNγ was neutralized (Figure 4.1).

We proceeded to investigate other potential factors promoting neutrophil infiltration. C5a of the complement system is known to be a neutrophil chemoattractant (Guo and Ward, 2005) and depletion of complement via cobra venom factor (CVF) did decrease intratumoral neutrophils (Figure 4.1). Antibody-mediated neutralization of MIP-2 also led to a decrease in intratumoral neutrophils (Figure 4.1), suggesting that both of these neutrophil chemoattractants play a role in neutrophil infiltration into the tumor. Furthermore, blockade of either factor during Fc/IL-2+TA99 treatment resulted in a significant reduction in treatment efficacy (Figure 4.2).

Functionally, we found that intratumoral neutrophils appear to be releasing cytosolic vesicles and granules, given the high surface expression of CD63 and CD11b (Kuijpers et al., 1991) compared to neutrophils in the peripheral blood (Figure 4.3). Moreover, the activation state of the neutrophils was affected by IFNγ, as observed by surface expression of CD16. While neutrophil surface expression of CD32 remains unchanged under activating conditions, CD16 surface expression is drastically reduced (Huizinga et al., 1988; Kuijpers et al., 1991). This effect is observed with Fc/IL-2+TA99, as intratumoral neutrophils showed decreased surface CD16/32 compared to peripheral blood neutrophils, but neutralization of IFNγ partially reversed this trend (Figure 4.3).

Another effector function of neutrophils is the production of reactive nitrogen species via iNOS (Fang, 2004). We found that only Fc/IL-2+TA99 treatment led to an increase in iNOS, but

those levels were reduced when either neutrophils were depleted or IFNγ was neutralized, suggesting that neutrophils may be a potential but not necessarily exclusive source of iNOS, and that IFNγ is important for the induction of iNOS (Figure 4.4). Furthermore, iNOS transcription was nearly undetectable in neutrophils from peripheral blood, but was significantly increased in intratumoral neutrophils (Figure 4.5). Overall, it would appear that Fc/IL-2+TA99 led to the infiltration and activation of neutrophils, releasing factors that contribute to inflammation and tumor killing.

4.3.2 Contribution of Eosinophils and Respiratory Burst

Another well-known cytotoxic function of neutrophils is the generation of reactive species through respiratory burst (Fang, 2004) and we hypothesized that neutrophils might contribute to tumor killing via respiratory burst whose activity can be quantified from the *in vivo* injection of luminol (Gross et al., 2009). Surprisingly, both Fc/IL-2 and Fc/IL-2+TA99 treated mice exhibited increased luminescent signal over initial background measurement (Figure 4.6).

Although the respiratory burst activity appeared to also be a result of synergy, as depletion of $CD8^+$ T-cells or neutralization of IFNγ resulted in a decrease in luminol-derived chemiluminescence (Figure 4.6), it seemed unlikely that the source of respiratory burst was from neutrophils, since Fc/IL-2 alone did not result in increased neutrophil infiltration (Figure 3.4). This was confirmed upon neutrophil depletion, as the chemiluminescence signal was essentially unchanged (Figure 4.6). Instead, we identified eosinophils as a likely source of this respiratory burst given an increase in intratumoral IL-5 and $CD11b^+Siglec\text{-}F^+$ eosinophils with both Fc/IL-2 and Fc/IL-2+TA99 (Figures 4.7 and 4.8). Moreover, depletion of eosinophils via anti-IL-5 antibody reduced luminol-derived chemiluminescence as well as dimished the therapeutic efficacy of Fc/IL-2+TA99 (Figures 4.6 and 4.9).

Given the apparent importance of respiratory burst, we proceeded to investigate its contribution to the efficacy of Fc/IL-2+TA99 regardless of the cellular source. We employed p47phox KO mice, which lack the p47phox subunit necessary for NADPH oxidase (Jackson et al., 1995), leading to a lack of luminol-derived chemiluminescence (Figure 4.10). Indeed, the efficacy of the therapy was reduced in the treatment of these mice (Figure 4.11), exhibiting the importance of respiratory burst in tumor control.

4.3.3. Fc/IL-2 Promotes NK Cell and CD8$^+$ T-Cell Activation and Cytotoxic Function

While NK cells and CD8$^+$ T-cells potentiated neutrophil infiltration and function, these cells themselves were likely contributing directly to therapeutic efficacy. As Fc/IL-2 or Fc/IL-2+TA99 significantly increased intratumoral NK cells and CD8$^+$ T-cells, we proceeded to investigate how Fc/IL-2 in either case may affect their effector functions. Fc/IL-2 significantly activated intratumoral NK cells as measured through the activation marker KLRG-1 (Huntington et al., 2007) (Figure 4.12). Fc/IL-2 also activated intratumoral CD8$^+$ T-cells as measured through the activation markers CD25, CD69, and CD71 (Neckers and Cossman, 1983; Schwartz, 2003), with CD25 and CD69 being highly significant (Figures 6.13 and 6.14) while CD71 showed a weaker trend (Figure 6.15). The immune check-point receptors PD-1 and CTLA-4 are also markers for T-cell activation (Keir et al., 2008; Walunas et al., 1994), but no differences were identified 3 days after treatment (Figures 4.16 and 4.17). Thus, although Fc/IL-2 alone led to significantly increased CD8$^+$ T-cell infiltration and activation in the tumor, it was apparent that T-cells alone were insufficient to account for the strong tumor growth inhibition caused by Fc/IL-2+TA99 (Figure 2.1).

We next wanted to investigate the cytotoxic function of NK cells and CD8$^+$ T-cells. With Fc/IL-2 or Fc/IL-2+TA99, NK cells appeared to secrete IFNγ and degranulate as measured through CD107a (Betts et al., 2003), although surprisingly both treatment conditions were comparable (Figure 4.18), suggesting that the presence of an anti-tumor antibody *in vivo* does not directly affect these particular functions assayed 2 days after treatment. A similar observation was made for CD8$^+$ T-cells (Figure 4.19), although infiltrating CD8$^+$ T-cells did exhibit reactivity against B16F10 as demonstrated by ELISPOT (Figure 4.20).

Given that CD8$^+$ T-cells produced IFNγ during anti-tumor responses, it was of interest to determine the contribution of IFNγ in controlling tumor growth. Administration of anti-IFNγ antibody demonstrated an intermediate reduction in therapeutic efficacy (Figure 4.21). The previously observed increase in intratumoral TNFa (Figure 3.8) could potentially be generated by infiltrating CD8$^+$ T-cells as well, but neutralization of this cytokine did not appear to reduce the efficacy of the therapy (Figure 4.22). It has also been shown that IFNγ upregulates MHC-I expression on B16F10 (Ju et al., 2005). Similarly, in our system, we confirmed via immunohistochemistry that an IFNγ-dependent increase of MHC-I expression on B16F10 occurred when tumors were treated with Fc/IL-2+TA99 (Figure 4.23).

4.4 Discussion

The demonstrated key components of the immune response induced by our combination immunotherapy are summarized in Figure 8. We find that our model reflects many observations of critical interactions between various effectors during administration of cancer immunotherapy reported in the literature. In syngeneic tumor models, the efficacy of antibody treatments has previously been shown to be dependent on and can synergize with $CD8^+$ T-cell activity (Abès et al., 2010; Park et al., 2010; Stagg et al., 2011). Stimulation of $CD8^+$ T-cells provides not only the benefit of direct tumor killing, but also the modulation of PMNs for ADCC, such as through the release of cytokines like IFNγ known to promote neutrophil activity (Pelletier et al., 2010). Significant interaction between neutrophils and other effector cells in our own system was evident, as infiltration and activation of neutrophils was dependent on IFNγ, and by association, the cells that produce it

To date, little focus has been placed on eliciting strong neutrophil responses against tumors. Tumor-associated neutrophils are often considered as pro-tumor "N2" polarized neutrophils (Fridlender and Albelda, 2012) and the immunosuppressive granulocytic-subtype of myeloid derived suppressor cells also possess a similar phenotype (Gabrilovich et al., 2012). However, there are examples where neutrophils are required for antibody therapeutic effects in xenograft tumor control studies (Eisenbeis et al., 2003; Schneider-Merck et al., 2010; Siders et al., 2010). In fact, it seems intuitive to utilize the underappreciated neutrophil to mount an anti-tumor response given that they are the most abundant of circulating leukocytes, and in other forms of immune challenge, neutrophils are the first responders, inducing massive cell-killing. Moreover, neutrophils have been shown to release chemotactic factors to recruit other effector cells (Lillard et al., 1999) and produce cytokines which can modulate T-cells (Cassatella, 1995). While a robust T-cell response is ultimately required for tumor rejection and immunological memory, the innate arm of the immune system may provide necessary support to boost existing T-cell-focused immunotherapies. This was demonstrated when we combined the existing Fc/IL-2+TA99 with adoptive T-cell transfer (Opel, 2015; Zhu et al., 2015).

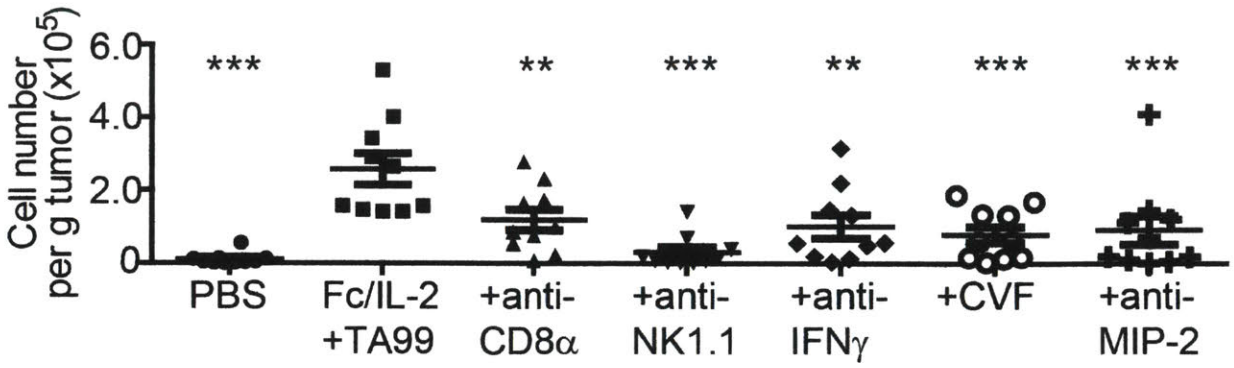

Figure 4.1 Analysis of $CD11b^{+}Ly\text{-}6C^{+}Ly\text{-}6G^{+}$ neutrophil infiltration into B16F10 tumors treated with PBS, Fc/IL-2+TA99, and with depletions/neutralizations as indicated, normalized to total tumor mass. Complement depleted by cobra venom factor (CVF). n = 10 per group. *p < 0.05, **p < 0.01, ***p < 0.001 v. Fc/IL-2+TA99. Data are mean ± SEM.

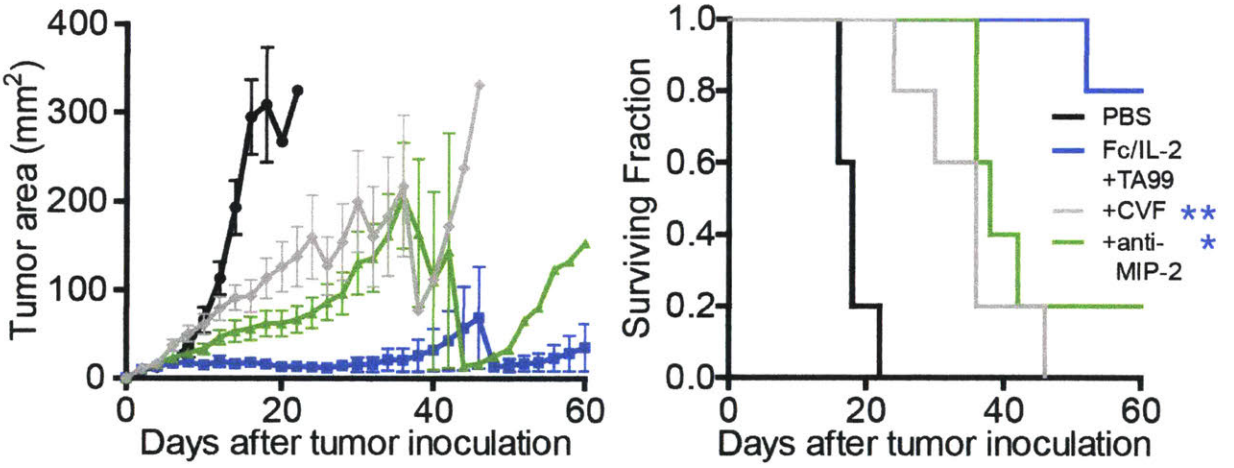

Figure 4.2 Tumor growth and survival curves of C57BL/6 mice bearing subcutaneous B16F10 tumors treated with PBS, Fc/IL-2+TA99, and with depletions/neutralizations as indicated. n = 5 per group. *p < 0.05, **p < 0.01 v. Fc/IL-2+TA99. Data are mean ± SEM.

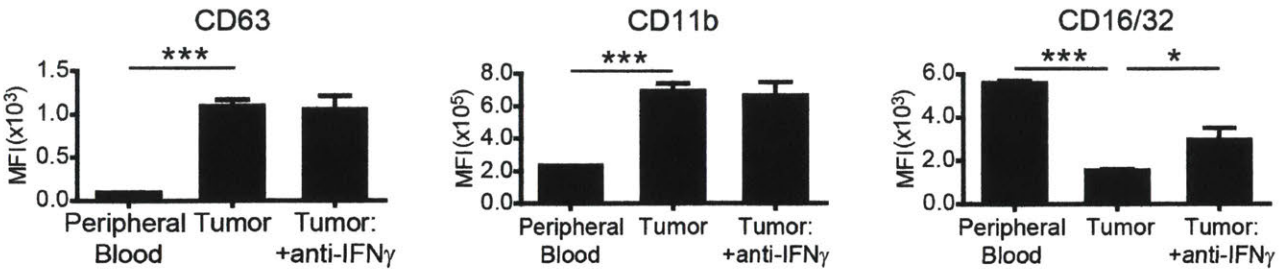

Figure 4.3 Analysis of degranulation and activation markers of neutrophils in mice treated with Fc/IL-2+TA99. n = 5 per group. *p < 0.05, ***p < 0.001 between indicated groups. Data are mean ± SEM.

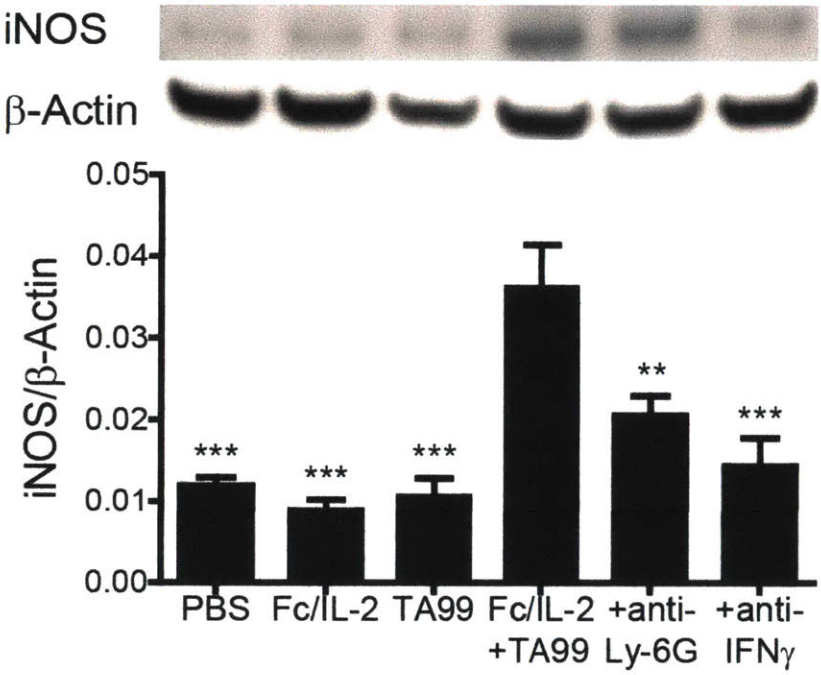

Figure 4.4 B16F10 tumors treated with the indicated conditions were assayed for iNOS as detected by western blot. β-Actin served as a loading control. Representative blot is shown. n = 5 per group. **p < 0.01, ***p < 0.001 v. Fc/IL2+TA99. Data are mean ± SEM.

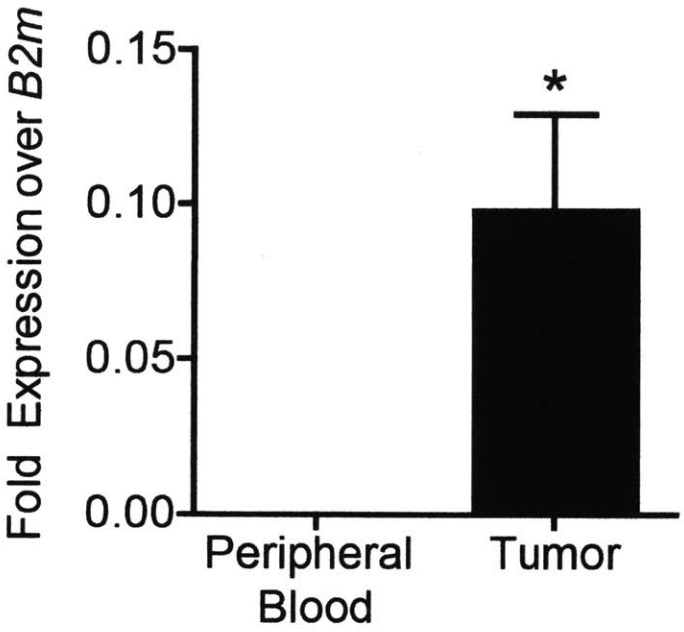

Figure 4.5 *Nos2* expression in CD11b^{+}Ly-6G^{+} neutrophils sorted from tumors or peripheral blood in mice treated with Fc/IL-2+TA99, normalized to beta-2 microglobulin (*B2m*) expression. n = 5 per group. *$p < 0.05$ v. Peripheral Blood. Data are mean $\pm$ SEM.

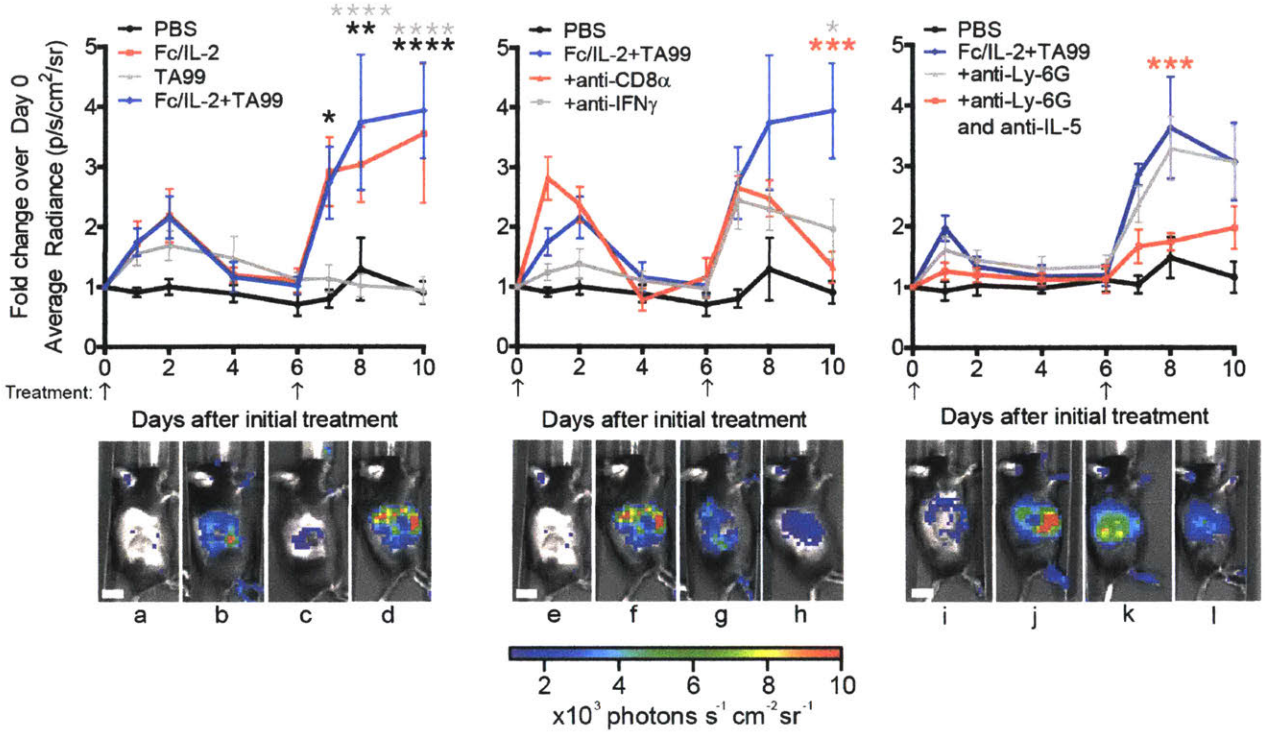

Figure 4.6 B16F10 tumors were treated with indicated treatments and depletions/neutralizations as applicable. On days of imaging, luminol was injected and average radiant luminescence was quantified. Representative images on day 8 are shown. a) PBS; b) Fc/IL-2; c) TA99; d) Fc/IL-2+TA99; e) PBS; f) Fc/IL-2+TA99; g) Fc/IL-2+TA99+anti-CD8α; h) Fc/IL-2+TA99+anti-IFNγ; i) PBS; j) Fc/IL-2+TA99; k) Fc/IL-2+TA99+anti-Ly-6G; l) Fc/IL-2+TA99+anti-Ly-6G+anti-IL-5. Arrows indicate points of treatment. n = 5 per group. *$p < 0.05$, **$p < 0.01$, ***$p < 0.001$, ****$p < 0.0001$ Fc/IL-2+TA99 v. corresponding color group in legend. Scale bar 1 cm. Data are mean ± SEM.

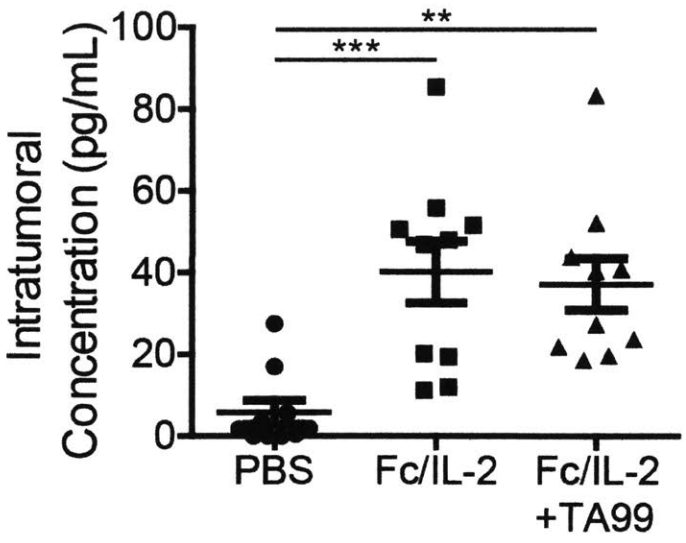

Figure 4.7 Analysis of intratumoral concentrations of IL-5 in tumors treated with PBS, Fc/IL-2, or Fc/IL-2+TA99. n = 10 per group. *p < 0.05, **p < 0.01, ***p < 0.001 between indicated groups. Data are mean ± SEM.

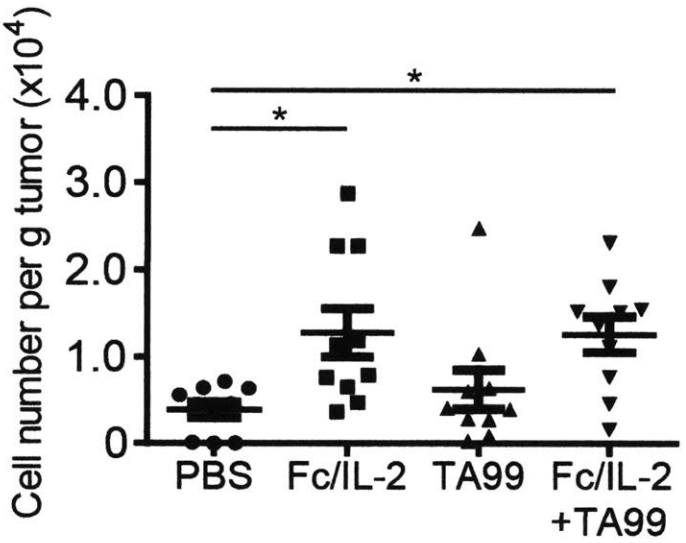

Figure 4.8 Analysis of CD11b$^+$Siglec-F$^+$ eosinophil infiltration into B16F10 tumors treated with PBS, Fc/IL-2, TA99, or Fc/IL-2+TA99, normalized to total tumor mass. n = 10 per group. *p < 0.05, **p < 0.01, ***p < 0.001 between indicated groups. Data are mean ± SEM.

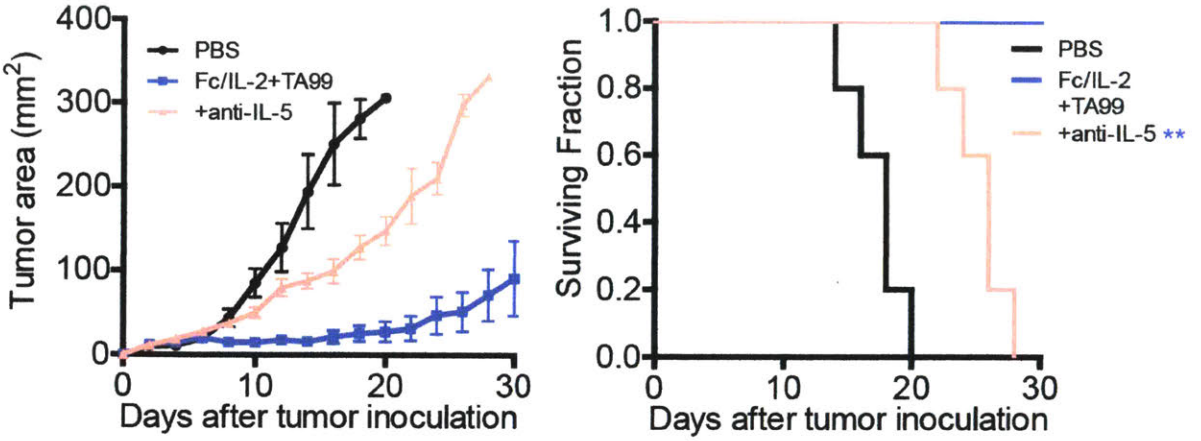

Figure 4.9 Tumor growth and survival curves of C57BL/6 mice bearing subcutaneous B16F10 tumors treated with PBS, Fc/IL-2+TA99, or Fc/IL-2+TA99 with anti-IL-5 antibody. n = 5 per group. **$p < 0.01$ v. corresponding color group as shown in legend. Data are mean $\pm$ SEM.

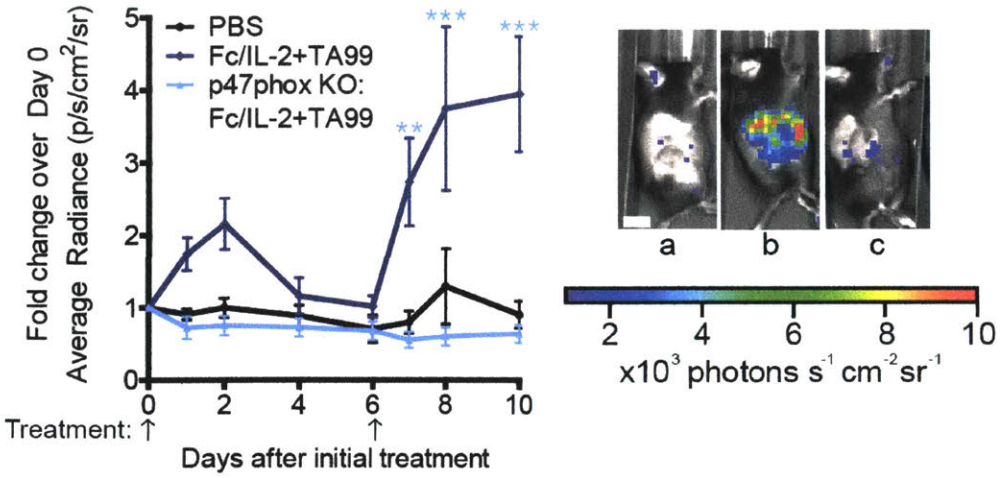

Figure 4.10 B16F10 tumors were treated with PBS or Fc/IL-2+TA99, in either WT C57BL/6 or p47phox KO mice. On days of imaging, mice were injected with 200 mg/kg of luminol in PBS and average radiant luminescence was quantified. Representative images on day 8 are shown. a) PBS; b) Fc/IL-2+TA99; c) p47phox KO: Fc/IL-2+TA99. Arrows indicate points of treatment. n = 5 per group. $^{**}p < 0.01$, $^{***}p < 0.001$ Fc/IL-2+TA99 v. p47phox KO: Fc/IL-2+TA99. Scale bar 1 cm. Data are mean $\pm$ SEM.

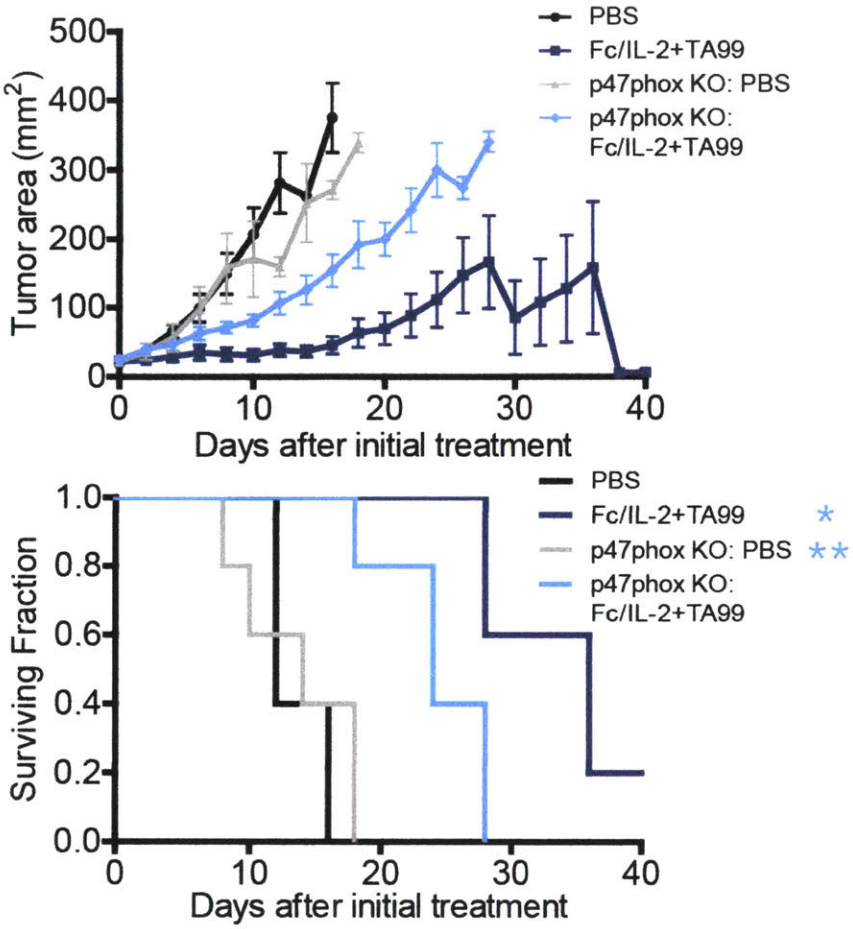

Figure 4.11 Tumor growth and survival curves of C57BL/6 mice or p47phox KO mice bearing subcutaneous B16F10 tumors treated with PBS or Fc/IL-2+TA99. n = 5 per group. *$p < 0.05$, **$p < 0.01$ v. p47phox KO: Fc/IL-2+TA99. Data are mean $\pm$ SEM.

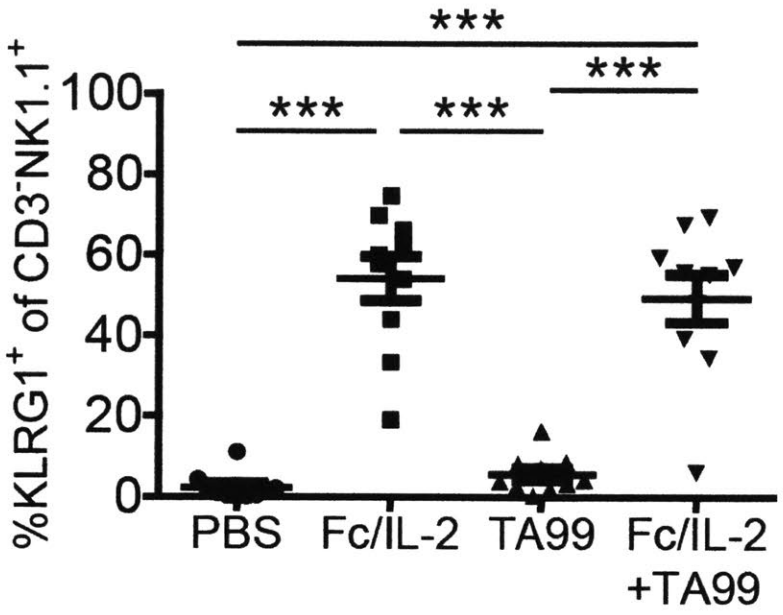

Figure 4.12 Analysis of NK cell activation marker as a percentage of the intratumoral NK cell population. $CD3^-NK1.1^+KLRG1^+$ cells. n = 10 per group. *p < 0.05, **p < 0.01, ***p < 0.001 between indicated groups. Data are mean ± SEM.

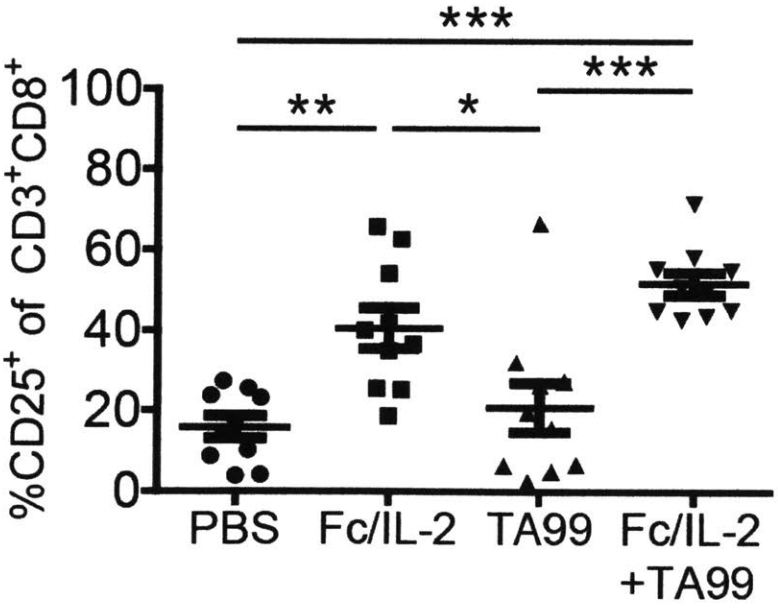

Figure 4.13 Analysis of $CD8^+$ T-cell activation markers as a percentage of the intratumoral $CD8^+$ T-cell population. $CD3^+CD8^+CD25^+$ cells. n = 10 per group. *p < 0.05, **p < 0.01, ***p < 0.001 between indicated groups. Data are mean ± SEM.

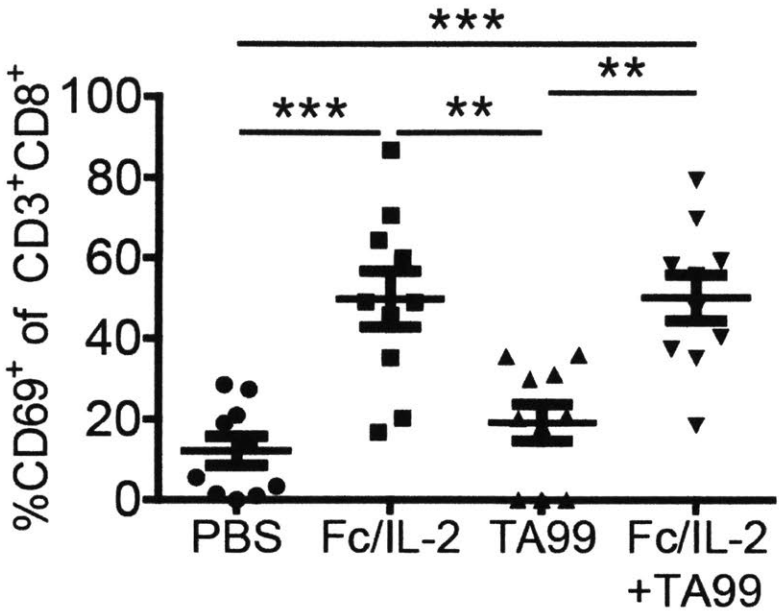

Figure 4.14 Analysis of $CD8^+$ T-cell activation markers as a percentage of the intratumoral $CD8^+$ T-cell population. $CD3^+CD8^+CD69^+$ cells. n = 10 per group. *p < 0.05, **p < 0.01, ***p < 0.001 between indicated groups. Data are mean ± SEM.

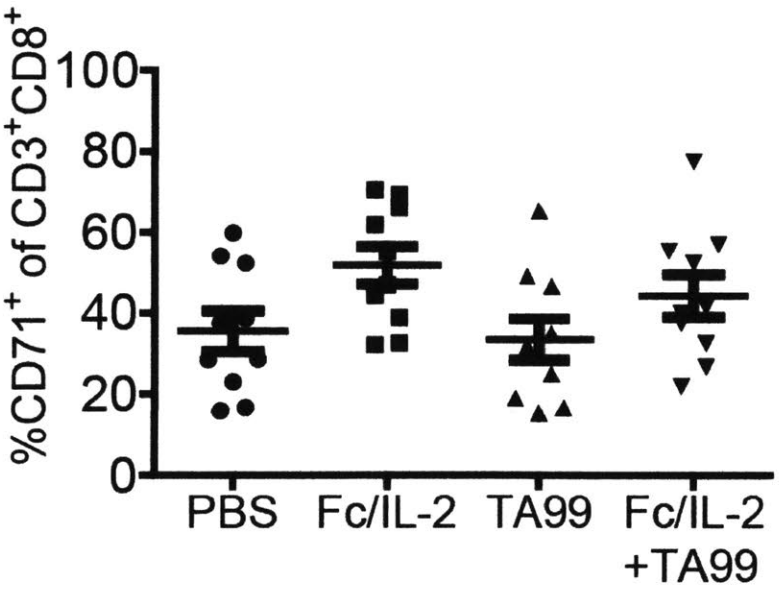

Figure 4.15 Analysis of $CD8^+$ T-cell activation markers as a percentage of the intratumoral $CD8^+$ T-cell population. $CD3^+CD8^+CD71^+$ cells. n = 10 per group. *p < 0.05, **p < 0.01, ***p < 0.001 between indicated groups. Data are mean ± SEM.

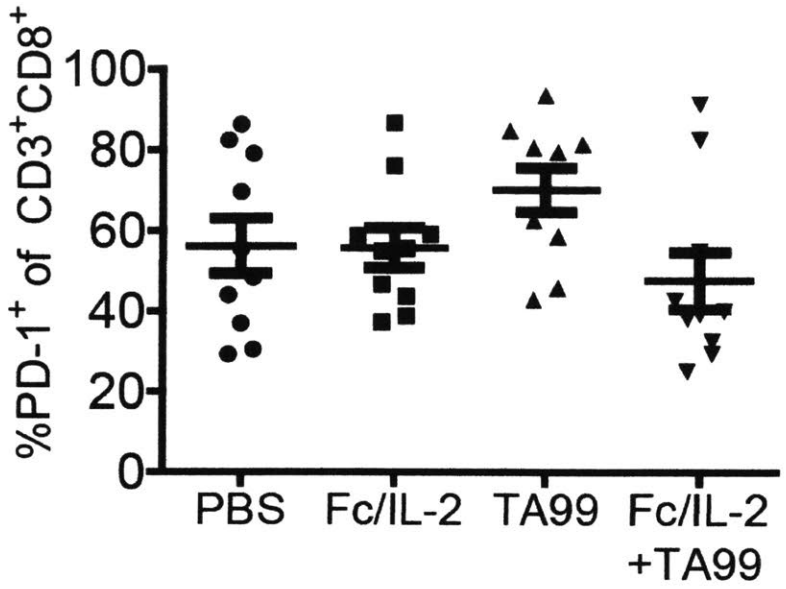

Figure 4.16 Analysis of $CD8^+$ T-cell activation markers as a percentage of the intratumoral $CD8^+$ T-cell population. $CD3^+CD8^+PD\text{-}1^+$ cells. n = 10 per group. *p < 0.05, **p < 0.01, ***p < 0.001 between indicated groups. Data are mean ± SEM.

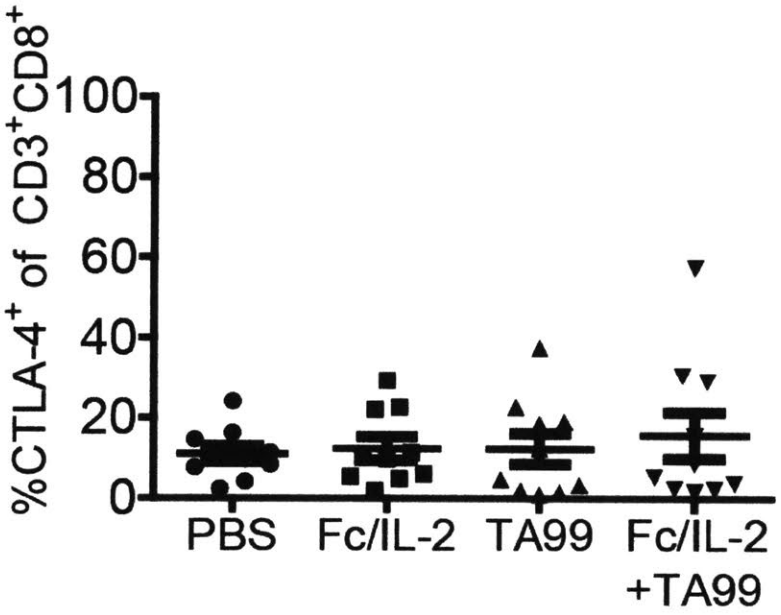

Figure 4.17 Analysis of $CD8^+$ T-cell activation markers as a percentage of the intratumoral $CD8^+$ T-cell population. $CD3^+CD8^+CTLA\text{-}4^+$ cells. n = 10 per group. *p < 0.05, **p < 0.01, ***p < 0.001 between indicated groups. Data are mean ± SEM.

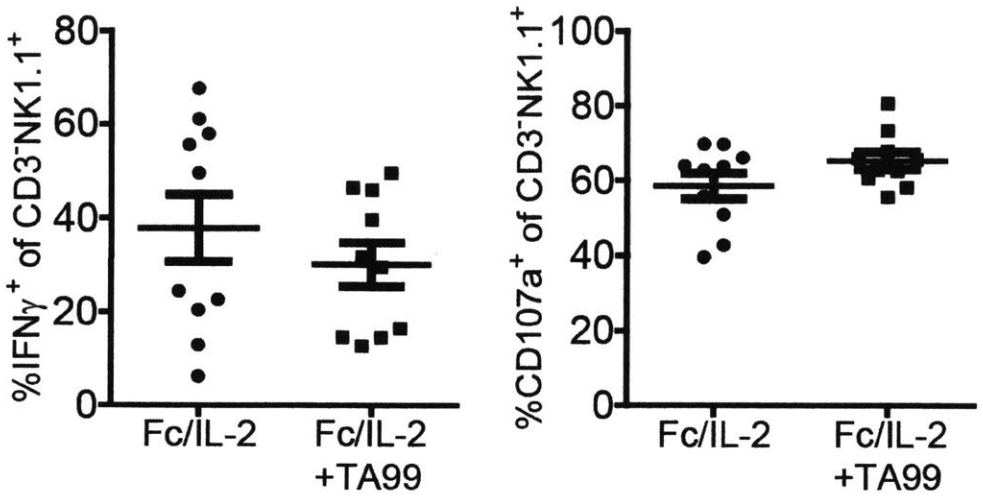

Figure 4.18 Analysis of IFNγ-producing or degranulating NK cells as a percentage of the intratumoral NK cell population. The following conditions were investigated: $CD3^-NK1.1^+IFN\gamma^+$ cells; $CD3^-NK1.1^+CD107a^+$ cells. n = 10 per group. *p < 0.05, **p < 0.01, ***p < 0.001 between indicated groups. Data are mean ± SEM.

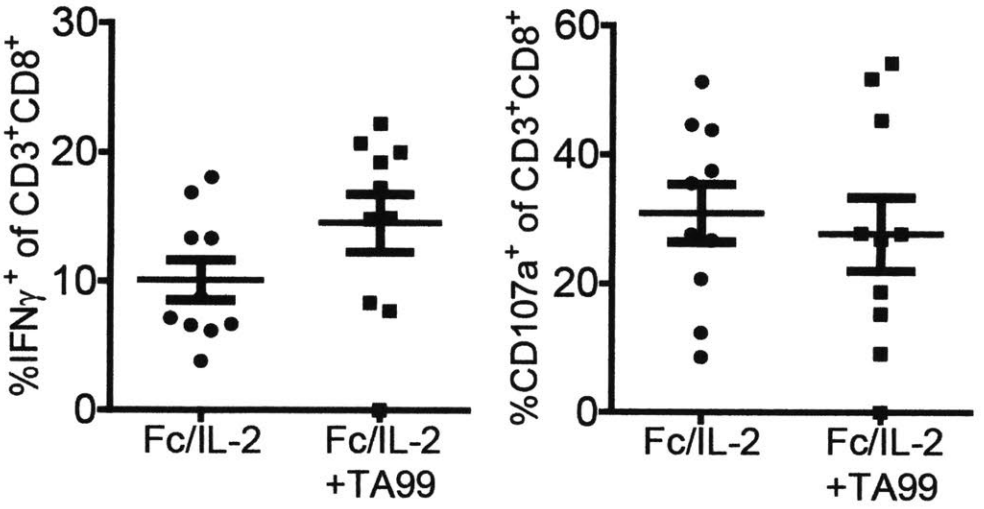

Figure 4.19 Analysis of IFNγ-producing or degranulating $CD8^+$ T-cells as a percentage of the intratumoral $CD8^+$ T-cell population. The following conditions were investigated: $CD3^+CD8^+IFN\gamma^+$ cells; $CD3^+CD8^+CD107a^+$ cells. n = 10 per group. *p < 0.05, **p < 0.01, ***p < 0.001 between indicated groups. Data are mean ± SEM.

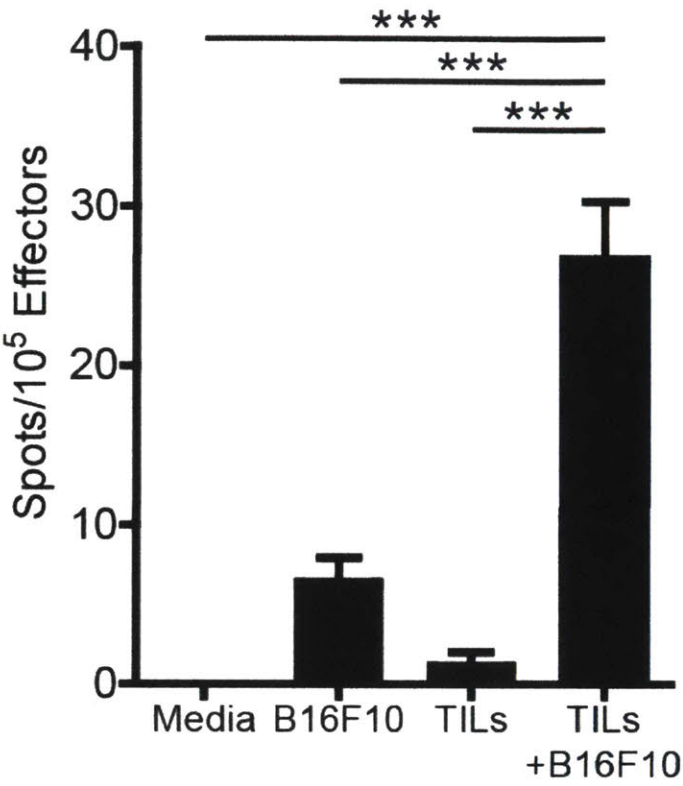

Figure 4.20 ELISPOT of $CD3^+CD8^+$ T-cells sorted from B16F10 tumors treated with Fc/IL-2+TA99. ***$p < 0.001$ between indicated groups. n = 5 per group. Data are mean ± SEM.

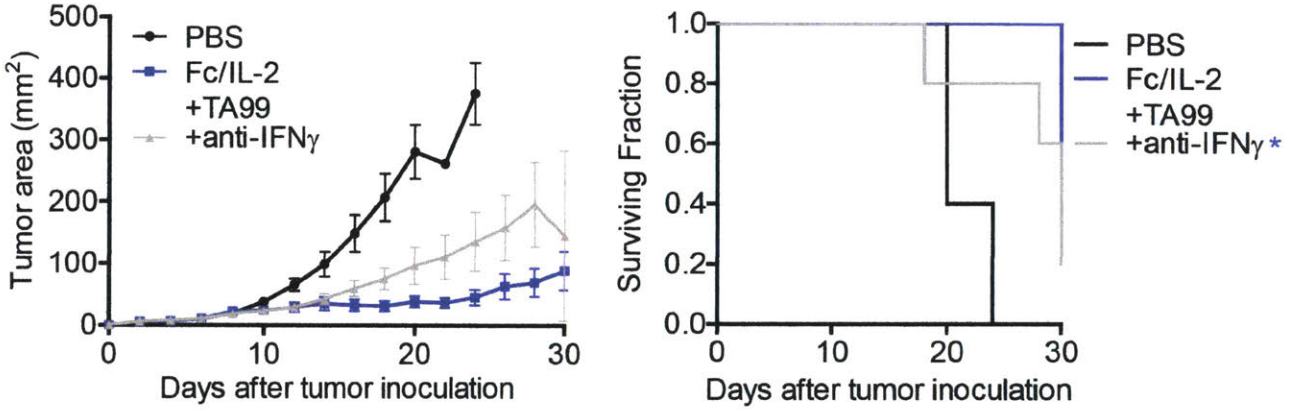

Figure 4.21 Tumor growth and survival curves of C57BL/6 mice bearing subcutaneous B16F10 tumors treated with PBS, Fc/IL-2+TA99, or Fc/IL-2+TA99 with anti-IFNγ antibody. n = 5 per group. *$p < 0.05$ v. Fc/IL-2+TA99. Data are mean ± SEM.

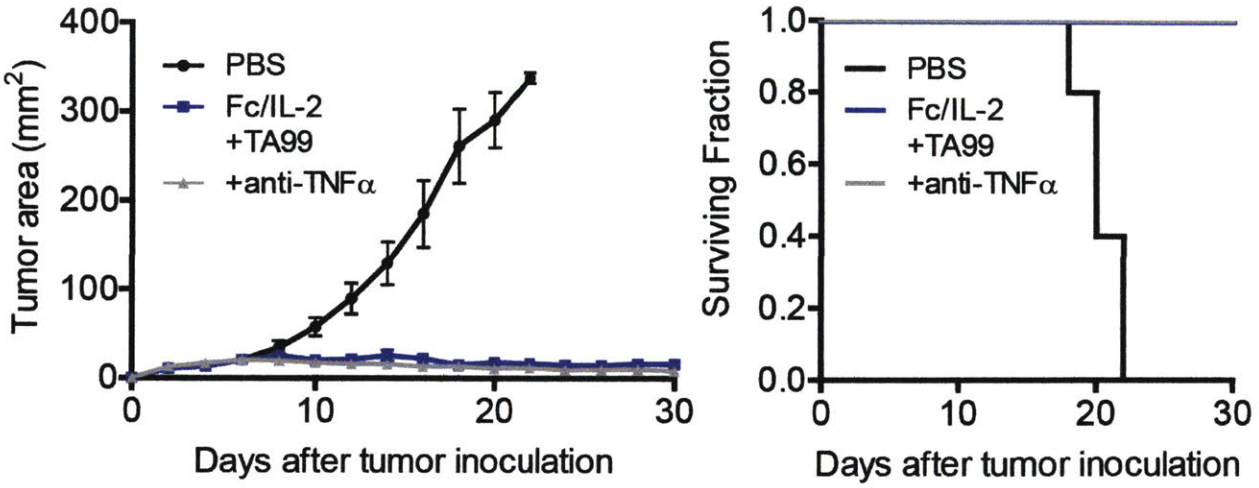

Figure 4.22 Tumor growth and survival curves of C57BL/6 mice bearing subcutaneous B16F10 tumors treated with PBS, Fc/IL-2+TA99, or Fc/IL-2+TA99 with anti-TNFα antibody. n = 5 per group. Data are mean ± SEM.

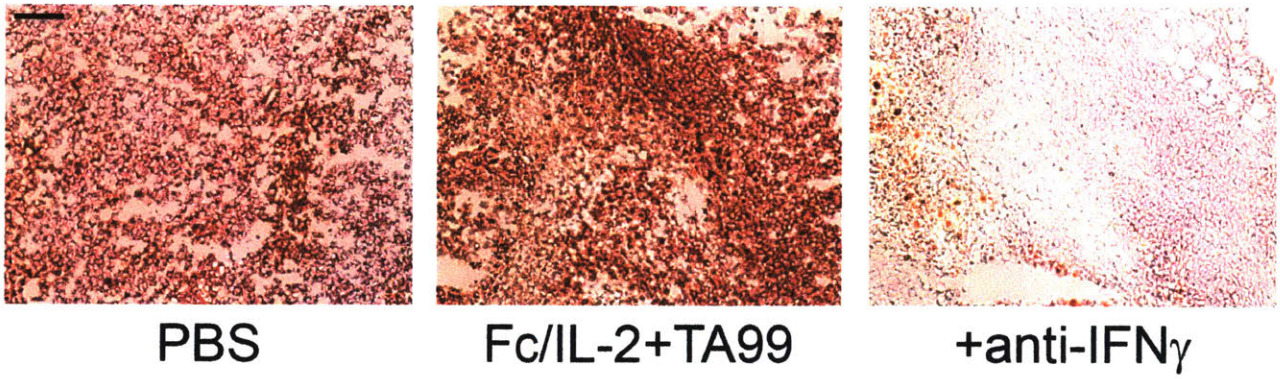

Figure 4.23 Representative immunohistochemistry of MHC-I expression using NovaRed stain in B16F10 tumors with the indicated conditions. Magnification 10x. Scale bar 100 microns.

5. Boosting Efficacy of Combination Immunotherapy through Timed Dendritic Cell Modulation

5.1. Introduction

It has been proposed that an effective immunotherapy regimen comprises three major characteristics: 1) immunogenic cancer cell death, 2) enhanced antigen presentation, and 3) blockade of immune-checkpoints (Stagg et al., 2007). In our previous work, we demonstrated that an immunotherapy combination consisting of an IL-2 protein fusion exhibiting extended serum persistence and anti-tumor antibodies resulted in stasis of tumor growth, suggesting some form of immunogenic cancer cell death (Zhu et al., 2015). However, we only sporadically observed cures in our therapy studies, and this is likely because our first generation combination immunotherapy did not meet the second and third criteria outlined above.

In order to prime an even stronger anti-tumor immune response, any resulting immunogenic cancer cell death must be coupled with enhancing antigen presentation. This is because although the former may release tumor-specific antigens, these may not be optimally presented by antigen presenting cells (APCs) such as dendritic cells (DCs). If an external agent is able to induce activation of DCs and their processing of these tumor-specific antigens, however, an even stronger anti-tumor T-cell response may be mounted. (Chen and Mellman, 2013)

There exist many therapeutics that could have the desired effect of maturing DCs. These include cytokines such as IFNα, antibodies such as anti-CD40, and small molecules which can bind a myriad of activating receptors on DCs such as α-galactosylceramide on CD1d, poly (I:C) on TLR3, or CpG motifs on TLR9 (Figdor et al., 2004; Fong and Engleman, 2000)
Another important factor that is often not considered in the rational combination of such immunotherapeutic agents is the timing of such agents. The development of an anti-tumor immune response is not an instantaneous function, but rather a temporal procession of different events that follow each other consecutively (Chen and Mellman, 2013). In order to mimic this natural progression, it may be important to explore how the timing of different agents may enhance or blunt the induction of the desired anti-tumor immune response.

5.2. Materials and Methods

Cloning

Vectors encoding the heavy and light chains of mouse TA99 antibody were gifts of Jeffrey V. Ravetch (The Rockefeller University). The DNA sequences encoding the heavy and light chains were cloned into gWIZ (Genlantis), yielding gWIZ-TA99-HC and gWIZ-TA99-LC. A vector encoding the heavy chain of mouse IgG2a from C57BL/6 mice was a gift of Jeffrey V. Ravetch (The Rockefeller University). A D265A mutation was introduced and the DNA encoding the non-lytic D265A Fc, henceforth referred to simply as Fc, was cloned into gWIZ. For cloning of Fc/IL-2, murine IL-2 (InvivoGen) with C-terminal 6xHis tags was subsequently cloned C-terminal to the Fc, separated by a short G_3S linker, yielding gWIZ-Fc/IL-2. To enable expression of monovalent heterodimeric Fc/IL-2, a vector encoding the Fc with a C-terminal FLAG tag, gWIZ-Fc/FLAG, was also constructed using similar methods. Plasmid DNA was transformed into XL-1 Blue (Agilent) for amplification and purified using EndoFree Plasmid Maxi Kit (Qiagen). Vectors encoding the heavy and light chains of mouse anti-CD40 antibody (clone 3/23) were gifts of Dr. Martin J. Glennie (University of Southampton). The DNA sequences encoding the heavy and light chains were cloned into gWIZ (Genlantis), yielding gWIZ-3/23-HC and gWIZ-3/23-LC.

Protein Production

TA99, 3/23 mAb, and Fc/IL-2 fusion proteins were produced using HEK293 cells (Life Technologies) according to manufacturer's instructions. HEK293 cells were transfected with gWIZ-TA99-HC and gWIZ-TA99-LC; gWIZ-3/23-HC and gWIZ-3/23LC; or gWIZ-Fc/IL-2 and gWIZ-Fc/FLAG; for TA99, 3/23 mAb, or Fc/IL-2, respectively, using polyethylenimine in FreeStyle 293 media supplemented with OptiPro (Life Technologies). TA99 and 3/23 mAb were purified by Protein A Agarose (Genscript), Fc/IL-2 was purified by TALON Metal Affinity Resin (Clontech) and followed by anti-FLAG M2 Affinity Gel (Sigma-Aldrich). All in-house produced protein were ensured to contain minimal levels of endotoxin (< 0.1 total EU/injection within 1 hour) using the QCL-1000 assay (Lonza).

Chemicals

α-galactosylceramide (KRN7000, Cayman Chemicals), was resuspended as follows: 1 mg KRN7000, 280 mg Sucrose (Sigma-Aldrich), 37.5 mg L-Histidine (Sigma-Aldrich), 25 mg poly-

sorbate 20 (Sigma-Aldrich) all in 5 mL of double-distilled water. This suspension was heated briefly at 40 °C until completely dissolved and the solution was clear. This solution was further diluted 1:1000 in double-distilled water.

Mice

C57BL/6NTac mice (Taconic) were aged between 6-10 weeks of age before tumor induction. All animal work was conducted under the approval of the MIT Division of Comparative Medicine, in accordance with federal, state, and local guidelines.

Tumor Cells

B16F10 cells (ATCC) were maintained in DMEM, supplemented with fetal bovine serum, L-alanyl-L-glutamine, and penicillin-streptomycin, all purchased from Life Technologies.

Tumor Inoculation and Treatment

For induction of B16F10 tumors, 10^6 cells in 100 μL of PBS were injected subcutaneously into the flanks of C57BL/6 mice and allowed to establish for 6 days before treatment. Retro-orbital injection of PBS, or Fc/IL-2 (25 μg) and TA99 (100 μg) was done on day 6 and 12 after tumor inoculation for a total of two treatments. For anti-CD40 3/23 mAb treatments, 100 μg was injected on day 5 and 11 for "early" staged treatments, or day 6 and 12 for "late" staged treatments. These injections were done retro-orbitally. For KRN7000 treatments, 0.025 μg (50 μL of the final stock) was injected on day 5 and 11 for "early" staged treatments, or on day 8 and 14 for "late" staged treatments. These injections were done retro-orbitally.

Statistics

Survival data were determined using a log-rank Mantel-Cox test.

5.3. Results

5.3.1. Timing of anti-CD40 and α-Galactosylceramide Administration Affects Therapeutic Efficacy of Combination Immunotherapy

We hypothesized that the addition of dendritic cell (DC) immunomodulatory agents to existing combination immunotherapy such as Fc/IL-2+TA99 could enhance therapeutic efficacy through increased $CD8^+$ T-cell priming by DCs. However, we found that the timing of administration of such DC modulatory agents significantly affected the therapeutic efficacy observed. With both the antibody 3/23 mAb (Figure 5.1) and the small molecule KRN7000 (Figure 5.2), the efficacy of Fc/IL-2+TA99 was actually abrogated when the third agent was given "early," in each case 24 hours prior to the administration of Fc/IL-2+TA99. However, when either agent was given at a "late" stage (3/23 mAb simultaneously with Fc/IL-2+TA99 and KRN7000 48 hours after Fc/IL-2+TA99), the therapeutic efficacy was enhanced with a strong trend for increased survival benefit.

5.4 Discussion

Although it is clear that combinations of immunotherapy can provide synergistic efficacy over their individual components (Zhu et al., 2015), the timing of dosing has not been highlighted. Yet, as we have observed in this study, sending incoherent immunological signals can have striking effects on the degree of therapeutic efficacy observed.

This was observed when DC maturation signals were given "early" or "late" with respect to the administration of Fc/IL-2+TA99. It was clear that when DC maturation agents were given "early," the efficacy of the original immunotherapy was abrogated. When given "late," an enhancement in survival was seen. Although survival enhancement was not deemed statistically significant, the maximal possible effect was likely not reached as the pharmacokinetics of 3/23 mAb and KRN7000 were not thoroughly investigated, and so optimal temporal spacing of these two agents was not determined. For example, the antibody would require a different timing than the small molecule due to their disparate clearance and tissue diffusion properties.

One hypothesis for the impact of timing is the presence of tumor antigen during DC activation. Fc/IL-2+TA99 is able to control tumor growth, and thus is likely causing cell death and release of tumor antigens. These tumor antigens can then be taken up by APCs such as DCs and used to prime $CD8^+$ T-cells. However, the phagocytic capability of DCs is regulated by their activation state. Once they receive a maturation signal, their phagocytic capabilities become reduced, whereas surface receptors involved in T-cell priming become up-regulated. (Albert et al., 1998).

If DCs are caused to mature before there is sufficient tumor antigen to be processed, in the "early" administration case," DCs lose their phagocytic capability before having taken up a significant amount of tumor antigen and would thus be ineffective in priming naïve T-cells. However, if DCs are forced to mature after having taken up a significant amount of circulating tumor antigen, in the "late" administration case, DCs could then effectively prime T-cells with tumor antigen and direct an endogenous $CD8^+$ T-cell response (Albert et al., 1998). Further work in this area could confirm this hypothesis, for example using a closely related tumor cell line with a tumor-associated protein that can be actively tracked using flow cytometry, such as a B16F10-EGFP cell line. The level of EGFP signal can then be quantified in draining-lymph node DCs in either the "early" or "late" DC agent cases. Several markers could also be observed, such as CD86, MHC-II, or CD40 (Banchereau and Steinman, 1998; Lutz and Schuler, 2002).

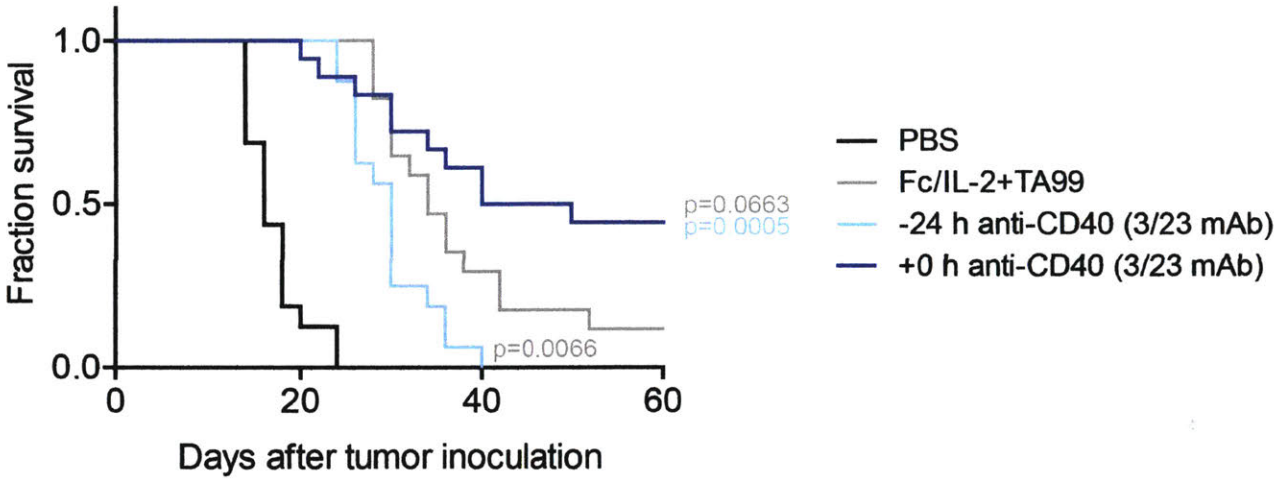

Figure 5.1 Tumor survival curves of C57BL/6 mice bearing subcutaneous B16F10 tumors treated with PBS or Fc/IL-2+TA99 treated on day 6 and 12. Anti-CD40 (3/23 mAb) was administered at the time indicated relative to that of Fc/IL-2+TA99 administration. n = 16-18 per group. p values indicated v. corresponding color group in legend. Data are mean ± SEM.

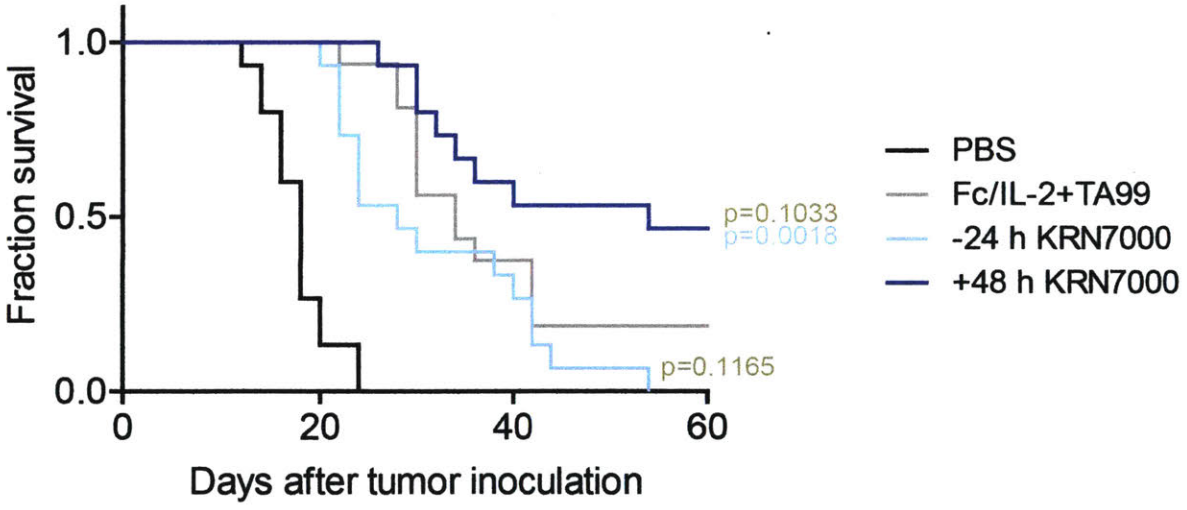

Figure 5.2 Tumor survival curves of C57BL/6 mice bearing subcutaneous B16F10 tumors treated with PBS or Fc/IL-2+TA99 treated on day 6 and 12. The small molecule α-galactosylceramide (KRN7000) was administered at the time indicated relative to that of Fc/IL-2+TA99 administration. n = 15-16 per group. p values indicated v. corresponding color group in legend. Data are mean ± SEM.

6. Combination Immunotherapy for Treatment of Autochthonous KP Lung Tumors

6.1. Introduction

While syngeneic subcutaneous murine tumor models have many benefits as a setting to test novel immunotherapies, in particular a fully immunocompetent *in vivo* system, there are still many drawbacks. These include the lesion often being grown in an ectopic anatomical site, the tumor microenvironment may not fully mimic those found in a clinical setting, and the tumor induction and latency are generally non-physiological, as they are induced through a bolus of numerous cells and grow extremely quickly (Dranoff, 2011; Teicher, 2006).

Recent developments in genetically-engineered mouse (GEM) models provide a superior alternative to subcutaneous models. These mice retain a fully functional immune system, but these tumors arise in the appropriate physiological site and are generated from a single transformation event, although the overall tumor burden may still be multi-focal in nature (Frese and Tuveson, 2007). There are numerous models that exist, such as the BRAF-Pten model of melanoma (Dankort et al., 2009) and the KP model of non-small cell lung carcinoma (NSCLC) (DuPage et al., 2009).

The KP model in particular is an intriguing model to use in the testing of immunotherapy. The progression of these lung adenocarcinomas follows closely the clinical temporal pathophysiology of human NSCLC (DuPage et al., 2009). Although it may be argued that such a model may be inappropriate for immunotherapy, given their low mutational loads compared to other models (Westcott et al., 2014), we would assert the opposite. Although immunotherapies such as anti-PD-1 and anti-CTLA-4 have experienced unprecedented success in the clinic, they benefit only a subset of cancer patients (Borghaei et al., 2015; Brahmer et al., 2015; Hodi et al., 2010a; Wolchok et al., 2013), often with malignances presenting high mutational load (Alexandrov et al., 2013).

In order to expand the utility of cancer immunotherapies to a broader range of tumors, we believe that it is imperative to utilize a model that is difficult to cure given its low mutational load and that expresses few tumor-specific antigens. It would follow that only the most potent and efficacious immunotherapy regimens would be effective in such a model. Moreover, only

these regimens would have a reasonable chance at clinical translation where tumors with lower mutational burden may not respond favorably to existing immunotherapeutic interventions.

From our first generation therapy described in our previous work, we have included three additional agents to meet all three characteristics of an effective immunotherapy. The first characteristic, immunogenic cell death, was met by our existing combination of IL-2 with extended serum persistence and anti-tumor antibodies (Zhu et al., 2015). The second characteristic, enhanced antigen presentation, has been met by the addition of an amphiphile vaccine system, which generates robust $CD8^+$ T-cell responses against the antigen vaccinated against (Liu et al., 2014). The third characteristic, blockade of checkpoint inhibitors, has been achieved through the use of anti-PD-1, anti-CTLA-4, or the combination of both. With this multi-pronged immunotherapy, it may be possible that tumor regression can be achieved in models that otherwise would be refractory to existing immunotherapy.

6.2. Materials and Methods

Cloning

Vectors encoding the heavy and light chains of mouse anti-CEA antibody (Sm3e) were previously described and generated in-house from yeast-display affinity-matured scFv. The DNA sequences encoding the heavy and light chains were cloned into gWIZ (Genlantis), yielding gWIZ-Sm3e-HC and gWIZ-Sm3e-LC. A vector encoding the heavy chain of mouse IgG2a from C57BL/6 mice was a gift of Jeffrey V. Ravetch (The Rockefeller University). For cloning of the recombinant fusion protein of mouse serum albumin fused to murine IL-2 (MSA/IL-2), the coding sequence for mouse serum albumin (Origene) was used to replace the sequence encoding the Fc in the existing gWIZ-Fc/IL-2 vector, generating the vector gWIZ-MSA/IL-2. For cloning of the recombinant fusion protein used in the vaccine of mouse serum albumin fused to CEA peptide, the same albumin and linker construct for gWIZ-MSA/IL-2 was used, but the IL-2 sequence was replaced with the DNA sequence encoding for RAYVSGIQNSVSANRSDP, generating the vector gWIZ-MSA-CEAVx. This amino acid sequence contains a known CD8 epitope against CEA, with additional, arbitrary numbers of amino acids of the full-length protein before and after (Mennuni et al., 2005). For cloning of aCTLA-4, the known sequence of the variable regions of the aCTLA-4 clone 9D9 was synthesized (IDT Technologies) and cloned into the mouse IgG2a of C57BL/6 mice, generating gWIZ-9D9-HC and gWIZ-9D9-LC. Plasmid DNA was transformed into XL-1 Blue (Agilent) for amplification and purified using EndoFree Plasmid Maxi Kit (Qiagen).

Protein Production

Sm3e, MSA/IL-2, and MSA-CEAVx fusion proteins were produced using HEK293 cells (Life Technologies) according to manufacturer's instructions. HEK293 cells were transfected with gWIZ-Sm3e-HC and gWIZ-Sm3e-LC; gWIZ-MSa/IL-2; or gWIZ-MSA-CEAVx; for Sm3e, MSA/IL-2, or MSA-CEAVx, respectively, using polyethylenimine in FreeStyle 293 media supplemented with OptiPro (Life Technologies). aCTLA-4 was produced using CHO cells at the Protein Expression Core Facility at EPFL using plasmids gWIZ-9D9-HC and gWIZ-9D9-LC. Sm3e and aCTLA-4 was purified by Protein A Agarose (Genscript). MSA-CEAVx and MSA/IL-2 was purified by TALON Metal Affinity Resin, and MSA/IL-2 was further purified using a HiLoad™ 16/600 Superdex™ 200 pg column (GE Healthcare Life Sciences) on an ÄKTAFPLC

protein purification system (GE Healthcare Life Sciences). All in-house produced protein were ensured to contain minimal levels of endotoxin (< 0.1 total EU/injection within 1 hour) using the QCL-1000 assay (Lonza).

Mice

CEA transgenic mice (CEA-Tg) on a C57/BL6 background were a kind gift from Dr. Jeffrey Schlom (NCI), and a colony was further propagated in-house. KP-CEA transgenic mice were generated by back-crossing CEA-Tg mice and KP mice for several generations until a uniform strain was obtained. KP mice (K-ras$^{LSL-G12D}$/p53$^{fl/fl}$ on a C57/BL6 background were a kind gift from Dr. Tyler Jacks (MIT). Mice were aged between 6-16 weeks of age before tumor induction. All animal work was conducted under the approval of the MIT Division of Comparative Medicine, in accordance with federal, state, and local guidelines.

Tumor Cells

KP2677 cells were a kind gift from Dr. Tyler Jacks (MIT). KP2677-CEA cells were generated by transduction of KP2677 using lenti-virus encoding Cre and the entire gene for human CEACAM5. Transduced cells were further sorted to gain a homogenous CEA+ cell line. Both KP2677 and KP2677-CEA cells were maintained in DMEM, supplemented with fetal bovine serum, L-alanyl-L-glutamine, and penicillin-streptomycin, all purchased from Life Technologies.

Viral Vector Cloning and Production

Lentivirus transfer plasmid containing Cre (Lenti-X) and lentiviral component plasmids psPAX2 and pCMV-VSV-G were a kind gift from Tyler Jacks (MIT) and were as previously described (DuPage et al., 2009). Full-length human CEA (Addgene) was cloned out and introduced into the Lenti-X plasmid under an EFS promoter, generating the plasmid Lenti-CEA. 293 FS* cells were plated at 80% confluence. Following 24 hours, lentiviruses were produced by co-transfection of Lenti-Cre-CEA construct with psPAX2 (gag/pol) and pCMV-VSV-G (env) plasmids at a 10:10:1 ratio using a calcium phosphate transfection kit (Clontech laboratories). Lentivirus containing supernatant was harvested 48 and 72 hours post-transfection. Supernatant was filtered through a 0.2 um syringe filter and ultracentrifuged at 25,000 rpm for 90 minutes to pellet the lentivirus. Virus pellet was re-suspended in 50 ul of 1:1 Optimem (Gibco) to sterile saline and allowed to dissolve overnight at 4° C. Lentiviruses were aliquoted and frozen at -80°C. Lentivirus titer was calculated by infecting Cre reporter cell line GreenGo 3TZ cells with decreasing dilutions of

lentivirus (1:10 to $1:10^8$) and calculating Cre expression by FACS for each dilution of viral infection in triplicate.

Lipo-CpG Synthesis

CpG amphiphiles were synthesized using an ABI 394 synthesizer on a 1.0 μmol scale. Immunostimulatory CpG used was a class B sequence known as 1826. Lipophilic phosphoramidites were conjugated as a final 'base' on the 5′ end of oligonucleotides. Lipophilic phosphoramidites were dissolved in dichloromethane and coupled to oligos using the so-called syringe synthesis technique. Briefly, lipid phosphoramidites (200 μL) were mixed with activator (0.2 mM 5-Ethylthio Tetrazole in 200 μL Acetonitrile), and the mixture were pushed back and forth through the column using 2 syringes for 10 min. Alternatively, lipophilic phosphoramidite could also be coupled using the DNA synthesizer (15 min coupling time). After the synthesis, DNA was cleaved from the solid support, deprotected, and purified by reverse phase HPLC using a C4 column (BioBasic-4, 200 mm x 4.6 mm, Thermo Scientific), 100 mM triethylamine-acetic acid buffer (TEAA, pH 7.5)- acetonitrile (0-30 min, 10-100%) as an eluent. Lipophilic CpG typically eluted at 20 min while unconjugated CpG eluted at 8 min. Lipophilic CpG was characterized by MALDI-TOF mass spectrometry.

Tumor Inoculation

For induction of flank KP2677 or KP2677-CEA tumors, 10^6 cells in 100 μL of PBS were injected subcutaneously into the flanks of CEA-Tg mice and allowed to establish for 6 days before treatment. For induction of autochthonous CEA-expressing lung tumors, 30,000 PFU of Lenti-CEA virus was administered via the trachea, as previously described.

Treatment

As applicable, I.P. injections of MSA/IL-2 (30 μg), Sm3e (200 μg), aCTLA-4 (200 μg), and aPD-1 (200 μg) were administered weekly. For injection of amphiphile vaccine, MSA-CEAVx (10 μg peptide equivalence) and Lipo-CpG (1.24 nanomoles) or cyclic di-guanylate monophosphate (CDN; 25 μg; Invivogen) were given as a subcutaneous tail base injection, consisting of one prime and 4 boosts for the former adjuvant and 3 boosts for the latter adjuvant, delivered weekly. All recombinant proteins produced in-house as described previously except for aPD-1, purchased from BioXCell.

Flow Cytometry

Tumor inoculation and treatment were done as previously described. For intracellular cytokine staining, 100 μL of blood was obtained through retro-orbital bleeding using heparin-coated capillary tubes (Fisher Scientific) and stored in MiniCollect blood collection tubes (Grenier Bio-One). Blood was transferred to V-bottom 96-well plates (BD Biosciences) and red blood cells were lysed using ACK Lysis Buffer (Life Technologies). Cells are incubated in T-cell media (Complete RPMI with 1x Sodium Pyruvate, 1x Non-Essential Amino Acids, 1x β-Mercaptoethanol, all purchased from Life Technologies) with a final MSA-CEAVx concentration of 20 mg/mL. After 16 hours of incubation at 37° C, Brefeldin A (Life Technologies) is added to a final concentration of 1X to each well and is further incubated for another 4 hours. Cells were first treated with Live/Dead Aqua (Life Technologies). Cells were subsequently treated with TruStain fcX (clone 95; Biolegend) and then stained with antibodies against CD3ε (clone 145-2C11) and CD8α (clone 53-6.7), both purchased from Biolegend. Following surface staining, samples were fixed, permeabilized, and stained with antibodies against IFNγ (clone XMG1.2; Biolegend) or isotype control (clone RTK2071; Biolegend). Samples were analyzed on a BD LSR-II flow cytometer (BD Biosciences) and data analysis was performed using FlowJo software (Tree Star).

Histology

Tumor inoculation and treatment were done as previously described. For H&E staining, animals were sacrificed a week after the final treatment. Lungs were inflated and fixed in 10% formalin, embedded in paraffin, and stained with hematoxylin and eosin.

qPCR Analysis

Tumor inoculation was done as previously described. All mice were sacrificed and tumors harvested for analysis 18 weeks after tumor induction. Tumor nodules were excised and made into single cell suspensions through mechanical dissociation between two glass slides. Cell suspensions were passed through 70 μm filters, pelleted, and resuspended in 96 well plates. Cell lysis and RT-PCR were then performed using an Ambion Cells-to-C_t kit (Life Technologies) according to manufacturer's instructions. qPCR was performed using TaqMan probes purchased from Life Technologies for the human gene *CEACAM5* and the mouse gene *B2m* as internal control, and the TaqMan Universal PCR Master Mix (Life Technologies) according to manufacturer's instructions, on a Roche Lightcycler 480 (Roche).

Statistics

Survival data were determined using a log-rank Mantel-Cox test and qPCR data were analyzed using a Fisher's exact test.

6.3. Results

6.3.1. CEA Expression in an *in vitro* KP Cell Line and *in vivo* in Autochthonous KP Lung Tumors

Because the KP lung model exhibits low mutational burden, there may exist only few tumor-associated antigens. However, because these antigens are currently unknown to us, we were forced to introduce an additional tumor-associated antigen into this tumor model. This allowed us to develop the two components of our combination immunotherapy—the anti-tumor antibody and vaccine—which require a targetable antigen.

We chose to incorporate human carcinoembryonic antigen (CEA), an oncofetal antigen that is associated with adenocarcinomas including NSCLC (Benchimol et al., 1989; Hammarström, 1999). However, because this antigen is not native to a murine system, CEA would have been a complete neoantigen in a wild-type BL6 mouse. To retain the physiological context of CEA, we thus crossed wild-type KP mice (DuPage et al., 2009) on a BL6 background to CEA-transgenic mice (Putten et al., 1994) on a BL6 background, achieving KP-CEA mice (Figure 6.1). Lung tumors can be induced in these mice through the standard lentiviral system, but because these mice are transgenic for CEA, any introduction of CEA antigen is no longer considered foreign. In this sense, we recapitulate the disease as it might be presented in humans.

In order to force tumors to express CEA, we designed a lentiviral vector incorporating Cre and CEA under two different promoters, allowing for transformation of the infected cells through oncogenic K-ras activation and p53 removal and also expression of the entire human CEA gene. We term this lentivirus Lenti-CEA (Figure 6.2). When GreenGo reporter cells are transduced with this vector, they begin to express GFP, indicating that the Cre is functional upon transduction (Figure 6.3). When a propagated line of KP tumor cells, KP2677, is transduced with Lenti-CEA, the large majority of this cell line begins to express CEA, as probed by the anti-CEA antibody Sm3e (Figure 6.4). This indicates that at least *in vitro*, Lenti-CEA is able to induce both Cre and CEA expression. KP2677 cells that were transduced with Lenti-CEA were further sorted by FACS to remove cells that had little to no CEA expression. The resulting cell line was named KP2677-CEA.

To determine if this result could be recapitulated in an *in vivo* setting, we infected the lungs of KP-CEA mice with Lenti-CEA through an intra-tracheal administration. We found that

uninfected lungs showed no tumor formation or CEA expression via qPCR after 12 weeks (Figure 6.5). However, mice infected with Lenti-CEA showed tumor nodules in the lung, and these nodules also demonstrated CEA expression via qPCR when excised from the healthy lung tissue (Figure 6.5). This suggests that Lenti-CEA is also able to induce lung tumor formation with a degree of tumor-associated CEA expression.

6.3.2. Combination Immunotherapy in Subcutaneous KP-CEA Flank Tumors

Because of the extended latency of the autochthonous lung tumor model, we decided to first test a proxy of the model using a subcutaneous model of KP2677-CEA cells. When discussing the contents of the immunotherapy, each agent is associated with a single letter as such:

A: Anti-CEA monoclonal murine IgG2a (Sm3e)
I: MSA/IL-2
P: Anti-PD-1 murine IgG1
C: Anti-CTLA-4 murine IgG2a
V: Amphiphile vaccine against CEA peptide composed of
    -MSA-CEA
    -LipoCPG

In previous manifestations of this therapy, AIPV was tested against various syngeneic subcutaneous models such as B16F10 melanoma and achieved a high rate of durable cures (Opel, 2015). However, it is notable that in the KP-2677-CEA subcutaneous model, tumor growth was only marginally delayed (Figure 6.6). If AIPV is replaced by AICV, curative potential is seen, but the maximal therapeutic response was seen only with AIPCV (Figure 6.6). This includes both checkpoint inhibitors in the combination immunotherapy, leading to 80% cures in the cohort. This suggests that the anti-PD-1 and anti-CTLA-4 components work in a complementary, non-overlapping mechanism, requiring both of their mechanisms of actions to achieve anti-tumor function in this lung tumor model.

We hypothesized that differences in efficacy may be due to the priming of T-cells to CEA. However, when we stimulated peripheral blood $CD8^+$ T-cells to CEA and perform intracellular cytokine staining, we find that the percentage of IFNγ-expressing T-cells is largely

equivalent (Figure 6.7). Moreover, the level of IFNγ does not appear to correlate with therapeutic efficacy, as AIPV generates a greater population of IFNγ-producing CEA-reactive $CD8^+$ T-cells (Figure 6.7), yet has the weakest therapeutic response (Figure 6.6).

6.3.3. Combination Immunotherapy in Autochthonous KP-CEA Lung Tumors

Because the subcutaneous model is not necessarily a faithful representation of the autochthonous model, we were curious if the more physiological model reflected characteristics of the subcutaneous model with regards to therapeutic response. We infected KP-CEA mice with Lenti-CEA, and allowed tumors to form until an "adenoma stage," at which point mice were either left untreated or treated with the relevant cohorts: AIPV, AICV, or AIPCV (Figure 6.8). We note here that the adjuvant component of the vaccine in the lung model was altered to provide more clinical translatability (Corrales et al., 2015).

V: Amphiphile vaccine against CEA peptide composed of

-MSA-CEA

-cyclic di-guanylate monophosphate (CDN)

We found that AIPCV exhibited toxicity not observed in the subcutaneous model, with some instances of lethality (Figure 6.9). Further dosing revealed that AIPV and AICV also exhibited toxicity (Figure 6.9). It is possible that the toxicity is related to the efficacy of the treatment and may be a sign of tumor lysis syndrome: the greater amount of tumor death induced by therapy may cause greater systemic toxicity.

Therapy was halted after 4 doses due to toxicity concerns and one week after the last administration, a randomized set of mice from each cohort were euthanized for mechanistic investigation (Figure 6.8). The remaining mice were left for survival purposes.

Gross examination of the lungs by the naked eye revealed the presence of tumor nodules in all groups except AIPCV (Figure 6.10). Upon histological analysis of H&E stained lung sections from each treatment cohort, we found a response that was very similar to that observed in the subcutaneous model, although there were no cured mice observed at the time-point investigated (Figure 6.11). A blinded study by a pathologist revealed that the number of tumor nodules was fewest in the AIPCV-treated cohort (Figure 6.12). It was also notable that all

cohorts except AIPCV had a sizeable fraction of Grade II tumors and some Grade III tumors (Figure 6.12). When an inflammation score corresponding to tumor-infiltrating lymphocyte (TIL) infiltration was given, we find that all treated groups had some tumors with a "severe" grade, indicating lymphocyte infiltration within the tumor mass itself (Figure 6.13). Although AIPCV exhibited few Grade I tumors (Figure 6.12), some of these tumors had no TILs associated with it (Figure 6.13). It is unclear if these tumors will become reactive to TILs later and be cleared, or if these nodules have somehow escaped the immune response and would have ultimately grown out. Nevertheless, degree of TIL infiltration does not necessarily explain the superiority of AIPCV, as the inflammation scores between AICV and AIPCV are largely comparable (Figure 6.13).

6.4 Discussion

We demonstrate that combination immunotherapy is able to exhibit anti-tumor efficacy, even in a model that is known to have a highly suppressive microenvironment due to Treg association (Joshi et al., 2015) and few neoantigens due to a low mutational burden (Westcott et al., 2014). In particular, AIPCV is the most effective in both the subcutaneous and autochthonous lung setting, and that excluding either component of checkpoint blockade leads to a weaker therapy.

Despite our attempts to date, we were unable to currently identify an effect unique to AIPCV that would explain its superior therapeutic efficacy. Because all of our metrics were based on bulk lung suspensions, we hypothesize that it is possible that architectural differences in the tumor may be important, but would not be captured through the assays used.

Anti-CTLA-4 and anti-PD-1 are known to have non-overlapping yet complementary effects on $CD8^+$ T-cell activation and function (Pardoll, 2012). Anti-CTLA-4 was thought to function mainly by improving cross-priming of $CD8^+$ T-cells by dendritic cells (DCs) (Leach et al., 1996), but more recent evidence shows that it can act as a potent Treg depletion strategy, provided the correct activating antibody isotype is used (Selby et al., 2013). Anti-PD-1, on the other hand, is thought to stimulate T-cells that have undergone exhaustion or anergy due to PD-1 engagement, as this receptor is upregulated in response to activation (Keir et al., 2008).

We hypothesize that anti-CTLA-4 may be transiently depleting tumor-associated Tregs, which may initially hinder $CD8^+$ T-cell infiltration into the tumor. This may be why AIPV therapies are fairly ineffective: the T-cells require no rescue from exhaustion if they have not yet infiltrated into the tumor in the first place. Nevertheless, anti-PD-1 is still required as once the $CD8^+$ T-cells do infiltrate and are activated in response to CEA, they may be anergized by PD-L1 expression on tumor or tumor-associated stromal cells.

Further analysis of this model, particularly through histology, will be required to fully understand the mechanism of this multi-component immunotherapy and the specific roles that anti-CTLA-4 and anti-PD-1 are playing in this lung cancer model.

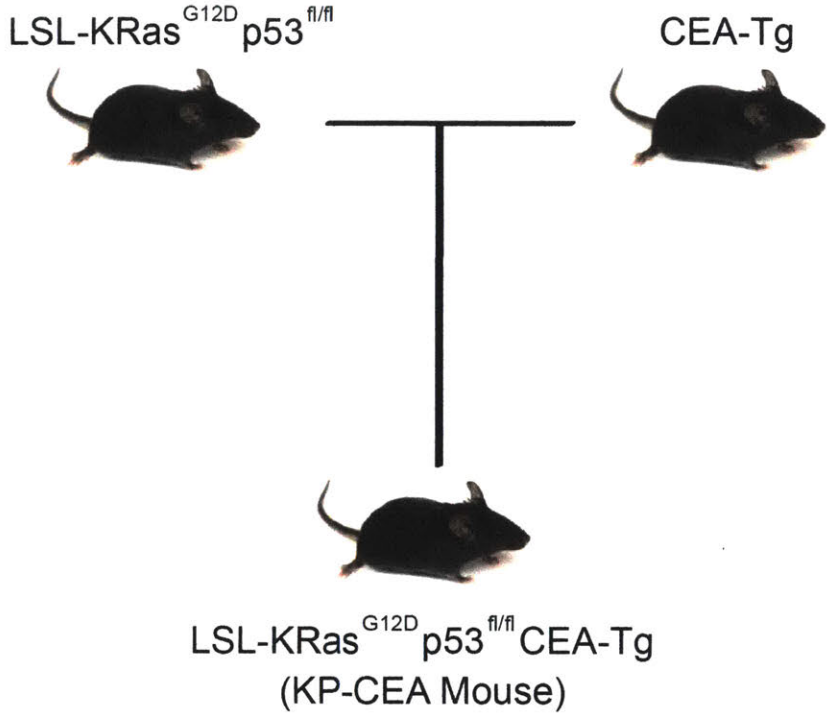

Figure 6.1 Schematic for breeding of KP-CEA mice. KP (LSL-KRas^{G12D}p53$^{fl/fl}$) mice were crossed with CEA-transgenic (CEA-Tg) mice, both on BL6 background. The resulting pups were backcrossed for several generations until KP-CEA mice were obtained.

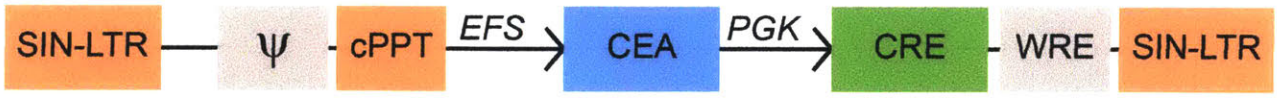

Figure 6.2 Schematic for lenti-viral vector for tumor induction in KP-CEA mice, containing both genes for CEA and Cre expression. This vector is termed Lenti-CEA. Full-length human CEA is driven by an EFS promoter, whereas expression of Cre is driven by a PGK promoter. The other components are standard for a lentiviral transfer plasmid.

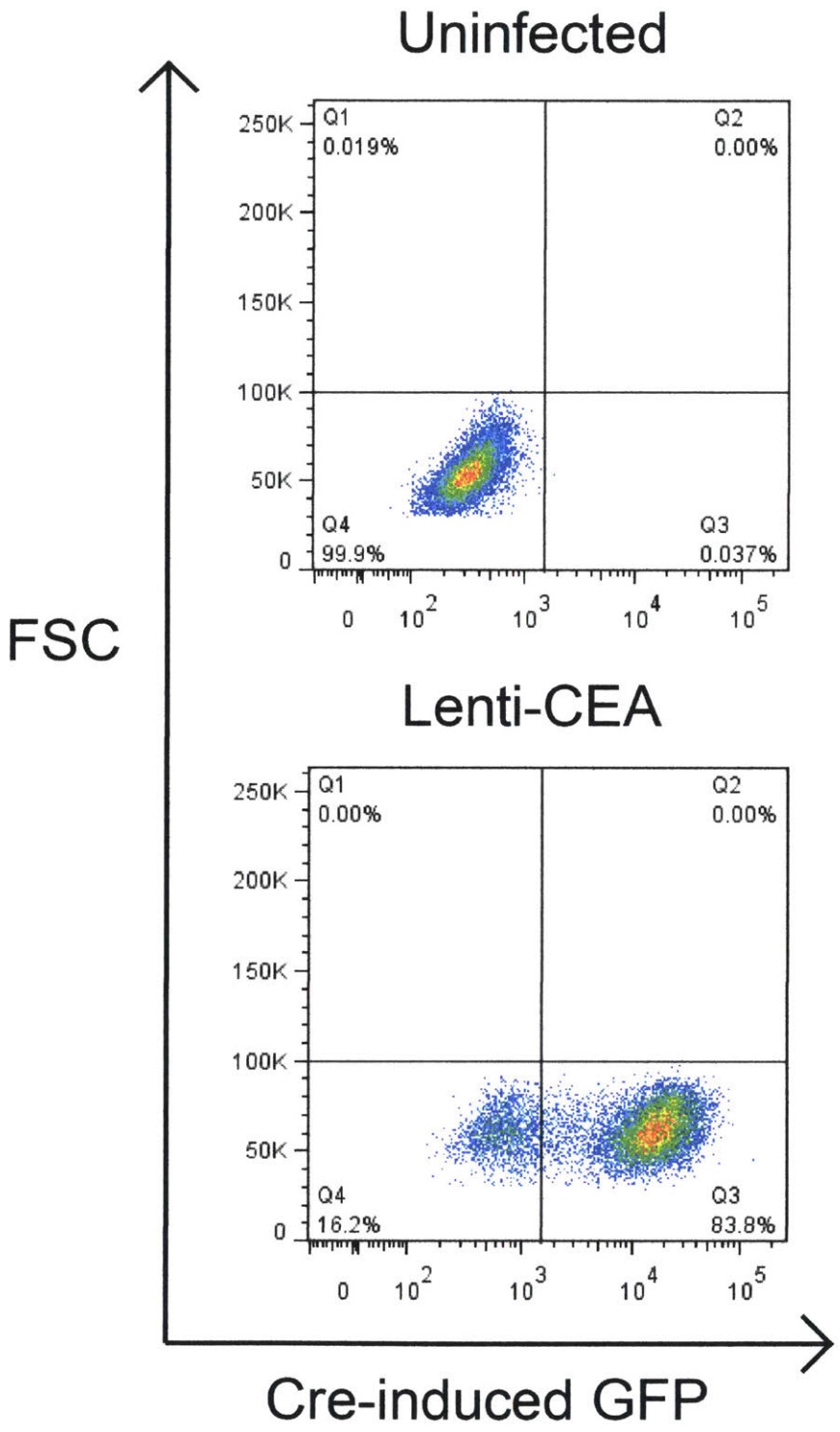

Figure 6.3 GreenGo cells induced with Lenti-CEA, indicating Cre-induced GFP expression.

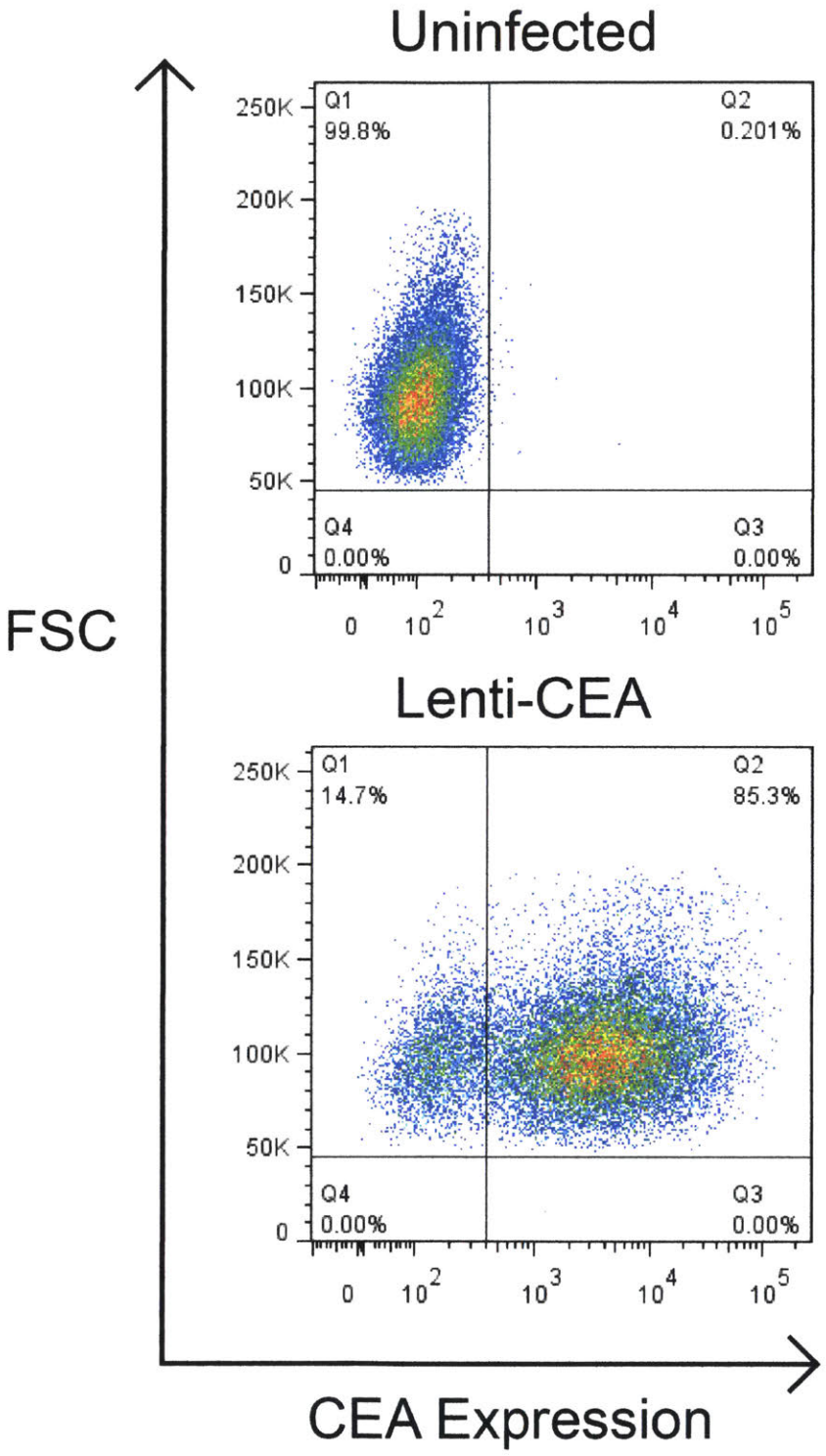

Figure 6.4 KP2677 transduced with Lenti-CEA, demonstrating Lenti-CEA integration of the CEA gene and expression of CEA as probed by the anti-CEA antibody Sm3e.

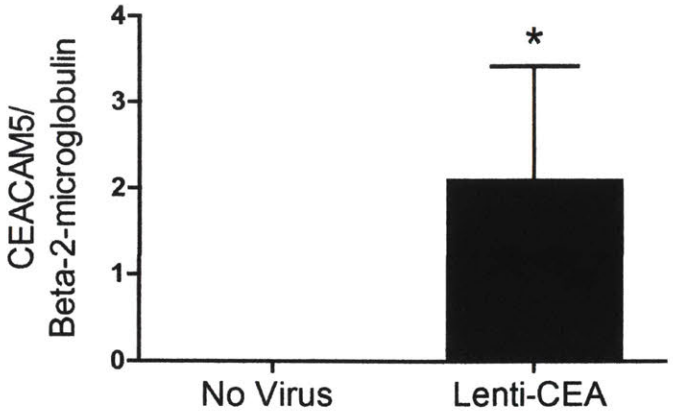

Figure 6.5 *CEACAM5* expression in lung cells either from a lung that did not Lenti-CEA or from distinct lung nodules excised from lungs that did receive Lenti-CEA. Expression was normalized to beta-2 microglobulin (*B2m*) expression. * $p < 0.05$. n = 3 per group. Data are mean ± SEM.

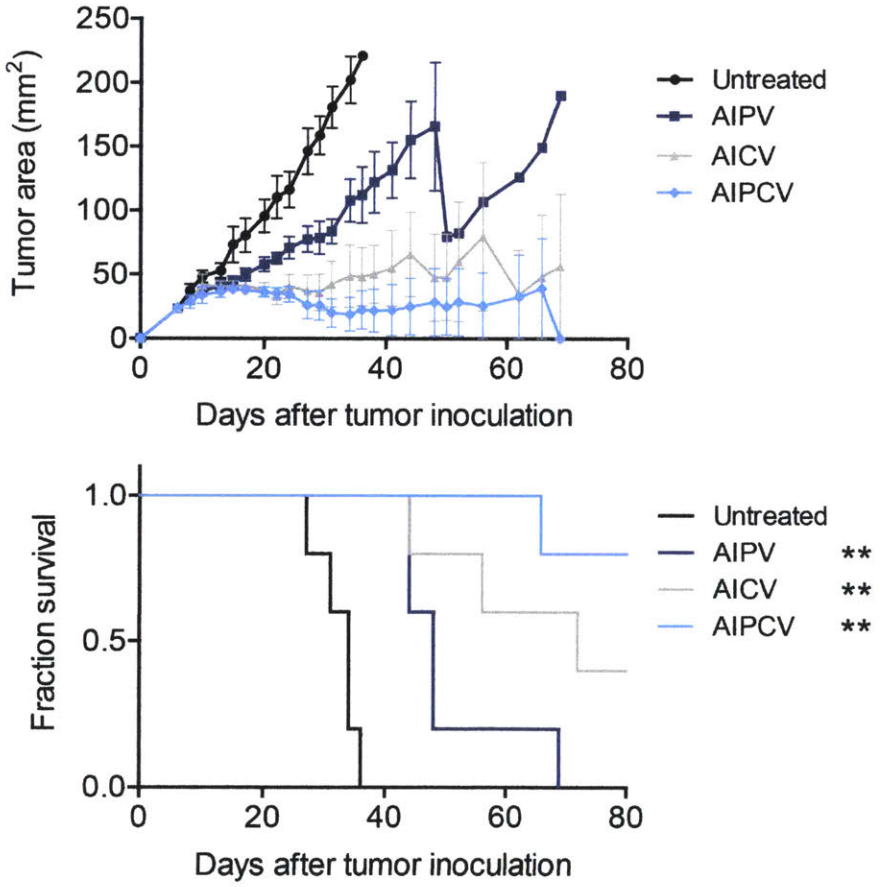

Figure 6.6 Tumor growth and survival curves of CEA-Tg mice bearing subcutaneous KP2677-CEA tumors treated as indicated. n = 5 per group. **$p < 0.01$ v. Untreated in legend. Data are mean ± SEM.

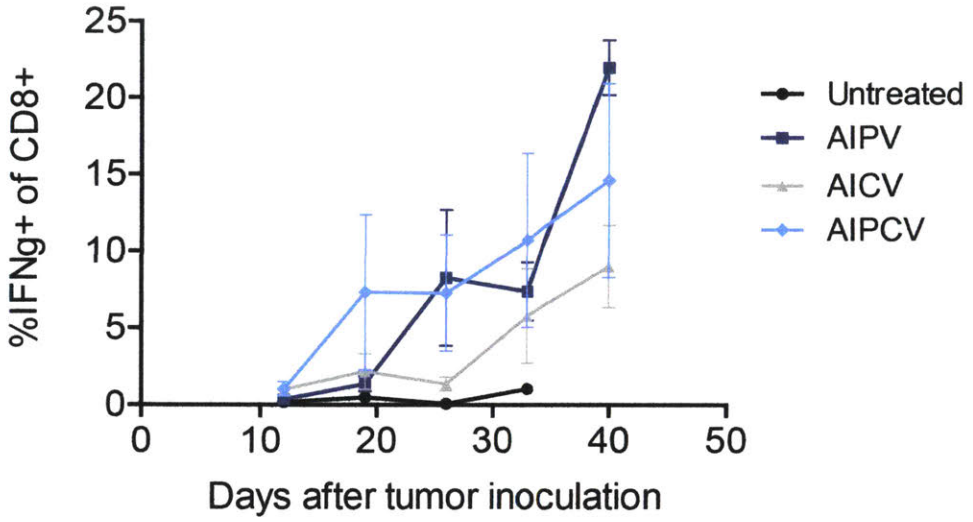

Figure 6.7 *In vitro* IFNγ production of peripheral blood $CD8^+$ T-cells stimulated with MSA-CEA, derived from mice treated with the indicated cohort. There was no statistically significant difference between the treated groups. n = 5 per group. Data are mean ± SEM.

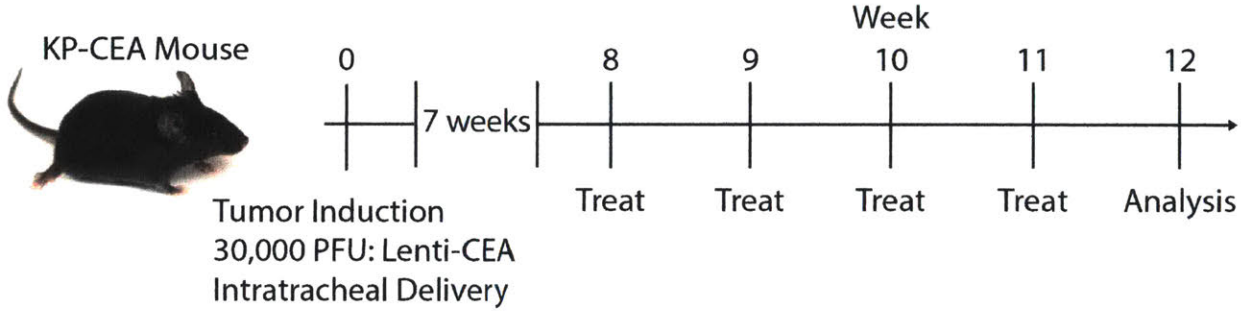

Figure 6.8 Schematic of autochthonous lung tumor model mechanistic experiments. KP-CEA mice on a BL6 background were infected with 30,000 PFU of Lenti-CEA via the trachea. On the 8^{th} week, treatment of various cohorts began weekly, for a total of 4 treatments. Mice were sacrificed on the 12^{th} week for either flow cytometric or histological analysis.

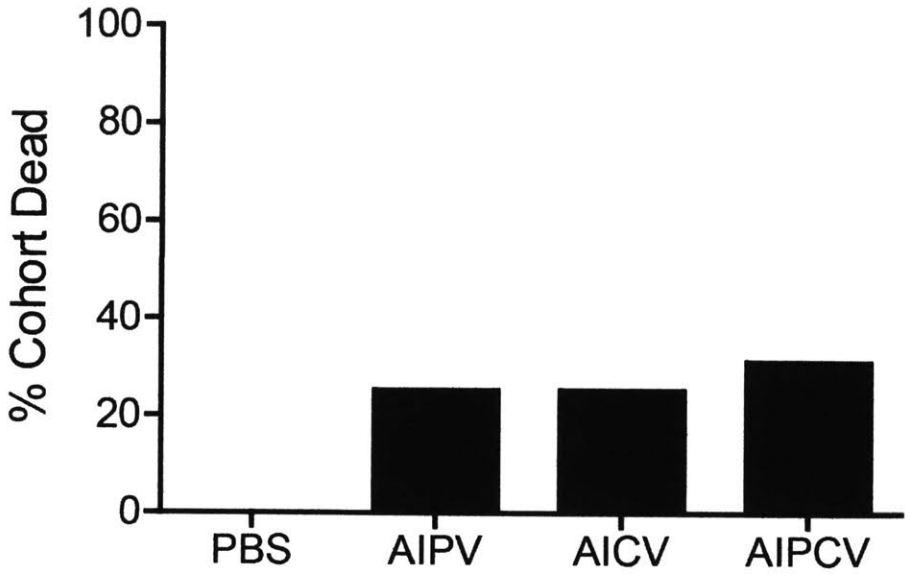

Figure 6.9 Percentage of autochthonous lung tumor-bearing mice from each cohort suffering lethal toxicities in response to immunotherapy administration.

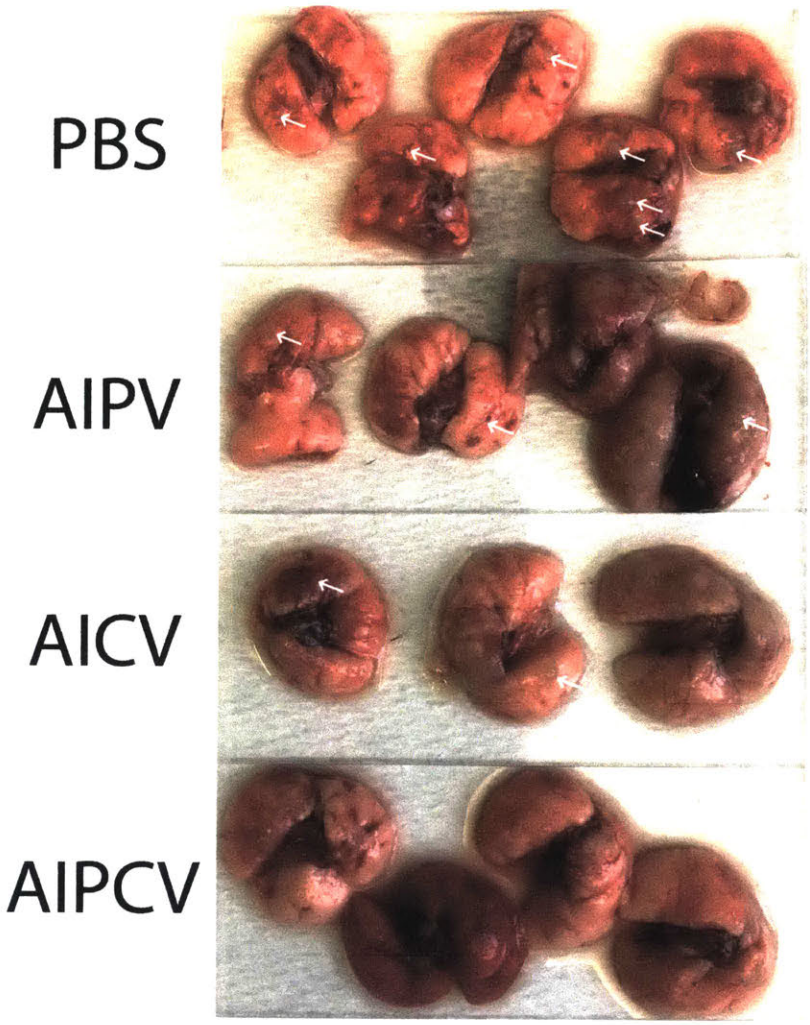

Figure 6.10 Whole lungs of mice treated with the indicated treatment condition. White arrows indicate observable tumor nodules.

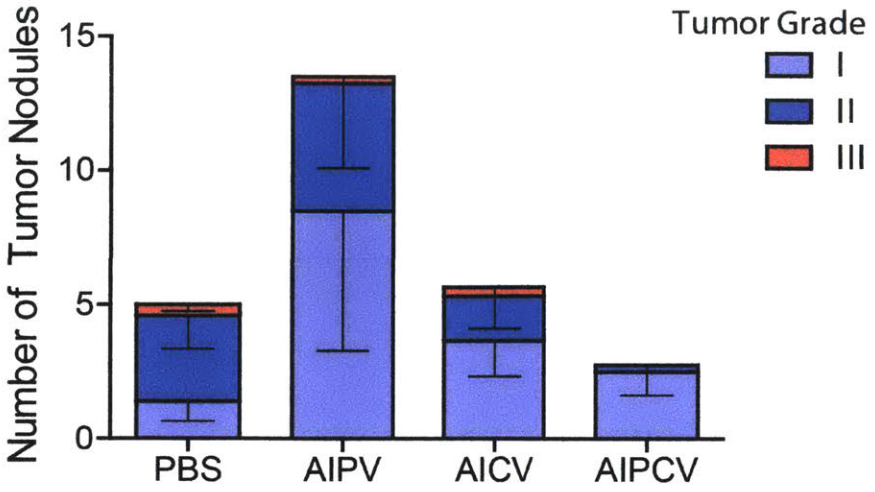

Figure 6.12 Analysis of H&E sections from mice treated with the indicated treatment. Pathologist was blinded to treatment conditions. Both distinct tumor masses and their grade were determined. Grade I refers to hyperplasias. Grade II refers to adenomas with sparse enlarged nuclei. Grade III refers to larger adenocarcinomas with extensive enlarged nuclei. n = 3-5 per group. Data are mean ± SEM.

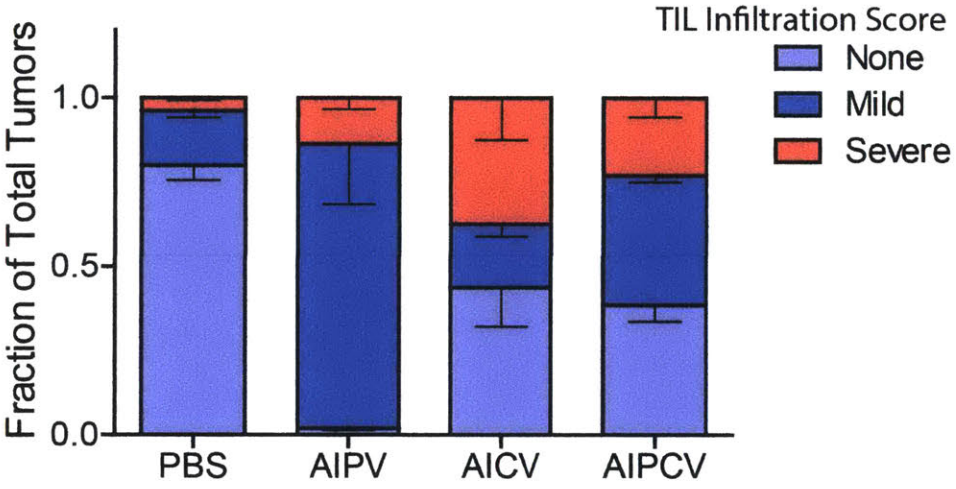

Figure 6.13 Analysis of H&E sections from mice treated with the indicated treatment. Pathologist was blinded to treatment conditions. The tumor infiltrating lymphocyte (TIL) infiltration score of each individual tumor mass was determined. None refers to no lymphocyte association. Mild refers to lymphocyte infiltration that is restricted to the peripheries. Severe refers to extensive infiltration both at the periphery but also within the tumor mass itself. n = 3-5 per group. Data are mean ± SEM.

References

1. Abès, R., Gélizé, E., Fridman, W.H., and Teillaud, J.-L. (2010). Long-lasting antitumor protection by anti-CD20 antibody through cellular immune response. Blood *116*, 926–934.
2. Ahmadzadeh, M., Johnson, L. a, Heemskerk, B., Wunderlich, J.R., Dudley, M.E., White, D.E., Rosenberg, S. a, and Dc, W. (2009). Tumor antigen − specific CD8 T cells infiltrating the tumor express high levels of PD-1 and are functionally impaired. Blood *114*, 1537–1544.
3. Albert, M.L., Pearce, S.F., Francisco, L.M., Sauter, B., Roy, P., Silverstein, R.L., and Bhardwaj, N. (1998). Immature dendritic cells phagocytose apoptotic cells via alphavbeta5 and CD36, and cross-present antigens to cytotoxic T lymphocytes. J. Exp. Med. *188*, 1359–1368.
4. Alexandrov, L.B., Nik-Zainal, S., Wedge, D.C., Aparicio, S. a J.R., Behjati, S., Biankin, A. V, Bignell, G.R., Bolli, N., Borg, A., Børresen-Dale, A.-L., et al. (2013). Signatures of mutational processes in human cancer. Nature *500*, 415–421.
5. Allavena, P., Sica, A., Vecchi, A., Locati, M., Sozzani, S., and Mantovani, A. (2000). The chemokine receptor switch paradigm and dendritic cell migration: its significance in tumor tissues. Immunol. Rev. *177*, 141–149.
6. Anderson, C.L., Chaudhury, C., Kim, J., Bronson, C.L., Wani, M.A., and Mohanty, S. (2006). Perspective-- FcRn transports albumin: relevance to immunology and medicine. Trends Immunol. *27*, 343–348.
7. Atkins, M.B., Lotze, M.T., Dutcher, J.P., Fisher, R.I., Weiss, G., Margolin, K., Abrams, J., Sznol, M., Parkinson, D., Hawkins, M., et al. (1999). High-dose recombinant interleukin 2 therapy for patients with metastatic melanoma: analysis of 270 patients treated between 1985 and 1993. J. Clin. Oncol. *17*, 2105–2116.
8. Azuma, T., Yao, S., Zhu, G., Flies, A.S., Flies, S.J., and Chen, L. (2008). B7-H1 is a ubiquitous antiapoptotic receptor on cancer cells. Blood *111*, 3635–3643.
9. Baden, L.R., Blattner, W.A., Morgan, C., Huang, Y., Defawe, O.D., Sobieszczyk, M.E., Kochar, N., Tomaras, G.D., McElrath, M.J., Russell, N., et al. (2011). Timing of plasmid cytokine (IL-2/Ig) administration affects HIV-1 vaccine immunogenicity in HIV-seronegative subjects. J. Infect. Dis. *204*, 1541–1549.

10. Bajorin, D.F., Chapman, P.B., Wong, G., Coit, D.G., Kunicka, J., Dimaggio, J., Cordon-cardo, C., Urmacher, C., Dantes, L., Templeton, M.A., et al. (1990). Phase I evaluation of a combination of monoclonal antibody R24 and interleukin 2 in patients with metastatic melanoma. Cancer Res. *50*, 7490–7495.

11. Baley, P. a, Yoshida, K., Qian, W., Sehgal, I., and Thompson, T.C. (1995). Progression to androgen insensitivity in a novel in vitro mouse model for prostate cancer. J. Steroid Biochem. Mol. Biol. *52*, 403–413.

12. Balkwill, F., Charles, K.A., and Mantovani, A. (2005). Smoldering and polarized inflammation in the initiation and promotion of malignant disease. Cancer Cell *7*, 211–217.

13. Banchereau, J., and Steinman, R.M. (1998). Dendritic cells and the control of immunity. Nature *392*, 245–252.

14. Baudino, L., Shinohara, Y., Nimmerjahn, F., Furukawa, J., Nakata, M., Martínez-Soria, E., Petry, F., Ravetch, J. V, Nishimura, S., and Izui, S. (2008). Crucial role of aspartic acid at position 265 in the CH2 domain for murine IgG2a and IgG2b Fc-associated effector functions. J. Immunol. *181*, 6664–6669.

15. Benchimol, S., Fuks, a, Jothy, S., Beauchemin, N., Shirota, K., and Stanners, C.P. (1989). Carcinoembryonic antigen, a human tumor marker, functions as an intercellular adhesion molecule. Cell *57*, 327–334.

16. Betts, M.R., Brenchley, J.M., Price, D. a., De Rosa, S.C., Douek, D.C., Roederer, M., and Koup, R. a. (2003). Sensitive and viable identification of antigen-specific CD8+ T cells by a flow cytometric assay for degranulation. J. Immunol. Methods *281*, 65–78.

17. Beyer, M., and Schultze, J.L. (2006). Regulatory T cells in cancer. Blood *108*, 804–811.

18. Blattman, J.N., and Greenberg, P.D. (2004). Cancer immunotherapy: a treatment for the masses. Science (80-.). *305*, 200–205.

19. Bleumera, I., Oosterwijka, E., Oosterwijk-Wakkaa, J.C., Völlera, M.C.W., Melchiorb, S., Warnaarc, S.O., Malac, C., Beckb, J., and Mulders, P.F.A. (2006). A clinical trial With chimeric monoclonal antibody WX-G250 and low dose interleukin-2 pulsing scheme for advanced renal cell carcinoma. J. Urol. *175*, 57–62.

20. Borghaei, H., Paz-Ares, L., Horn, L., Spigel, D.R., Steins, M., Ready, N.E., Chow, L.Q., Vokes, E.E., Felip, E., Holgado, E., et al. (2015). Nivolumab versus Docetaxel in

Advanced Nonsquamous Non-Small-Cell Lung Cancer. N. Engl. J. Med. *373*, 1627–1639.

21. Brahmer, J., Reckamp, K.L., Baas, P., Crino, L., Eberhardt, W.E.E., Poddubsakay, E., Antonia, S., Pluzanski, A., Vokes, E.E., Holgado, E., et al. (2015). Nivolumab versus Docetaxel in Advanced Nonsquamous Non-Small-Cell Lung Cancer. N. Engl. J. Med. *373*, 1627–1639.
22. Carlo, E. Di, Forni, G., Lollini, P., Colombo, M.P., Modesti, A., and Musiani, P. (2001). The intriguing role of polymorphonuclear neutrophils in antitumor reactions. Blood *97*, 339–345.
23. Carretero, R., Sektioglu, I.M., Garbi, N., Salgado, O.C., Beckhove, P., and Hämmerling, G.J. (2015). Eosinophils orchestrate cancer rejection by normalizing tumor vessels and enhancing infiltration of CD8(+) T cells. Nat. Immunol. *16*, 609–617.
24. Carson, W.E., Parihar, R., Lindemann, M.J., Personeni, N., Dierksheide, J., Meropol, N.J., Baselga, J., and Caligiuri, M. a (2001). Interleukin-2 enhances the natural killer cell response to Herceptin-coated Her2/neu-positive breast cancer cells. Eur. J. \Immunology *31*, 3016–3025.
25. Cassatella, M.A. (1995). The production of cytokines by polymorphonuclear neutrophils. Immunol. Today *16*, 21–26.
26. Chen, D.S., and Mellman, I. (2013). Oncology meets immunology: The cancer-immunity cycle. Immunity *39*, 1–10.
27. Chong, C.R., and Jänne, P. a (2013). The quest to overcome resistance to EGFR-targeted therapies in cancer. Nat. Med. *19*, 1389–1400.
28. Clemente, C., Mihm, M.J., Bufalino, R., Zurrida, S., Collini, P., and Cascinelli, N. (1996). Prognostic value of tumor infiltrating lymphocytes in the vertical growth phase of primary cutaneous melanoma. Cancer *77*, 1303–1310.
29. Clynes, R.A., Towers, T.L., Presta, L.G., and Ravetch, J. V (2000). Inhibitory Fc receptors modulate in vivo cytotoxicity against tumor targets. Nat. Med. *6*, 443–446.
30. Coley, W.B. (1894). Treatment of inoperable malignant tumors with the toxines of Erysipelas and the Bacillus Prodigiosus. Am. J. Med. Sci. *108*, 50–66.
31. Colotta, F., Re, F., Polentarutti, N., Sozzani, S., and Mantovani, A. (1992). Modulation of granulocyte survival and programmed cell death by cytokines and bacterial products.

Blood *80*, 2012–2020.

32. Corrales, L., Glickman, L.H., McWhirter, S.M., Kanne, D.B., Sivick, K.E., Katibah, G.E., Woo, S.R., Lemmens, E., Banda, T., Leong, J.J., et al. (2015). Direct Activation of STING in the Tumor Microenvironment Leads to Potent and Systemic Tumor Regression and Immunity. Cell Rep. *11*, 1018–1030.

33. Dankort, D., Curley, D.P., Cartlidge, R. a, Nelson, B., Karnezis, A.N., Damsky, W.E., You, M.J., DePinho, R. a, McMahon, M., and Bosenberg, M. (2009). Braf(V600E) cooperates with Pten loss to induce metastatic melanoma. Nat. Genet. *41*, 544–552.

34. Dillman, R.O., Church, C., Oldham, R.K., West, W.H., Schwartzberg, L., and Birch, R. (1993). Inpatient continuous-infusion interleukin-2 in 788 patients with cancer. Cancer *71*, 2358–2370.

35. Dong, H., Strome, S.E., Salomao, D.R., Tamura, H., Hirano, F., Flies, D.B., Roche, P.C., Lu, J., Zhu, G., Tamada, K., et al. (2002). Tumor-associated B7-H1 promotes T-cell apoptosis: a potential mechanism of immune evasion. Nat. Med. *8*, 793–800.

36. Dranoff, G. (2011). Experimental mouse tumour models: what can be learnt about human cancer immunology? Nat. Rev. Immunol. *12*, 61–66.

37. Dunn, G., Bruce, A., Ikeda, H., and Old, L. (2002). Cancer immunoediting: from immunosurveillance to tumor escape. Nature *3*, 991–998.

38. Dunn, G.P., Old, L.J., and Schreiber, R.D. (2004a). The three Es of cancer immunoediting. Annu. Rev. Immunol. *22*, 329–360.

39. Dunn, G.P., Old, L.J., Schreiber, R.D., Louis, S., Burnet, F.M., and Thomas, L. (2004b). The Immunobiology of Cancer Immunosurveillance and Immunoediting. Immunity *21*, 137–148.

40. DuPage, M., Dooley, A.L., and Jacks, T. (2009). Conditional mouse lung cancer models using adenoviral or lentiviral delivery of Cre recombinase. Nat. Protoc. *4*, 1064–1072.

41. Eisenbeis, C.F., Caligiuri, M.A., and Byrd, J.C. (2003). Rituximab : converging mechanisms of action in non-hodgkin's lymphoma ? Clin. Cancer Res. *9*, 5810–5812.

42. Eisenbeis, C.F., Grainger, A., Fischer, B., Baiocchi, R.A., Carrodeguas, L., Roychowdhury, S., Chen, L., Banks, A.L., Davis, T., Young, D., et al. (2004). Combination immunotherapy of B-Cell Non-Hodgkin's Lymphoma with rituximab and interleukin-2 : a preclinical and phase I study. Clin. Cancer Res. *10*, 6101–6110.

43. Facciabene, A., Motz, G.T., and Coukos, G. (2012). T-Regulatory cells: Key players in tumor immune escape and angiogenesis. Cancer Res. *72*, 2162–2171.

44. Fang, F.C. (2004). Antimicrobial reactive oxygen and nitrogen species: concepts and controversies. Nat. Rev. Microbiol. *2*, 820–832.

45. Feau, S., Arens, R., Togher, S., and Schoenberger, S.P. (2011). Autocrine IL-2 is required for secondary population expansion of CD8(+) memory T cells. Nat. Immunol. *12*, 908–913.

46. Ferris, R.L., Jaffee, E.M., and Ferrone, S. (2010). Tumor antigen-targeted, monoclonal antibody-based immunotherapy: clinical response, cellular immunity, and immunoescape. J. Clin. Oncol. *28*, 4390–4399.

47. Figdor, C.G., de Vries, I.J.M., Lesterhuis, W.J., and Melief, C.J.M. (2004). Dendritic cell immunotherapy: mapping the way. Nat. Med. *10*, 475–480.

48. Fleming, G.F., Meropol, N.J., Rosner, G.L., Hollis, D.R., Carson, W.E., Caligiuri, M., Mortimer, J., Tkaczuk, K., Parihar, R., Schilsky, R.L., et al. (2002). A phase I trial of escalating doses of trastuzumab combined with daily subcutaneous interleukin 2 : report of cancer and leukemia group B 9661. Clin. Cancer Res. *8*, 3718–3727.

49. Flies, D.B., Sandler, B.J., Sznol, M., and Chen, L. (2011). Blockade of the B7-H1/PD-1 pathway for cancer immunotherapy. Yale J. Biol. Med. *84*, 409–421.

50. Fong, L., and Engleman, E.G. (2000). Dendritic Cells in Cancer Immunotherapy. Annu. Rev. Immunol. *18*, 245–273.

51. Freeman, G.J., Long, a J., Iwai, Y., Bourque, K., Chernova, T., Nishimura, H., Fitz, L.J., Malenkovich, N., Okazaki, T., Byrne, M.C., et al. (2000). Engagement of the PD-1 immunoinhibitory receptor by a novel B7 family member leads to negative regulation of lymphocyte activation. J. Exp. Med. *192*, 1027–1034.

52. Frese, K.K., and Tuveson, D. a (2007). Maximizing mouse cancer models. Nat. Rev. Cancer *7*, 654–658.

53. Fridlender, Z.G., and Albelda, S.M. (2012). Tumor-associated neutrophils: friend or foe? Carcinogenesis *33*, 949–955.

54. Fridlender, Z.G., Sun, J., Kim, S., Kapoor, V., Cheng, G., Ling, L., Worthen, G.S., and Albelda, S.M. (2009). Polarization of tumor-associated neutrophil phenotype by TGF-beta: "N1" versus "N2" TAN. Cancer Cell *16*, 183–194.

55. Fyfe, G., Fisher, R.I., Rosenberg, S.A., Sznol, M., Parkinson, D.R., and Louie, A.C. (1995). Results of treatment of 255 patients with metastatic renal cell carcinoma who received high-dose recombinant interleukin-2 therapy. J. Clin. Oncol. *13*, 688–696.

56. Gabrilovich, D.I., and Nagaraj, S. (2009). Myeloid-derived suppressor cells as regulators of the immune system. Nat. Rev. Immunol. *9*, 162–174.

57. Gabrilovich, D.I., Ostrand-Rosenberg, S., and Bronte, V. (2012). Coordinated regulation of myeloid cells by tumours. Nat. Rev. Immunol. *12*, 253–268.

58. Gaffen, S.L. (2001). Signaling Domains of the Interleukin 2 Receptor. Cytokine *14*, 63–77.

59. Gajewski, T.F., Meng, Y., Blank, C., Brown, I., Kacha, A., Kline, J., and Harlin, H. (2006). Immune resistance orchestrated by the tumor microenvironment. Immunol. Rev. *213*, 131–145.

60. Gajewski, T.F., Schreiber, H., and Fu, Y.-X. (2013). Innate and adaptive immune cells in the tumor microenvironment. Nat. Immunol. *14*, 1014–1022.

61. Grivennikov, S.I., Greten, F.R., and Karin, M. (2010). Immunity, Inflammation, and Cancer. Cell *140*, 883–899.

62. Gross, S., Gammon, S.T., Moss, B.L., Rauch, D., Harding, J., Heinecke, J.W., Ratner, L., and Piwnica-Worms, D. (2009). Bioluminescence imaging of myeloperoxidase activity in vivo. Nat. Med. *15*, 455–461.

63. Guo, R.-F., and Ward, P. a (2005). Role of C5a in inflammatory responses. Annu. Rev. Immunol. *23*, 821–852.

64. Hammarström, S. (1999). The carcinoembryonic antigen (CEA) family: structures, suggested functions and expression in normal and malignant tissues. Semin. Cancer Biol. *9*, 67–81.

65. Hammers, H., Plimack, E.R., Infante, J.R., Ernstoff, M., Rini, B.I., McDermott, D.F., Razak, A., Pal, S.K., Voss, M., Sharma, P., et al. (2014). Phase I Study of Nivolumab in Combination With Ipilimumab in Metastatic Renal Cell Carcinoma (MRCC). Ann. Oncol. *25*, iv361–iv362.

66. Hodi, F., O'Day, S., McDermott, D., Weber, R., Sosman, J., Haanen, J., Gonzalez, R., Robert, C., Schadendorf, D., Hassel, J., et al. (2010a). Improved Survival with Ipilimumab in Patients with Metastatic Melanoma. N. Engl. J. Med. *363*, 711–723.

67. Hodi, S.F., O'Day, S.J., McDermott, D.F., Weber, R.W., Sosman, J.A., Haanen, J.B., Gonzalez, R., Robert, C., Scahdendorf, D., Hassel, J.C., et al. (2010b). Improved Survival with Ipilimumab in patients with Metastatic Melanoma. N. Engl. J. Med. *363*, 711–723.

68. Homey, B., Müller, A., and Zlotnik, A. (2002). Chemokines: Agents for the Immunotherapy of Cancer? Nat. Rev. Immunol. *2*, 175–184.

69. Huizinga, T.W.J., van der Schoot, C.E., Jost, C., Klaassen, R., Kleijer, M., von dem Borne, A.E.G.K., Roos, D., and Tetteroo, P.A.T. (1988). The PI-linked receptor FcRIII is released on stimulation of neutrophils. Nature *333*, 667–669.

70. Huntington, N.D., Tabarias, H., Fairfax, K., Brady, J., Hayakawa, Y., Degli-Esposti, M. a., Smyth, M.J., Tarlinton, D.M., and Nutt, S.L. (2007). NK cell maturation and peripheral homeostasis is associated with KLRG1 up-regulation. J. Immunol. *178*, 4764–4770.

71. Jackson, S.H., Gallin, J.I., and Holland, S.M. (1995). The p47phox mouse knock-out model of chronic granulomatous disease. J. Exp. Med. *182*, 751–758.

72. Jones, S. a. (2005). Directing Transition from Innate to Acquired Immunity: Defining a Role for IL-6. J. Immunol. *175*, 3463–3468.

73. Joshi, N.S., Akama-Garren, E.H., Lu, Y., Lee, D.Y., Chang, G.P., Li, A., DuPage, M., Tammela, T., Kerper, N.R., Farago, A.F., et al. (2015). Regulatory T Cells in Tumor-Associated Tertiary Lymphoid Structures Suppress Anti-tumor T Cell Responses. Immunity *43*, 579–590.

74. Ju, S.-A., Lee, S.-C., Kwon, T.-H., Heo, S.-K., Park, S.-M., Paek, H.-N., Suh, J.-H., Cho, H.R., Kwon, B., Kwon, B.S., et al. (2005). Immunity to melanoma mediated by 4-1BB is associated with enhanced activity of tumour-infiltrating lymphocytes. Immunol. Cell Biol. *83*, 344–351.

75. June, C.H. (2007). Principles of adoptive T cell cancer therapy. J. Clin. Invest. *117*, 1204–1212.

76. Kalia, V., Sarkar, S., Subramaniam, S., Haining, W.N., Smith, K.A., and Ahmed, R. (2010). Prolonged interleukin-2Ralpha expression on virus-specific CD8+ T cells favors terminal-effector differentiation in vivo. Immunity *32*, 91–103.

77. Katayama, R., Khan, T.M., Benes, C., Lifshits, E., Ebi, H., Rivera, V.M., Shakespeare, W.C., Iafrate, A.J., Engelman, J.A., and Shaw, A.T. (2011). Therapeutic strategies to

overcome crizotinib resistance in non-small cell lung cancers harboring the fusion oncogene EML4-ALK. Proc. Natl. Acad. Sci. *108*, 7535–7540.

78. Keir, M.E., Butte, M.J., Freeman, G.J., and Sharpe, A.H. (2008). PD-1 and its ligands in tolerance and immunity. Annu. Rev. Immunol. *26*, 677–704.

79. Khan, K.D., Emmanouilides, C., Benson, D.M., Hurst, D., Garcia, P., Michelson, G., Milan, S., Ferketich, A.K., Piro, L., Leonard, J.P., et al. (2006). A phase 2 study of rituximab in combination with recombinant interleukin-2 for rituximab-refractory indolent non-Hodgkin's lymphoma. Clin. Cancer Res. *12*, 7046–7053.

80. Konrad, M.W., Hemstreet, G., Hersh, E.M., Mansell, P.W.A., Mertelsmann, R., Kolitz, J.E., and Bradley, E.C. (2009). Pharmacokinetics of recombinant interleukin 2 in humans. Cancer Res. *50*, 2009–2017.

81. Kowanko, I.C., and Ferrante, A. (1987). Stimulation of neutrophil respiratory burst and lysosomal enzyme release by human interferon-gamma. Immunology *62*, 149–151.

82. Kuijpers, T.W., Tool, a T., van der Schoot, C.E., Ginsel, L. a, Onderwater, J.J., Roos, D., and Verhoeven, a J. (1991). Membrane surface antigen expression on neutrophils: a reappraisal of the use of surface markers for neutrophil activation. Blood *78*, 1105–1111.

83. Kusmartsev, S., and Gabrilovich, D.I. (2002). Immature myeloid cells and cancer-associated immune suppression. Cancer Immunol. Immunother. *51*, 293–298.

84. Lacy, P., and Stow, J.L. (2011). Cytokine release from innate immune cells: association with diverse membrane trafficking pathways. Blood *118*, 9–18.

85. Leach, D.R., Krummel, M.F., and Allison, J.P. (1996). Enhancement of antitumor immunity by CTLA-4 blockade. Science (80-.). *271*, 1734–1736.

86. Leen, A., Rooney, C., and Foster, A. (2007). Improving T cell therapy for cancer. Annu. Rev. Immunol. *25*, 243–265.

87. Legha, S.S., Gianan, M.A., Plager, C., Eton, O.E., and Papadopoulous, N.E. (1996). Evaluation of interleukin-2 administered by continuous infusion in patients with metastatic melanoma. Cancer *77*, 89–96.

88. Lillard, J.W., Boyaka, P.N., Chertov, O., Oppenheim, J.J., and McGhee, J.R. (1999). Mechanisms for induction of acquired host immunity by neutrophil peptide defensins. Proc. Natl. Acad. Sci. U. S. A. *96*, 651–656.

89. Lindau, D., Gielen, P., Kroesen, M., Wesseling, P., and Adema, G.J. (2013). The

immunosuppressive tumour network: myeloid-derived suppressor cells, regulatory T cells and natural killer T cells. Immunology *138*, 105–115.

90. Liu, H., Moynihan, K.D., Zheng, Y., Szeto, G.L., Li, A. V, Huang, B., Van Egeren, D.S., Park, C., and Irvine, D.J. (2014). Structure-based programming of lymph-node targeting in molecular vaccines. Nature *507*, 519–522.

91. Liu, V.C., Wong, L.Y., Jang, T., Shah, A.H., Park, I., Yang, X., Zhang, Q., Lonning, S., Teicher, B.A., and Lee, C. (2007). Tumor Evasion of the Immune System by Converting CD4+CD25- T Cells into CD4+CD25+ T Regulatory Cells: Role of Tumor-Derived TGF-β. J. Immunol. *178*, 2883–2892.

92. Lutz, M.B., and Schuler, G. (2002). Immature, semi-mature and fully mature dendritic cells: Which signals induce tolerance or immunity? Trends Immunol. *23*, 445–449.

93. Malek, T.R. (2008). The biology of interleukin-2. Annu. Rev. Immunol. *26*, 453–479.

94. Mani, A., Roda, J., Young, D., Caligiuri, M. a, Fleming, G.F., Kaufman, P., Brufsky, A., Ottman, S., Carson, W.E., and Shapiro, C.L. (2009). A phase II trial of trastuzumab in combination with low-dose interleukin-2 (IL-2) in patients (PTS) with metastatic breast cancer (MBC) who have previously failed trastuzumab. Breast Cancer Res. Treat. *117*, 83–89.

95. Mantovani, A., Sozzani, S., Locati, M., Allavena, P., and Sica, A. (2002). Macrophage polarization: tumor-associated macrophages as a paradigm for polarized M2 mononuclear phagocytes. Trends Immunol. *23*, 549–555.

96. Mantovani, A., Cassatella, M. a, Costantini, C., and Jaillon, S. (2011). Neutrophils in the activation and regulation of innate and adaptive immunity. Nat. Rev. Immunol. *11*, 519–531.

97. Melder, R.J., Osborn, B.L., Riccobene, T., Kanakaraj, P., Wei, P., Chen, G., Stolow, D., Halpern, W.G., Migone, T.-S., Wang, Q., et al. (2005). Pharmacokinetics and in vitro and in vivo anti-tumor response of an interleukin-2-human serum albumin fusion protein in mice. Cancer Immunol. Immunother. *54*, 535–547.

98. Mennuni, C., Calvaruso, F., Facciabene, A., Aurisicchio, L., Storto, M., Scarselli, E., Ciliberto, G., and La Monica, N. (2005). Efficient induction of T-cell responses to carcinoembryonic antigen by a heterologous prime-boost regimen using DNA and adenovirus vectors carrying a codon usage optimized cDNA. Int. J. Cancer *117*, 444–455.

99. Motz, G., and Coukos, G. (2013). Deciphering and reversing tumor immune suppression. Immunity *39*, 61–73.

100. Müller, I., Munder, M., Kropf, P., and Hänsch, G.M. (2009). Polymorphonuclear neutrophils and T lymphocytes: strange bedfellows or brothers in arms? Trends Immunol. *30*, 522–530.

101. Neckers, L.M., and Cossman, J. (1983). Transferrin receptor induction in mitogen-stimulated human T lymphocytes is required for DNA synthesis and cell division and is regulated by interleukin 2. PNAS *80*, 3494–3498.

102. Nelson, B.H., and Willerford, D.M. (1998). Biology of the interleukin-2 receptor. Adv. Immunol. *70*, 1–81.

103. Nishimura, H., and Honjo, T. (2001). PD-1: An inhibitory immunoreceptor involved in peripheral tolerance. Trends Immunol. *22*, 265–268.

104. Nishimura, H., Nose, M., Hiai, H., Minato, N., and Honjo, T. (1999). Development of lupus-like autoimmune diseases by disruption of the PD-1 gene encoding an ITIM motif-carrying immunoreceptor. Immunity *11*, 141–151.

105. Opel, C.F. (2015). T Cell Mediated Combination Immunotherapy.

106. Overwijk, W.W. (2005). Breaking tolerance in cancer immunotherapy: time to ACT. Curr. Opin. Immunol. *17*, 187–194.

107. Overwijk, W.W., Theoret, M.R., Finkelstein, S.E., Surman, D.R., de Jong, L.A., Vyth-Dreese, F.A., Dellemijn, T.A., Antony, P.A., Spiess, P.J., Palmer, D.C., et al. (2003). Tumor regression and autoimmunity after reversal of a functionally tolerant state of self-reactive CD8+ T cells. J. Exp. Med. *198*, 569–580.

108. Pardoll, D.M. (2012). The blockade of immune checkpoints in cancer immunotherapy. Nat. Rev. Cancer *12*, 252–264.

109. Park, S., Jiang, Z., Mortenson, E.D., Deng, L., Radkevich-Brown, O., Yang, X., Sattar, H., Wang, Y., Brown, N.K., Greene, M., et al. (2010). The therapeutic effect of anti-HER2/neu antibody depends on both innate and adaptive immunity. Cancer Cell *18*, 160–170.

110. Pelletier, M., Micheletti, A., and Cassatella, M.A. (2010). Modulation of human neutrophil survival and antigen expression by activated CD4+ and CD8+ T cells. J. Leukoc. Biol. *88*, 1163–1170.

111. Pipkin, M.E., Sacks, J.A., Cruz-Guilloty, F., Lichtenheld, M.G., Bevan, M.J., and Rao, A. (2010). Interleukin-2 and inflammation induce distinct transcriptional programs that promote the differentiation of effector cytolytic T cells. Immunity *32*, 79–90.

112. Poiré, X., Kline, J., Grinblatt, D., Zimmerman, T., Conner, K., Muhs, C., Gajewski, T., Besien, K. Van, and Smith, S.M. (2010). Phase II study of immunomodulation with granulocyte-macrophage colony-stimulating factor, interleukin-2, and rituximab following autologous stem cell transplant in patients with relapsed or refractory lymphomas. Leuk. Lymphoma *51*, 1241–1250.

113. Pollard, J.W. (2004). Tumor-educated macrophages promote tumour progression and metastasis. Nat. Rev. Cancer *4*, 71–78.

114. Pollard, J.W. (2009). Trophic macrophages in development and disease. Nat. Rev. Immunol. *9*, 259–270.

115. Putten, H. Van Der, Hirth, A., Hirth, A., Thompson, J., Neumaler, M., Kleist, S. Von, and Zimmermann, W. (1994). Mice Transgenic for the Human Carcinoembryonic Antigen Gene Maintain Its Spatiotemporal Expression Pattern Mice Transgenic for the Human Carcinoembryonic Antigen Gene Maintain Its Spatiotemporal Expression Patternâ €. Cancer Res. 4169–4176.

116. Rabinovich, G.A., Gabrilovich, D., and Sotomayor, E.M. (2007). Immunosuppressive strategies that are mediated by tumor cells. Annu. Rev. Immunol. *25*, 267–296.

117. Rao, B.M., Driver, I., Lauffenburger, D.A., and Wittrup, K.D. (2004). Interleukin 2 (IL-2) variants engineered for increased IL-2 receptor alpha-subunit affinity exhibit increased potency arising from a cell surface ligand reservoir effect. Mol. Pharmacol. *66*, 864–869.

118. Rao, B.M., Driver, I., Lauffenburger, D.A., and Wittrup, K.D. (2005). High-affinity CD25-binding IL-2 mutants potently stimulate persistent T cell growth. Biochemistry *44*, 10696–10701.

119. Repka, T., Chiorean, E.G., Gay, J., Herwig, K.E., Kohl, V.K., Yee, D., and Miller, J.S. (2003). Trastuzumab and interleukin-2 in HER2-positive metastatic breast cancer : a pilot study. Clin. Cancer Res. *9*, 2440–2446.

120. Rini, B.I., and Atkins, M.B. (2009). Resistance to targeted therapy in renal-cell carcinoma. Lancet Oncol. *10*, 992–1000.

121. Rosenberg, H.F., Dyer, K.D., and Foster, P.S. (2013). Eosinophils: Changing

perspectives in health and disease. Nat. Rev. Immunol. *13*, 9–22.

122. Sakaguchi, S., Sakaguchi, N., Asano, M., Itoh, M., and Toda, M. (1995). Immunological self-tolerance maintained by activated T cells expressing IL-2 receptor alpha-chains (CD25). Breakdown of a single mechanism of self-tolerance causes various autoimmune diseases. J. Immunol. *155*, 1151–1164.

123. Sansom, D.M. (2000). CD28, CTLA-4 and their ligands: Who does what and to whom? Immunology *101*, 169–177.

124. Schneider-Merck, T., Lammerts van Bueren, J.J., Berger, S., Rossen, K., van Berkel, P.H.C., Derer, S., Beyer, T., Lohse, S., Bleeker, W.K., Peipp, M., et al. (2010). Human IgG2 antibodies against epidermal growth factor receptor effectively trigger antibody-dependent cellular cytotoxicity but, in contrast to IgG1, only by cells of myeloid lineage. J. Immunol. *184*, 512–520.

125. Schreiber, R.D., Old, L.J., and Smyth, M.J. (2011). Cancer Immunoediting : Integrating Immunity ' s Roles in Cancer Suppression and Promotion. *331*, 1565–1570.

126. Schwartz, R.H. (2003). T cell anergy. Annu. Rev. Immunol. *21*, 305–334.

127. Selby, M.J., Engelhardt, J.J., Quigley, M., Henning, K.A., Chen, T., Srinivasan, M., and Korman, A.J. (2013). Anti-CTLA-4 antibodies of IgG2a isotype enhance antitumor activity through reduction of intratumoral regulatory T cells. Cancer Immunol. Res. *1*, 32–42.

128. Siders, W.M., Shields, J., Garron, C., Hu, Y., Boutin, P., Shankara, S., Weber, W., Roberts, B., and Kaplan, J.M. (2010). Involvement of neutrophils and natural killer cells in the anti-tumor activity of alemtuzumab in xenograft tumor models. Leuk. Lymphoma *51*, 1293–1304.

129. Sliwkowski, M.X., Lofgren, J.A., Lewis, G.D., Hotaling, T.E., Fendly, B.M., and Fox, J.A. (1999). Nonclinical studies addressing the mechanism of action of trastuzumab (Herceptin). Semin. Oncol. *26*, 60–70.

130. Smyth, M.J., Godfrey, D.I., and Trapani, J. a (2001). A fresh look at tumor immunosurveillance and immunotherapy. Nat. Immunol. *2*, 293–299.

131. Smyth, M.J., Hayakawa, Y., Takeda, K., and Yagita, H. (2002). New aspects of natural-killer cell surveillance and therapy of cancer. Nat. Rev. Cancer *2*, 850–861.

132. Stagg, J., Johnstone, R.W., and Smyth, M.J. (2007). From cancer immunosurveillance to

cancer immunotherapy. Immunol. Rev. *220*, 82–101.

133. Stagg, J., Loi, S., Divisekera, U., Foong, S., Duret, H., Yagita, H., Teng, M.W., and Smyth, M.J. (2011). Anti – ErbB-2 mAb therapy requires type I and II interferons and synergizes with anti – PD-1 or anti-CD137 mAb therapy. PNAS *108*, 10–15.

134. Suntharalingam, G., Perry, M.R., Ward, S., Brett, S.J., Castello-Cortes, A., Brunner, M.D., and Panoskaltsis, N. (2006). Cytokine storm in a phase 1 trial of the anti-CD28 monoclonal antibody TGN1412. N. Engl. J. Med. *355*, 1018–1028.

135. Sznol, M., and Chen, L. (2013). Antagonist antibodies to PD-1 and B7-H1 (PD-L1) in the treatment of advanced human cancer. Clin. Cancer Res. *19*, 1021–1034.

136. Teft, W.A., Kirchhof, M.G., and Madrenas, J. (2006). A molecular perspective of CTLA-4 function. Annu. Rev. Immunol. *24*, 65–97.

137. Teicher, B.A. (2006). Tumor models for efficacy determination. Mol. Cancer Ther. *5*, 2435–2443.

138. Tokuda, Y., Ohnishi, Y., Shimamura, K., Iwasawa, M., Yoshimura, M., Ueyama, Y., Tamaoki, N., Tajima, T., and Mitomi, T. (1996). In vitro and in vivo anti-tumour effects of a humanised monoclonal antibody against c-erbB-2 product. Br. J. Cancer *73*, 1362–1365.

139. Tsuruo, T., Naito, M., Tomida, A., Fujita, N., Mashima, T., Sakamoto, H., and Haga, N. (2003). Molecular targeting therapy of cancer : drug resistance , apoptosis and survival signal. Cancer Sci. *94*, 15–21.

140. Vivier, E., Tomasello, E., Baratin, M., Walzer, T., and Ugolini, S. (2008). Functions of natural killer cells. Nat. Immunol. *9*, 503–510.

141. Walunas, T.L., Lenschow, D.J., Bakker, C.Y., Linsley, P.S., Freeman, G.J., Green, J.M., Thompson, C.B., and Bluestone, J. a (1994). CTLA-4 can function as a negative regulator of T cell activation. Immunity *1*, 405–413.

142. Wang, S., Astsaturov, I.A., Bingham, C.A., McCarthy, K.M., von Mehren, M., Xu, W., Alpaugh, R.K., Tang, Y., Littlefield, B.A., Hawkins, L.D., et al. (2012). Effective antibody therapy induces host-protective antitumor immunity that is augmented by TLR4 agonist treatment. Cancer Immunol. Immunother. *61*, 49–61.

143. Ward, P.L., Koeppen, H., Hurteau, T., and Schreiber, H. (1989). Tumor antigens defined by cloned immunological probes are highly polymorphic and are not detected on

autologus normal cells. J. Exp. Med. *170*, 217–232.

144. Waugh, D.J.J., and Wilson, C. (2008). The interleukin-8 pathway in cancer. Clin. Cancer Res. *14*, 6735–6741.

145. Weiner, L.M., Dhodapkar, M. V, and Ferrone, S. (2009). Monoclonal antibodies for cancer immunotherapy. Lancet *373*, 1033–1040.

146. Weiner, L.M., Surana, R., and Wang, S. (2010). Monoclonal antibodies: versatile platforms for cancer immunotherapy. Nat. Rev. Immunol. *10*, 317–327.

147. Weng, W.-K., and Levy, R. (2003). Two immunoglobulin G fragment C receptor polymorphisms independently predict response to rituximab in patients with follicular lymphoma. J. Clin. Oncol. *21*, 3940–3947.

148. Westcott, P.M.K., Halliwill, K.D., To, M.D., Rashid, M., Rust, A.G., Keane, T.M., Delrosario, R., Jen, K., Gurley, K.E., Kemp, C.J., et al. (2014). The mutational landscapes of genetic and chemical models of Kras-driven lung cancer. Nature *517*, 489–492.

149. Whiteside, T.L. (2008). The tumor microenvironment and its role in promoting tumor growth. Oncogene *27*, 5904–5912.

150. Whiteside, T.L. (2014). Tumor-infiltrating lymphocytes and their role in solid tumor progression. In Interaction of Immune and Cancer Cells, pp. 111–121.

151. Winkler, U., Jensen, M., Manzke, O., Schulz, H., Diehl, V., and Engert, A. (1999). Cytokine-release syndrome in patients with B-cell chronic lymphocytic leukemia and high lymphocyte counts after treatment with an anti-CD20 monoclonal antibody (Rituximab, IDEC-C2B8). Blood *94*, 2217–2224.

152. Wolchok, J.D., Kluger, H., Callahan, M.K., Postow, M.A., Rizvi, N.A., Lesokhin, A.M., Segal, N.H., Ariyan, C.E., Gordon, R.-A., Reed, K., et al. (2013). Nivolumab plus Ipilimumab in Advanced Melanoma. N. Engl. J. Med.

153. Wolpe, S.D., Sherry, B., Juers, D., Davatelis, G., Yurt, R.W., and Cerami, A. (1989). Identification and characterization of macrophage inflammatory protein 2. PNAS *86*, 612–616.

154. Yang, J.C., Topalian, S.L., Schwartzentruber, D.J., Parkinson, D.R., Marincola, F.M., Weber, J.S., Seipp, C.A., White, D.E., and Rosenberg, S.A. (1995). The use of polyethylene glycol-modified interleukin-2 (PEG-IL-2) in the treatment of patients with

metastatic renal cell carcinoma and melanoma. Cancer *76*, 687–694.

155. Yang, L., Pang, Y., and Moses, H.L. (2010). TGF-beta and immune cells: an important regulatory axis in the tumor microenvironment and progression. Trends Immunol. *31*, 220–227.

156. Yu, A.L., Gilman, A.L., Ozkaynak, M.F., London, W.B., Kreissman, S.G., Chen, H.X., Smith, M., Anderson, B., Villablanca, J.G., Matthay, K.K., et al. (2010). Anti-GD2 antibody with GM-CSF, interleukin-2, and isotretinoin for neuroblastoma. N. Engl. J. Med. *363*, 1324–1334.

157. Zhang, H., Zhang, S., Cheung, N.-K. V., Ragupathi, G., and Livingston, P.O. (1998). Antibodies against GD2 Ganglioside Can Eradicate Syngeneic Cancer Micrometastases. Cancer Res. *58*, 2844–2849.

158. Zhu, E.F., Gai, S.A., Opel, C.F., Kwan, B.H., Surana, R., Mihm, M.C., Kauke, M.J., Moynihan, K.D., Angelini, A., Williams, R.T., et al. (2015). Synergistic innate and adaptive immune response to combination immunotherapy with anti-tumor antigen antibodies and extended serum half-life il-2. Cancer Cell *27*, 489–501.

159. Zimmerman, R.J., Aukerman, S.L., Katre, N. V, Winkelhake, J.L., and Young, J.D. (1989). Schedule dependency of the antitumor activity and toxicity of polyethylene glycol-modified interleukin 2 in murine tumor models. Cancer Res. *49*, 6521–6528.